In situ measurements of pH and O2 by planar optodes: improvements and adaptations for soil and rhizosphere applications

Gabrielle Daudin

le cnam

CONSERVATOIRE NATIONAL DES ARTS ET METIERS

PARIS

MEMOIRE

présenté en vue d'obtenir

le DIPLOME d'INGENIEUR CNAM

SPECIALITE : MESURE ANALYSE

OPTION : ANALYSE CHIMIQUE ET BIOANALYSE

par

DAUDIN Gabrielle

In situ measurements of pH and O_2 by planar optodes: improvements and adaptations for soil and rhizosphere applications

---

Soutenu le 4 octobre 2018

JURY

PRESIDENT : Christophe MOULIN (Professeur CNAM, Paris)

MEMBRES : Marie-Christine MOREL (Maitre de conférence CNAM, Paris)

Chouki ZERROUKI (Maitre de conférence CNAM, Paris)

Eva OBURGER (Dipl-Ing. Dr. BOKU, Vienne)

Philippe HINSINGER (DR INRA, Montpellier)

le cnam

CONSERVATOIRE NATIONAL DES ARTS ET METIERS

PARIS

MEMOIRE

présenté en vue d'obtenir

le DIPLOME d'INGENIEUR CNAM

SPECIALITE : MESURE ANALYSE

OPTION : ANALYSE CHIMIQUE ET BIOANALYSE

par

DAUDIN Gabrielle

In situ measurements of pH and O_2 by planar optodes: improvements and adaptations for soil and rhizosphere applications

---

Soutenu le 4 octobre 2018

JURY

PRESIDENT : Christophe MOULIN (Professeur CNAM, Paris)

MEMBRES : Marie-Christine MOREL (Maitre de conférence CNAM, Paris)

Chouki ZERROUKI (Maitre de conférence CNAM, Paris)

Eva OBURGER (Dipl-Ing. Dr. BOKU, Vienne)

Philippe HINSINGER (DR INRA, Montpellier)

Acknowledgements

This manuscript is not just an assessment of 9 months of exciting internship. This work is the end point of 9 months of a great experience in Austria, in two research teams, and … almost 9 years of evening course at CNAM Montpellier and Paris. When I took this path, I didn't know where it would lead me. Today, I could not even say what pushed me to do such a long trip. It was a long trip, requiring a lot of perseverance, whereas during 4 hours, the course is only a succession of internet breaks..." Why? Why am I doing this?" And the next day, the motivation is still there. The CNAM is a school of perseverance, motivation, autonomy… It was a very rich professional and personal experience, sometimes challenging, always exciting. This adventure could not have succeeded without all the people who supported me, help me and believed in this project.

I would like to express my deep gratitude for Eva Oburger to welcome me within The Terrestrial Ecosystem Research group, University of Vienna, Vienna, and the Rhizosphere Ecology and Biogeochemistry group, BOKU, University of Natural Resources and Life Sciences, Tulln. It was really pleasant to work on her sides, between autonomy, trust and guidance. I learnt a lot during this internship! I would also thank warmly Hannès Schmidt, to welcome in his project and the pleasant collaboration during the first part of this internship. Thanks to them for giving me the opportunity to attend EGU 2017.

I would like to express my grateful thanks to Sergey Borisov, for providing prototypes, fluorescent probes, as well as for his expertise on the manufacture of optode and enlightening advice.

Of course, many thanks to Christina, without whom I could not have completed the experiments. And to your dad too... magic black box!!! No need to fix black curtains to windows anymore, and work in a black room, with a headlamp. Two intense months, but always in a good mood, even when the experiment were going wrong. I wish you every success for your PhD thesis.

I thank the colleagues of both teams, for their welcome, kindness and help. Especially to Daniel for his help for soil preparation and Veronika, always available and helpful. And also to Christoph, who kindly shared his knowledge about optodes and DGT. I also thank the students of the two labs, between barbecue evenings (even in winter!) and snowshoe expedition. Great time!

This course at CNAM and especially this internship would not have been possible without the support of Jean-Luc Chotte and Philippe Hinsinger. I would address my grateful thanks for allowing me to leave the team and do this internship. I particularly thank Philippe for proposing me to work on optode six years ago. It was completely new, and so, very exciting. Even if, we met a lot of setback, I got the virus, and I discovered the fascinating world of roots. Thanks a lot for having trusted me since the beginning of the EiCnam adventure, for

having followed my internship, taken time to answer my questions, and corrected this manuscript. It helped me to improve and progress during this internship. I thank INRA for having financially supported this course. Thanks to Farid and Candie for their essential administrative assistance. To all the Eco&Sols colleagues who supported me during all these years of CNAM, a big thank you! With a special thanks to Agnès and Claire, for your useful advices and warm talks. A special thought for Céline, and our optode team in Brazil… for sure optodes will go in-depth!

I also thank Marie-Christine Morel, for the help and support during the Paris step of the CNAM course, and for her constructive advice during the internship. The CNAM in Paris was not so easy, but the teaching by distance was most of the time very good. Thanks to all the analytical chemistry team.

Thank to my family for having always supported and encouraged me in this course and to my friends, for their support throughout this marathon. And finally, to the one who showed an unfailing support during this long road. Sometimes, you probably have wondered why I spent so many evenings in course and so many week-ends to study… It is a little bit crazy, isn't it? Yes, the CNAM is quite a venture!

"Argue for your limitations and you get to keep them". E. Gilbert

Abbreviations

CCD	Charge Coupled Device
CMOS	Complementary Metal Oxide Semiconductor
DClFODA	2’,7’-dichloro-5(6)-N-octadecyl-carboxamidofluorescein
DGT	Diffusive Gradients in Thin film
DSLR	Digital Single-Lens Reflex
FOCS	Fiber-Optic Chemical Sensor
HO	High pH Optode
HPTS	8-hydroxypyrene-1,3,6-trisulfonate
d-HPTS	lipophilic 8-hydroxypyrene-1,3,6-trisulfonate
LA-ICP-MS	Laser Ablation Inductively Coupled Plasma Mass Spectrometry
LED	Light Emitting Diodes
LO	Low-pH Optode
MWHC	Maximum Water Holding Capacity
MY	Macrolex Yellow
OxO	Oxygen Optode
PBS	Phosphate Buffered Saline
PtOEP	Platinum (II)-octaethylporphyrin
PtTFPP	Platinum (II)-tetra(pentafluorophenyl) porphyrin
RGB	Red Green Blue
ROI	Region Of Interest
ROL	Radial Oxygen Loss
RSD	Relative Standard Deviation
SD	Standard Deviation
SE	Standard Error
t-DLR	time-domain Dual Lifetime Referencing
Ru-ddp	Ruthenium (II)-tris-4,7-diphenyl-1,10-phenantroline

Figures index

Table index

Table of contents

General introduction

Soil is a highly complex matrix at the interface between atmosphere, biosphere, lithosphere and hydrosphere. It is a natural resource essential for sustaining human societies as it plays a central role in providing food, clean water and clean air. In soil, complex biogeochemical interactions drive key ecosystem functions such as plant productivity, regulation of greenhouse gas emissions, filtering and buffering of nutrients and contaminants [1]. Soil physical, chemical and biological heterogeneities induce spatial and temporal variabilities from the nanometre scale to the landscape scale [2]. Elucidating theses spatial and temporal dynamics at a fine scale is essential to better understand the interaction between inorganic and organic particles, roots, fungi and microorganisms in soil. However, accurate investigations of these dynamics require non-invasive approaches at the microscale avoiding disturbance of soil processes.

Planar optodes combine advantages of non-invasive and reversible methods. Based on the reversible changes of luminescence properties of a fluorescent probe, it allows the imaging of pH, O_2 and CO_2 at sub-mm scale, at high spatial and temporal resolution. Two decades ago, planar optodes were first applied in marine sediment to monitor oxygen gradients at the water-sediment interface *in situ* [3]. Ten years later, planar optodes were first applied to image spatio-temporal pH dynamics in rhizosphere of plant species growing under waterlogged conditions [4]. This has opened new possibilities to obtain information of pH and O_2 gradients in soil systems in a non-invasive way and to study rhizosphere processes at the microscale. Oxygen and pH constitute the main parameters reflecting biogeochemical activities in soil, especially interactions between roots and soil [5]. Nonetheless, planar optode application in soil is still challenging. Soil is a highly heterogeneous system with complex physical and chemical properties. Optodes therefore have to be adapted to the specific environmental conditions [6].

This work presents the development and adaptation of oxygen and pH optodes for application in soil environments. In addition to the extensive developmental work, two distinct soil application studies were carried out. In the first one, oxygen dynamics in the rhizosphere of paddy field rice were monitored to reveal oxygen hotspots due to a radial loss of oxygen around roots in anoxic environment. In the second soil application study, pH optodes suitable for both, neutral and alkaline pH range, were applied to assess pH changes

around metallic tungsten sources in soils. The heavy metal tungsten is considered a green alternative to lead, however, little is known about the pH dependent solubility and therefore bioavailability of tungsten in soil environments.

The objectives were therefore (1) to design reliable optodes recipes to monitor oxygen and pH gradients in soil that are applicable in a laboratory not specialized in sensor chemistry, (2) to adapt optode construction and deployment for specific soil as well as soil-root interface applications, (3) to conduct two case studies using the improved planar optode setups.
Development and application work was conducted in the laboratories of two research groups in Austria 40 km apart: The Terrestrial Ecosystem Research group, University of Vienna, Vienna, and the Rhizosphere Ecology and Biogeochemistry group, BOKU, University of Natural Resources and Life Sciences, Tulln. The work related to oxygen optodes was carried out mostly in Vienna, whereas development and application of pH optodes were done in the laboratories in Tulln.

The manuscript is divided in three chapters. Chapter 1 will be dedicated to a description of optode technology, focusing on oxygen and pH planar optodes. It will also present the scientific context of optode application in soils. Furthermore, it will include a critical overview of the current state of the art of optode applications in soil, addressing potentials, limitations and possible improvements. General information about important soil biogeochemical processes will also be presented. Chapter 2 will focus on the practical work, describing the conducted oxygen and pH optode development process followed by specific adaptations for soil and rhizosphere applications. Finally, the third chapter will present the two application projects

Chapter I

State of the art and context

1. What is an optode?

1.1. Principles and generality

1.1.1. Definition

An optode (from the greek *optós* visible or optical and *odós* way*)* is an optical and chemical sensor. As defined by Cambridge [7], a chemical sensor is "*a miniaturized analytical device which can deliver real-time, online information on the presence of specific compounds or ions in complex samples".* Optodes have been developed since 1980s with the emergence of opto-electronics devices, such as low-cost miniaturized light sources and high quality fiber-optics, as it met the needs of biomedical and industrial of real-time and continuous monitoring.

An optode can be describe as two connected platforms: (1) the sensing platform or transducer, in contact with the analyte of interest and (2) the signal processing platform that detects and records the optical signal related to the analyte concentration. Figure 1 features the schemes of an optode. The sensing platform is the chemical part of the sensor. It interacts with the analyte of interest by changing the optical properties of the sensors. Then, the signal processing platform records the change of optical properties.

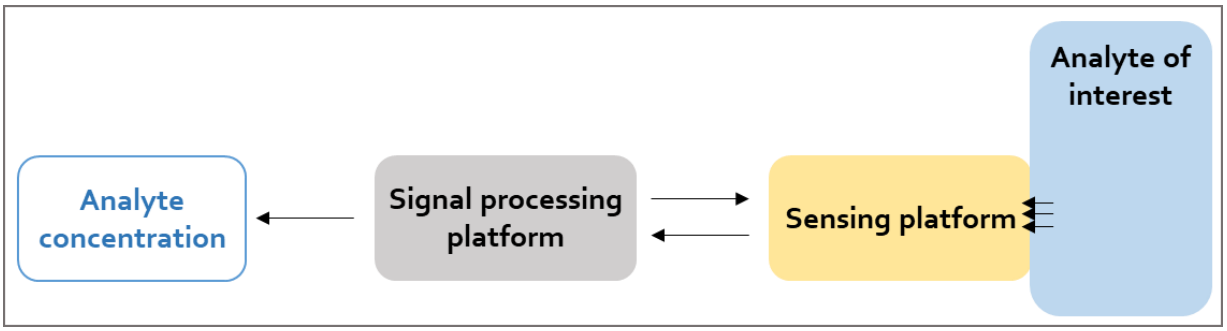

Figure 1: Schemes of an optical and chemical sensor (adapted from Wencel, 2014 [6])

Most optical chemical sensors are based on changes of absorption and fluorescence properties [6]. The optical sensing platforms include optical fibers and planar platforms that record and transduce optical signals emitted by the chemical sensor into data related to the concentration of analyte. Fiber-optics and planar platforms differ by their geometry and the format of output data. Fiber-optic records signal from the chemical sensor in one point whereas planar platform gives a data matrix with a spatial dimension (Figure 2). Consequently, fiber-optic can be defined as a 1-D optical platform and planar platform as a 2-D one. Optode sensors using planar platform are called planar optode and are associated with an imaging optical system.

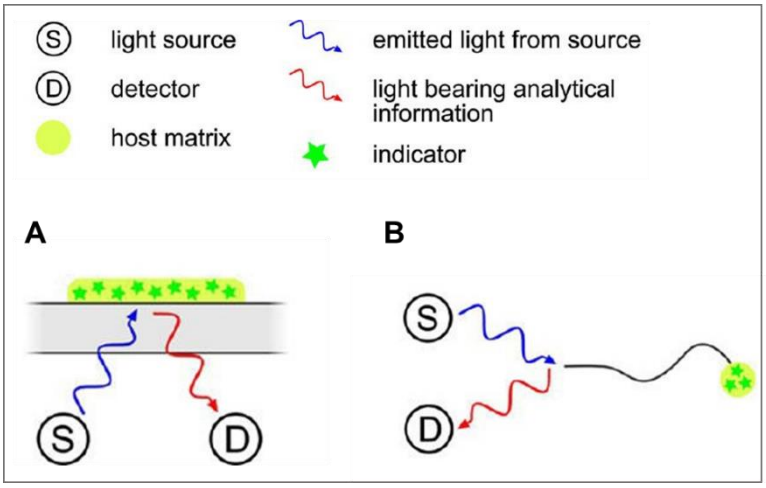

Figure 2: Schematic representation of planar platform (A) and fiber-optic sensor (B). (Adapted from Wencel, 2014 [6]).

One typical fiber-optic chemical sensor (FOCS) is a doped cladding system with the coating of the chemical sensing platform at the tip. Contrast to the planar platforms, it cannot be used for non-invasive measurement as the chemical sensing part is integrated to the optical platform. These widely used FOCS are beyond the scope of this document, as we focus on 2-D optical platform giving a spatial information.

Optodes have numerous advantages. They are easy to handle and often reach higher sensitivity than electrochemical sensors. Moreover, remote systems allow non-invasive and multi-analyte measurements [8].

While optical chemical sensor is a very wide topic, this review will focus on planar optode based on fluorescence transduction and summarize the principles of luminescence-based optode (sensing schemes), optical platforms and the chemical part of the optode. Analytes of interest and application areas will also be presented.

1.1.2. Sensing schemes of luminescence-based optode

Luminescence based optodes use the change in optical properties of a luminescent probe when interacting with the analyte of interest. Luminescence is the light emission of a molecule occurring from excited states due to photon absorption [9]. This process is described by the Jablonski diagram, as presented in Figure 3. When absorbing light, a fluorophore, in electronically fundamental state S_0, is excited to a higher electronic state S_1 or S_2. A fluorophore in S_2 state relaxes quickly to the excited state S_1 by internal conversion. Then, to return to the ground state S_0, the fluorophore can follow two ways. The first one is de-excitation by light

emission, called fluorescence. The relaxation occurs in the nanosecond range. The second one is the intersystem crossing with a conversion from the singlet state S_1 to a triplet electronic state T_1. Then, there is relaxation to the ground state S_0 by light emission called phosphorescence occurring at a longer time (millisecond).

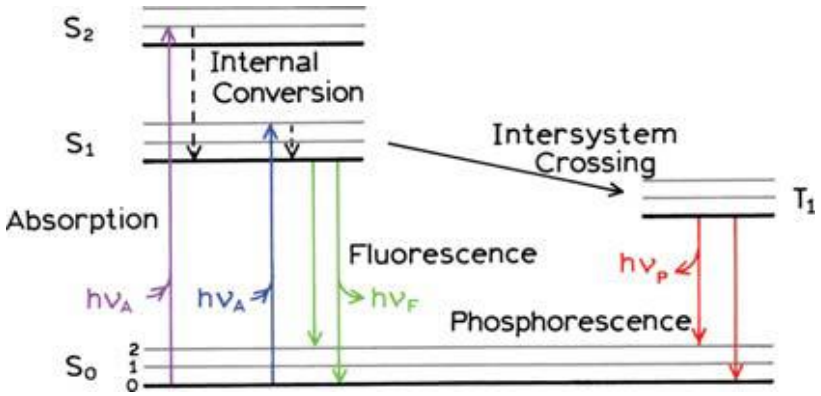

Figure 3: A typical Jablonski diagram (from Lakowicz, 2006 [9])

Luminescence properties of a probe can be described by two parameters: luminescence intensity and decay-time of luminescence. The choice of the parameters will define the chemical construction of the optode as well as the optical sensing platform.

- *Fluorescence intensity*

The measure of fluorescence intensity under continuous light-excitation is the easiest method to perform optode measurements. However, fluorescence intensity is not only dependent on the concentration of the fluorophore as described by Parker's law:

$$I = I_0 . \varepsilon . C . l . Q . k \quad (1)$$

Where $\boldsymbol{I}$ is the intensity of luminescence, $\boldsymbol{I_0}$ the intensity of the light source, $\boldsymbol{\varepsilon}$ the molar absorption coefficient ($L.mol^{-1}.cm^{-1}$), $\boldsymbol{C}$ the concentration of fluorophore ($mol.L^{-1}$), $\boldsymbol{l}$ the length of the penetrated layer or thickness (cm), $\boldsymbol{Q}$ the quantum yield of the fluorophore and $\boldsymbol{k}$ a coefficient related to the geometry of the optical set-up.

Fluorescence intensity is also affected by the disturbance of the light source, ambient light, inhomogeneity of probe distribution and thickness of the sensor, as well as background luminescence. Also, leaching of the probe or photobleaching will decrease the fluorescence

intensity. Two methods can overcome these critical drawbacks of fluorescence intensity measurement: (1) Time-resolved fluorescence, (2) Ratiometric measurements [10].

Time resolved fluorimetry is the measurement of the fluorescence intensity at a certain time interval after excitation by a short light pulse. This method can only be applied with a long-decay time probe. It enables to background fluorescent to be suppressed (in the case of short-decay time signal), but does not eliminates heterogeneity of excitation light, artefacts from ambient light, probes inhomogeneity or probes leaching [8].

Ratiometric approach is more widely used and based on the fluorescence intensity measurement at dual excitation wavelengths and/or dual emission wavelengths. Two approaches can be used. The first approach relies on the excitation and/or emission wavelength shift when the sensitive dye reacts with the analyte. For example, 8-hydroxypyrene-1,3,6-trisulfonate (HPTS) pH sensitive probe exhibits a pH-dependent shift of its absorption band. As result, HPTS excitation spectra present two separated fluorescence peaks at 428 nm and 505 nm for the acidic and basic form of HPTS. The ratiometric approach can thus be applied by measuring the fluorescence emission at 540 nm at both excitation wavelength [11]. The second approach consist of combining an inert fluorophore with the sensitive probe and measure fluorescence intensity of both probes. The fluorescence of the inert fluorophore acts as reference signal. To provide sufficient signal sensitivity, the sensitive and non-sensitive dye have to present a sufficient Stokes shift to discriminate reference signal from analyte dependent signal. The ratiometric approach overcomes some disadvantages of intensity measurement, such as the drift of the light source, sensor thickness heterogeneity or inhomogeneity of the fluorophore distribution in the sensor layer (to some extent). Combination of two probes might be prone to drifts due to photobleaching or probe leaching as both probes may have different physical and chemical properties. The intensity ratiometric approach is mainly combined with an imaging sensing platform, particularly, the combination of sensitive and non-sensitive dyes combined with digital camera as reported for few years [12].

- *Fluorescence decay time*

The decay time or lifetime of a fluorescent probe is unique and independent on wavelength emission. It is defined as the time available for a fluorophore to get information about its

emission, or the time to decay from the excited state S_1 to the ground state S_0 with light emission [9]. Fluorescence lifetime-based measurement aims to record lifetime of excited state of the fluorophore after a short pulse of light. This approach is classified by two domains: the time-domain and the frequency-domain [9].

Lifetime measurement is superior to intensity measurement as it is not affected by the concentration of fluorophore and it is independent of wavelength dependant interferences [13]. However, it requires a highly sensitive and fast gateable optical set-up to record signals in the 10^{-6}s time range. Optical set-ups are fiber-optic or expensive CCD (Charge Coupled Device) camera.

To overcome the complexity of lifetime measurement, especially with short decay time fluorophore, a referenced time domain method was developed by Liebsch, called time-domain Dual Lifetime Referencing (t-DLR) [13]. A short-lived sensitive probe and a long-lived reference probe are excited by a short pulse of light. Images are taken at two different times: the first one during the short pulse, the second when the excitation light is off. The first image records intensity from the sensitive probe and the reference probe. The second image records the signal during the decay time of the long-lived reference probe.

1.1.3. Chemical part

The sensing platform is built of three parts: the support layer, the sensor layer and a supplementary layer as described in the Figure 4.

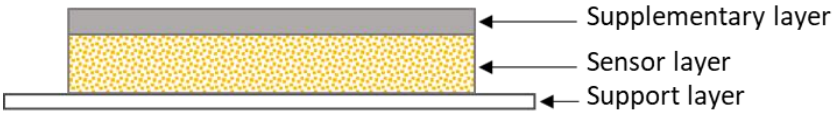

Figure 4: Schematic cross-section of planar optode (not to scale)

The **support layer** is designed to make the optode easy to handle. It has to be optically transparent, chemically compatible and inert with the sensor layer. The most common support material is transparent polyester foil [12]. It also possible to use glass or Perspex support [14], or even to spray sensor directly on to the sample surface [15].

The **sensor layer**, coated onto the support layer, is made of a matrix containing fluorescent probes. Matrix serves as a physical support for the probes immobilization, prevents it from

diffusion into the measurement environment and helps to achieve a homogenous distribution of the probes. Also, matrix properties play an important role for the diffusion of the analyte towards the probes and therefore can define the sensitivity of the sensor [16]. The most common material is a polymer class matrix covering among others, like polystyrene [17] and polyvinyl-alcohol [18], cellulose acetate [19], ethyl cellulose [20] and hydrogels (e.g. polyurethane) [21]. Recently, sol-gel based materials were also introduced as they present better optical transparency and can be tuned for specific chemical and physical properties [22]. Fluorescent probes are immobilized in the matrix in three mains ways: adsorption, covalent binding and entrapment. Adsorption method is the least reliable as the probe can easily leach out. Covalent binding is a complex process, time consuming and needs appropriate materials. This method is very reliable and eliminates probes leaching issues. However, covalent binding may cause a change of optical properties of the dye and therefore reduce the sensor performance [6]. Entrapment is the easiest one and it is a fast method. It is also the method used most widely, especially for teams that do not specialize in sensor chemistry. However, slow leaching of probes can occur over time. Additives can also be included in the sensor matrix to improve performance of the sensor. A typical one is scattering particles as SiO_2 and TiO_2 to enhance excitation efficiency by a multiple light scattering in the sensor layer [23].

On top of the sensor layer, a **supplementary layer** can be coated to protect from interfering sample fluorescence. This layer act as an optical insulation. It has to be permeable to the analyte and requires good adhesion properties to the sensor layer. Optical insulation may result in an increase of the sensor time response due to a longer path between the sample and the probe immobilized in the matrix. Polymer layers such as hydrogel in which carbon black is entrapped and coated on to the sensor layer are most frequently used as supplementary layer [24]. White membranes applied between the optode and the sample were also reported [25].

1.1.4. Optical part

The signal processing platform aims to measure luminescence properties emitted by the sensing part. It requires a light source and a photodetector that records light emitted by the optode.

Excitation light is delivered by a light source such as Xenon lamps [18] or LEDs (light emitting diodes) [21]. As LEDs are low-cost light source and exhibit interesting spectral properties with narrow spectral band, they are more currently encountered in optode measurement set-ups.

Photodetectors record light emitted by the sensor. In the case of planar optodes, imaging set-up use CCD (Charge Coupled Device) or CMOS (Complementary Metal Oxide Semiconductor) cameras. Lifetime measurements are performed with high expensive CCD cameras as they require a very fast shutter to be able to record signal at a short time interval [13]. CMOS cameras are preferred for intensity measurement. Recently, low-cost imaging system has appeared with commercial digital DSLR (Digital Single-Lens Reflex) cameras [18]. These colour cameras provide red, green and blue signals for each pixel (RGB approach) due to its Bayer filters (Figure 5). Depending on spectral properties of fluorophore probes, each individual channel can be used for ratiometric measurements. Thus, it is possible to combine up to three indicators with discriminated emission wavelengths allowing a dual sensing [26].

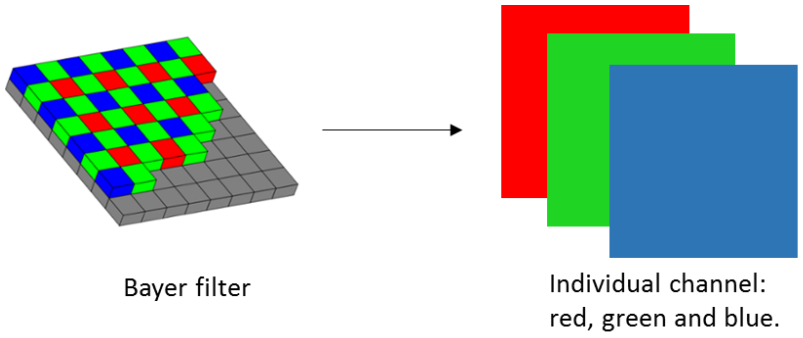

Figure 5: Bayer filter with Red, Green and Blue channels

It has been shown that the RGB approach presented a reduced spatial standard deviation and a higher signal-to-noise ratio compared to black/white CCD camera [27]. CMOS camera is therefore an affordable system (<1000€), very easy to handle, portable, and can be used with or without optical filters. However, digital cameras do not protect from excitation light inhomogeneity or dye photobleaching. Even if lifetime measurements by CCD cameras represent the most accurate system with the best spatial homogeneity, the RGB approach provides a good compromise between robustness and cost. It will therefore be used for the experimental work. Therefore, hue parameter (tint) of DSLR color camera can also be exploited for imaging approach with a better quantification that ratiometric intensity RGB approach as recently reported [28].

1.1.5. Application

Planar optodes are used in a wide range of applications. The first environmental/ecological optode application was carried out on marine sediments to study oxygen profiles at the water-

sediment interface [3]. Since then, numerous studies have been published reporting spatial and temporal dynamics of oxygen and pH profiles in sediments [11,18,29]. Another current application in sediment is the imaging of oxygen in the rhizosphere of plants grown under waterlogged conditions (e.g. paddy field rice) as these plants develop strategies to withstand the anoxic environment and toxic elements [30]. During the past decade, planar optode have been applied to investigate rhizosphere processes in soil under both upland (aerobic) and paddy field (anaerobic) conditions by imaging of O_2, pH and CO_2 gradients around roots from different plant species, like chickpea and wheat and rice [31,32,33]. More recently, optodes were also used in soil to study the impact of oxygen on N_2O emissions in soils amended with manure [34]. Finally, planar optodes are also used for bioprocess monitoring [25] and even in medical application to follow in vivo wound healing [35].

In terms of target analyte, most of optodes are dedicated to oxygen and pH imaging as cited above. Then CO_2 optodes were developed [36]. Other analytes were also explored, like nitrate [37], ammonium [38], ammonia [39], hydrogen sulfide [40], potassium [41]. Optodes can also be applied to monitor physical parameter as temperature [42] or pressure [10]. An optode was also developed to monitor the enzymatic activity of leucine-aminopeptidase [43]. Finally, some optodes were developed for multi-sensing such pH and O_2 dual sensing [44] and even a multilayer optode for simultaneous imaging of O_2, CO_2, pH and temperature [42].

1.2. Oxygen planar optode

1.2.1. Principles

Oxygen optodes are based on the ability of oxygen to quench the fluorescence of many dyes [45]. The oxygen quenching responds to the model of dynamic quenching due to the collision between oxygen and the fluophore. It is described by the Stern-Volmer equation [9]:

$$\frac{I_0}{I} = 1 + k_q \,.\, \tau_0 \,.\, [Q] \tag{2}$$

Where, $\boldsymbol{I_0}$ and $\boldsymbol{I}$ are the fluorescence intensities in the absence and presence of quencher respectively; $\boldsymbol{k_q}$ is the bimolecular quenching constant; $\boldsymbol{\tau_0}$ is the lifetime of the fluorophore in absence of quencher, and **[*Q*]** is the concentration of quencher.

The Stern-Volmer quenching constant is given by:

$$K_{sv} = k_q \,.\, \tau_0 \tag{3}$$

$\boldsymbol{K_{sv}}$ is generally related to the overall quenching efficiency of the oxygen probe. The quenching plot or Stern-Volmer plot is often represented by the ratio $\frac{I_0}{I}$ in function of [Q]. In theory, this plot should be linear. Thus, K_{sv}^{-1} is the concentration of the quencher when half of I_0 is lost. The bimolecular quenching constant k_q reflects the efficiency of the quenching or in other words the accessibility of the fluorophores to the quenchers. Also, as τ_0 influences K_{sv} constant, a probe with a long-lived excited state lifetime is a more efficient fluorescence quencher.

In an optode, the probe is entrapped in a matrix reducing probe accessibility to oxygen. The Stern-Volmer plot of an oxygen optode is not linear and is incurved towards *x* axis (Figure 6).

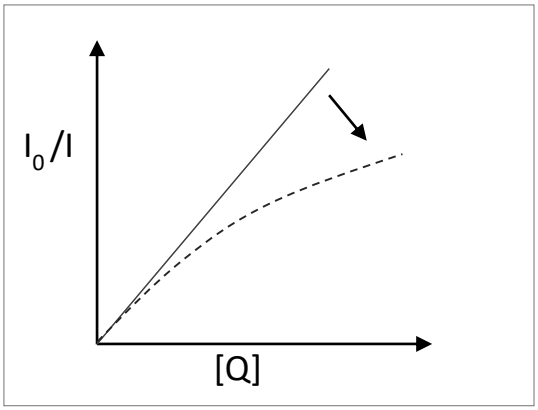

Figure 6: Stern-Volmer plot. Theoretical (solid line) and incurved plot (dotted line).

It is generally described by a modified Stern-Volmer equation [46]:

$$\frac{I_0}{I} = \left(\frac{1-\alpha}{1 + K_{sv} \,.\, [O_2]} + \alpha\right)^{-1} \tag{4}$$

Where $\boldsymbol{I_0}$ and $\boldsymbol{I}$ are the fluorescence intensities in the absence and presence of quencher respectively, $\boldsymbol{K_{sv}}$ is the overall quenching constant, $\boldsymbol{\alpha}$ is the fraction of fluorescence of the probe which is not quenched significantly by oxygen.

Finally, as the collisional quenching is affected by temperature (Figure 7), oxygen optode measurement are cross-sensitive to temperature [47]. It means that oxygen measurements with optodes should be carried out at constant temperature or results have to be corrected.

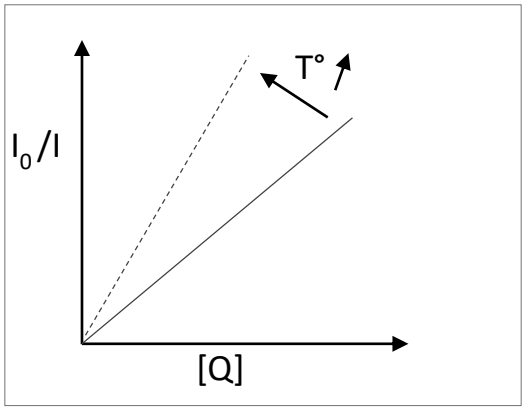

Figure 7: Stern-Volmer plot affected by temperature.

1.2.2. Fluorescent oxygen probes

Oxygen fluorescent probes available are numerous and grouped into several chemical classes. As the subject is very wide and well documented, I will present it briefly and focus especially on dyes most commonly used.

The two main classes of oxygen probes are (i) organic probes and (ii) metal-ligand complexes. Organic probes include polycyclic aromatic hydrocarbons (PAHs) and fullerene. Pyrene based PAH probes are considered as the first generation of oxygen probes [23]. They present a strong luminescence and a good photostability. Fullerene based probes possess also interesting chemical properties like a large conjugate structure resulting in a high sensitivity for oxygen. For example, fullerene C70 was used as for oxygen trace sensor in the ppbv range [48].

The second main class are metal-ligand complexes which are nowadays most commonly used in oxygen sensors. It is a wide class of probes with useful properties such as relatively long lifetime, absorption band in the visible and a large Stokes shift. This class of probes contains transition metal complexes such as ruthenium and iridium complexes, and the large group of porphyrins and metalloporphyrines. Ruthenium complexes, especially ruthenium(II)-tris-4,7-diphenyl-1,10-phenantroline (Ru-ddp) have been widely used as it possesses long-lived emission, from micro-second to millisecond. It has suitable properties for the decay time approach as described by Holst and Frederiksen who applied oxygen planar optodes based on

Ru-ddp with lifetime measurement on the sediment-water interface [49], as well as on the rhizosphere of flooded plant species in sediment [50]. In contrast, iridium complexes possess a short response time, high sensitivity, higher brightness and they are less sensitive to temperature. For example, cyclomateleted iridium(III) coumarin complexe based oxygen sensors present an outstanding brightness and a low cross-sensitivity to temperature. Its spectral properties allow the application of both, the ratiometric or the decay time approach, but its photostability is poor and much lower than that of Ru-ddp [47].

The most frequently used oxygen probes are metalloporphyrin complexes with platinum or palladium. These probes show strong absorption and a high quenching efficiency. Among the large group of metalloporphyrins, fluorinated ones such as platinum(II)-tetra(pentafluorophenyl) porphyrin (PtTFPP) and the non-fluorinated, platinum(II)-octaethylporphirin (PtOEP) are most common [23]. Both have an absorption band in the visible and present a large Stokes shift. PtTFPP is more photostable than PtOEP. It was used during several months in sediments without major shifts [51]. However, PtOEP is highly sensitive to low oxygen concentrations and preferred for oxygen depleted environments as showed by Oguri, with the highest sensitivity in the oxygen concentration range of 0-50 µmol.L^{-1} and a higher brightness than PtTFPP [17]. This study also revealed no shift of the signal during 19 hours of continuously light exposure.

As oxygen probes rely on long lived emission properties insuring high quenching efficiency, oxygen sensors are often combined with the fluorescence decay time approach. However, with the emergence of low cost imaging systems, and the large Stokes shift of some sensor, especially for metalloporphyrin, the ratiometric approach is also available. Larsen proposed an oxygen planar optode made up of PtOEP oxygen probes mixed with the non-sensitive probe Macrolex Yellow, entrapped in polystyrene matrix [12]. PtOEP emits in the red part of the spectrum whereas Macrolex Yellow emits in the green. Measurement are typically carried out with a RGB camera and results are reported based on ratiometric calculations between the intensity recorded by the red and green channel. This simple approach makes the method accessible to non-specialists with significantly lower cost than decay time measurement.

1.3. pH planar optode

1.3.1. Principle

pH optode measurement is based on a difference in optical properties of protonated and deprotonated forms of a weak organic acid. A change of proton concentrations modifies the concentration ratio between acidic and basic form of the pH probe. The fluorescence intensity measured is correlated to this change of equilibrium between protonated and deprotonated form of the pH probes [52]. Thus, optical pH sensors measure the concentration ratio between acidic and basic form of the fluorophore. As for electrochemical pH sensors, pH changes follow the Henderson-Hasselbach equation:

$$pH = pKa + log\frac{[A]}{[AH]} + log\frac{f_A}{f_{AH}} \quad (5)$$

Where $\boldsymbol{pKa}$ is the negative logarithm of the acid dissociation constant, [$\boldsymbol{A}$] and [$\boldsymbol{AH}$] are the concentration of acidic and basic form of the probes, $\boldsymbol{f_A}$ and $\boldsymbol{f_{AH}}$ are the activity coefficient of the acidic and basic form of the probe.

As described by the equation (5), pH value is defined also in terms of activities, meaning that pH optodes are cross sensitive to ionic strength. Figure 8 presents the pH response of a pH sensor based on 8-hydroxy-1,3,6-pyrenetrisulfonic acid (HPTS) in buffer solution with different ionic strengths [18]. The interference varies with the charge of the fluorophore and the ionic strength of the environment.

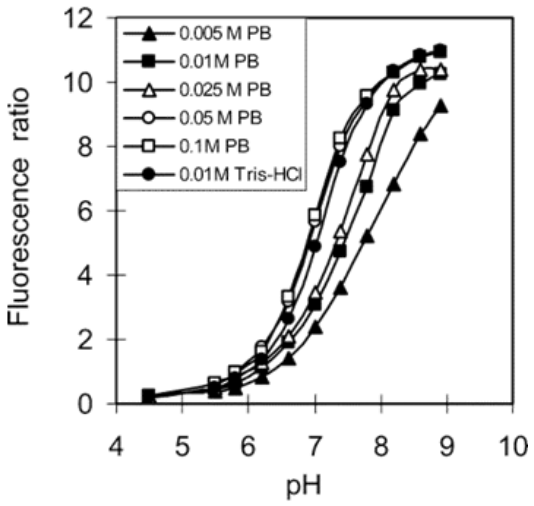

Figure 8: pH sensor response in phosphate buffers with different ionic strengths. (From Zhu, 2005 [18])

Since the changes of fluorescence intensity with pH are described by a sigmoidal relationship, the dynamic pH range is limited to pKa ± 1.5 [6]. In addition, the pKa of the pH probes inserted in a matrix is different and will be called $\boldsymbol{pKa'}$ in the manuscript. Thus, pH dynamic range of a probe can be tuned with the host matrix and methods of immobilization. For example, the pKa' of pH probe 8-Hydroxy-1,3,6-pyrenetrisulfonic acid (HPTS) has found to be at 6.7 in ethyl-cellulose [20], 7.7 in Dowex resin [25], and 7.1 in polyvinyl alcohol [18].

1.3.2. Fluorescent pH probes

HPTS and its derivatives as well as fluorescein based probes are typical pH fluorophores with HPTS based probes being most widely used. It is a great choice for ratiometric approach, as its excitation spectra is pH dependant [11]. The ratiometric approach can be applied at dual excitation wavelength and single emission. Also, as explained above, its dynamic range can be changed with the matrix, from neutral range towards alkaline range. In addition, it exhibits a good photostability. However, HPTS presents high sensitivity to ionic strength [53]. Also, as it is very hydrophilic, HPTS can be chemically modified to render it more lipophilic [54]. Thus, modified HPTS can be entrapped in a matrix and not only covalently bound [12].

The main alternative to HPTS is fluorescein and its derivatives. In contrast to HPTS, it exhibits a low photostability. However, it is less sensitive to ionic strength [55]. A series of chlorofluorescein esters were designed that were lipophilic and can be entrapped in a hydrogel matrix. These fluorescein derivatives probes show a marginal shift of their pKa' with ionic strength changes. Also, depending on the halide substituent added to the fluorescein ester base, the pKa varied from 5.5 to 7.3 allowing different pH dynamic ranges [55]. Moreover, these chlorofluorescein pH probes exhibited higher photostability than the fluorescein chromophore. Another lipophilic and low sensitive to ionic strength fluorescein derivative is carboxyamidofluorescein class designed for marine sediment application [21]. They also presented high quantum yield and pH dynamic range in the alkaline range, from 7.2 to 9.2. However, these probes showed poor stability in light exposure [56]. Finally, a commercial available fluorescein derivative, 5-hexadecanoylaminofluorescein, present also lipophile properties as well as low cross sensitivity to ionic strength. With a pKa' in hydrogel at 6.6, this pH probe was used to study pH dynamics in rhizosphere of lupin combined with intensity based approach [57].

Due to the sigmoid response of pH probes, the dynamic range is limited to 3 pH unit. In consequence, it is not possible to monitor pH across a wide range. This is only possible by mixing two pH probes in the matrix as presented by Weidgans [55]. Two lipophilic fluorescein esters were combined in hydrogel matrix with a dynamic range of pH 4.5 to pH 8.5. Also, a larger dynamic range was proposed by Schreml to investigate pH changes of wound healing in humans *in situ* [58]. Alternative to the combination of two probes, fluorescein-5-isothiocyanate (FITC) pH sensitive probe was covalently bound to aminocellulose particles and mixed to a reference dye in hydrogel matrix. It exhibited reliable pH measurement in a range of pH 3 to 9, and was suitable to detect inflammatory phase within wound healing.

The dynamic range of fluorescent pH probes is usually between 5 and 9. Optodes suitable for acidic environments below pH 5 are rare. One optode for a pH range between 2.5 to 4.5 was developed by PreSens GmbH [59]. In the extreme alkaline pH range, a recent publication described a planar optode for alkaline sediment based on chloro phenyl imino propenyl aniline (CPIPA) with a dynamic range from pH 7.5 to pH 10.5 and a negligible cross sensitivity to ionic strength if below 0.1 mol. L^{-1} [60].

2. Soil and rhizosphere

2.1. Principles and generality

Soil is a highly complex and heterogeneous living environment in the biosphere. It consists of a mineral and organic matrix (such as humus), as well as living organisms (microorganisms (bacteria, fungus) and fauna. This heterogeneous environment is the place of many interactions at fine scales with consequences on soil functioning at landscape scale. In particular, biogeochemical interactions at microscale are of abiotic and biotic origin. Abiotic processes include freezing/thawing as well as drying/wetting and they alter soil structures (aggregates and pores) and redox conditions. Biotic factors involve living roots and rhizodeposition, root turnover, litter fall, fauna activity (burrowing). This factors induced chemical and biological processes such as denitrification/nitrification or carbon mineralisation [61].

One of the main hotspot of biogeochemical activity is the rhizosphere. Defined as the amount of soil around living roots which is influenced by root activity [5], the rhizosphere is the place of intense interactions between soil particles and roots: water and nutrient absorption, anions

and cations exchange, release of organic and inorganic (H^+, OH^-) molecules, and respiration. This exchange between roots and soil modifies the chemical equilibrium around roots potentially changing rhizosphere soil pH and redox conditions. Rhizosphere processes are highly dynamic, both at the temporal and spatial scale. Figure 9 summarizes the main biogeochemical processes in the rhizosphere [62].

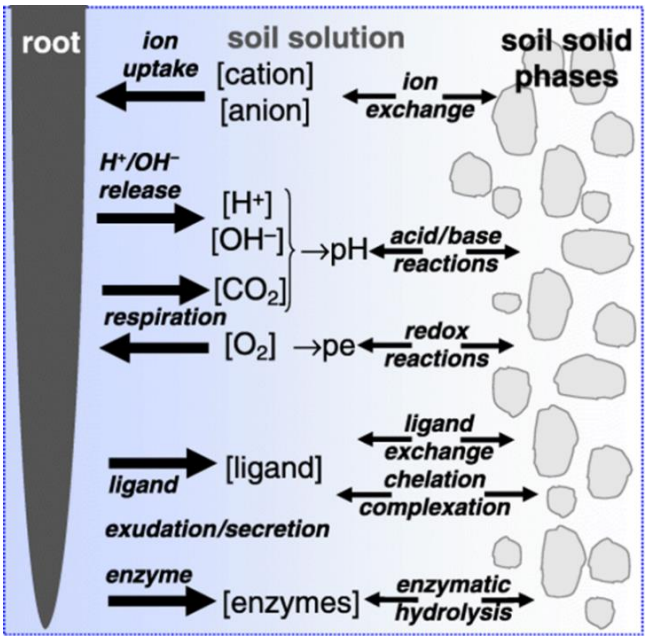

Figure 9: Schematic representation of chemical processes occurring in the rhizosphere. (From Hinsinger, 2005 [60])

Plant-soil interactions induce pH changes in the rhizosphere that affect the bioavaibility of nutrients and toxic elements. The flux of protons and hydroxyls between soil and roots is triggered by many interactions: balance of cation and anion exchange, release of organic root exudates and CO_2 (respiration of roots and rhizosphere microorganisms), and is affected by redox conditions, soil buffering capacity, nutritional constrains [63]. pH is thus of major ecological relevance in roots and soil functioning.

A particular important parameter is oxygen as redox conditions drive lot of chemical reaction in soil. In addition, oxygen is required by the plant for root cell respiration which is of major importance for wetland plant living in anoxic condition. In order to uphold root respiration under flooded conditions, plants developed aerenchyma tissue (gas channel) to transport oxygen from leaves to roots. This oxygen transferred to the rhizosphere by a phenomena called radial oxygen loss, additionally protects roots from toxic element that are highly soluble under reduced conditions (e.g. H_2S) [64].

2.2. Measurement of biogeochemical processes in bulk and rhizosphere soil

Biogeochemical heterogeneity in soils and rhizosphere can be measured by two approaches: destructive and no destructive.

2.2.1. Destructives approaches

Destructives approaches involve sampling of soils and analysis of target analyte after extraction steps. These approaches are subject to international standards such as pH, phosphate or organic carbon measurement in soils. However, these widely used methods have some disadvantages. Firstly, the sampling of particular soil compartments can be very challenging. Indeed, the separation of rhizosphere from bulk soil is highly challenging. As defined above, rhizosphere soil is the amount of soil subject to root-induced activity. However, this influence varies for different elements or parameters of interest [65]. For example, the phosphorus depletion zone around the root is about 3 mm while that of nitrate is about 2 cm as displayed in Figure 10.

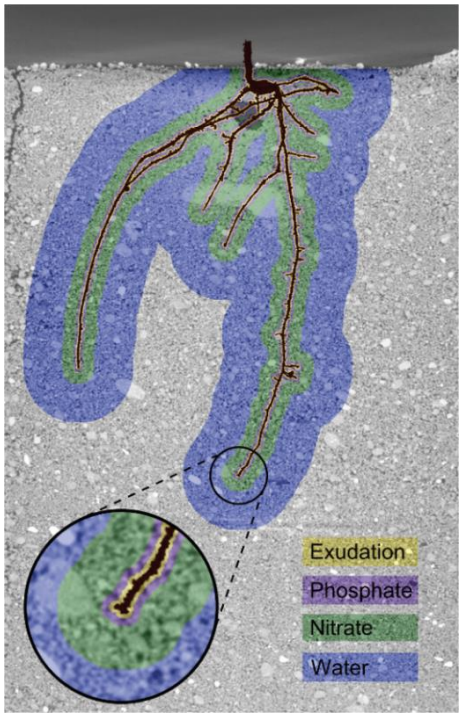

Figure 10: Rhizospheric boundaries regarding to chemical species: exudates accumulation, phosphate, nitrate and water depletion (From York, 2016 [65])

From a practical point of view, it is common to define the rhizosphere soil as the soil adhering to the roots. However, the thickness of this soil layer is highly dependent on soil texture and moisture level, as well as root morphological properties which makes this sampling random and imprecise. Secondly, with sampling being destructive, a temporal analysis of the same plant/

rhizosphere spot is not possible. Destructive spatial analysis at the millimetre scale is also tricky since a sufficient amount of soil (mostly several gram) is needed to carry out the analyses.

2.2.2. Non destructives approaches

Non-destructive approaches aim to measure biogeochemical properties of soils *in situ*. Experimental approaches can be classified into two main categories: (1) invasive methods and (2) non-invasive methods.

The invasive methods include electrodes and microelectrodes, and optical microsensors. Electrodes are based on electrochemical principles and are specific to a target analyte. They are mainly used for pH, gas such as N_2O, CO_2, H_2S et O_2, and ions (e.g. NH_4^+, NO_3^-). Microelectrodes, with a small sensor tip (micrometer scale) have the advantages to allow high spatial measurement with a fast response [66]. However, these tools present some limitations in soils application as the sensor tip can be polluted by organic matter and soil components meaning a drift of the signal overtime. They can also consume a significant amounts of the target analyte. The optical microsensor, also called micro-optode, are based on optical fibers with a luminophore coated at the end tip. They present a fast response time (range of second), a long-term stability, does not consume target analyte and less fragile than microelectrodes. They are mainly used to monitore O_2, H_2S, H_2, N_2O, NO, pH and redox potential [66].

Even if microsensors allow *in situ* measurements over time, the procedure remains invasive and disturbing for the root-soil system. Also, spatial monitoring along roots requires the insertion of many microsensors in the study area. An alternative is the implementation of non-invasive methods providing 2D measurements.

The first non-invasive, 2D chemical imaging method was used to monitor pH in the rhizosphere in 80's. It required the application of an agar gel around the root system containing a pH-sensitive colour indicator [67]. This method was then improved by the use of video densitometry to correlate color change and pH value [68]. Figure 11 presents an image of pH monitoring in the rhizosphere of tobacco in agarose gel containing the pH dye bromocresol purple becoming yellow with pH decrease [5]. While clearly demonstrating the spatial

heterogeneity of root induced pH changes, this method cannot be used in complex system as soil.

Figure 11: Root-induced pH changes in Fe-deficient tobacco. (from Hinsinger et al, 2009) [5]

Davison and Zhang proposed a new approach to measure inorganic species in a non-invasive way called DGT (Diffusive gradients in thin film) [69]. It is based on the exposure of a soil or sediment layer to a diffusive gel acting as a sink for anionic or cationic species. Then, species taken up by the gel are desorbed and analysed. By scanning gels with LA-ICP-MS (Laser Ablation Inductively Coupled Plasma Mass Spectrometry), it has recently been demonstrated that DGT is a suitable tool to mirror solubility gradients of nutrients and/or pollutants in the rhizosphere [70]. Also, enzymatic activity in soil can be mapped by *in situ* (i.e. zymography). Gel (e.g. agarose) with enzymatic substrates are applied to soil surfaces and enzymatic activities are revealed by colorimetric reaction and imaged with a scanner [71]. Both DGT-LA-ICP-MS and zymography are non-invasive and give useful information about heterogeneity of biogeochemical processes in soil. However, as both are based on irreversible interaction, temporal monitoring of the same area of interest is not possible unless a new image device is re-applied at a later stage.

To sum up, invasive methods allow temporal monitoring at high spatial resolution of pH, gas and mineral ionic species, but need many single measurements to get a spatially resolved map. Non-invasive ones are available to spatially map inorganic species and enzymatic activities at a larger area than invasive methods with a single measurement.

To complete this box of *in situ* tools for measuring biogeochemical heterogeneity in soil, planar optodes meet the need of spatial and temporal monitoring in a non-invasive way, and are thus frequently applied to study O_2 and pH dynamics.

2.3. Planar optodes applied to soil and rhizosphere environment

As presented above (section 1.1.5), planar optodes have been first used in sediment environments and are a useful approach to image oxygen distribution in the rhizosphere of flooded plant species or to obtain oxygen profiles in sediments disturbed by fauna. Soils are highly heterogeneous and even more complex than sediments. Planar optodes applied to soil environments has only emerged since the last ten years with the number of publications only slowly increasing.

Blossfeld and Gansert first used planar optodes in soil in 2007, to map pH at soil-root interface of *Juncus effusus L*, a flooded plant species [4]. The experiment was carried out in waterlogged rhizoboxes and planar optodes were fixed on to the inner transparent side. This experiment was conducted with commercially available optodes and an optical fiber as optical set-up (PreSens GmbH). The combination of discrete pH values resulted in a pH map with a 1.5 to 3 mm of spatial resolution, as displayed in Figure 12.

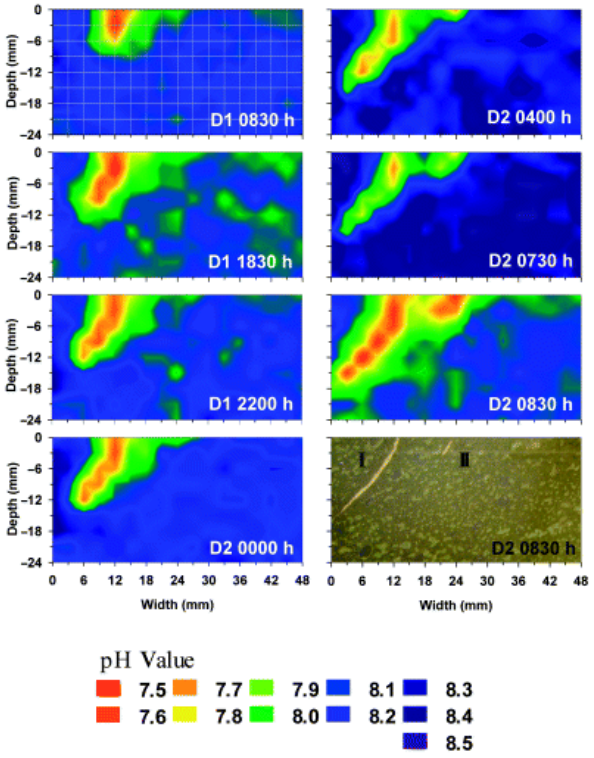

Figure 12: pH dynamics in Juncus effusus during 24h. (from Blossfeld and Gansert, 2007 [4]).

Daily patterns of acidification around roots were observed with a broader and stronger acidification area at daytime. The pH decreased from 8.5 to 7.5 around growing roots and acidification strongly occurred only 30 min after illumination at day 2 (0.5 pH unit). This first experiment demonstrated the great potential of planar optodes to study spatial and temporal dynamics of biogeochemical processes at the soil-root interface.

Investigating rhizosphere oxygen or pH dynamics are the main application of optode in soil. It is also possible to combine pH and oxygen optodes using the same optical detection system. Hybrid sensors allowing dual sensing were first described by Blossfeld, 2011 [31]. Oxygen and pH probes were fixed into polymeric particles and dispersed into a matrix permeable to oxygen and protons/hydroxyl ions. Oxygen concentrations and pH were monitored with fiber-optics based on t-DLR and multifrequency approach (PreSens GmbH). In another study combining O_2 and pH measurements, home-made oxygen and pH optodes were applied simultaneously to the rhizosphere of young maize plants and optode measurements were combined with neutron radiography for water content determination [72]. The experiment was carried out in a thin rhizobox (1.5 cm width) and optodes were applied on each side of the rhizobox. Results highlighted different patterns of pH, oxygen and water content related to type of root. Strong acidification (up to 1 pH unit) was observed around the main roots whereas only a slight acidification occurred around lateral roots, and pH changes were more pronounced under dry conditions. In addition, oxygen profiles revealed a higher oxygen consumption by crown roots than laterals ones. These studies demonstrated the great potential of multi-imaging approaches to inter-relate key processes at soil-root interface.

The works of Blossfeld and Rudolph-Mohr are based on two different approaches. Blossfeld used commercially available optodes and optical system (PreSens GmbH) whereas Rudolph-Mohr proposed home-made optodes combined with a CCD camera. These optodes were made by entrapping an oxygen or pH sensitive fluorescent probe in a polymeric matrix coated onto a transparent polyester foil. CCD camera recorded fluorescence intensity emitted by the planar foil. Successive publications of Rudolph-Mohr and co-authors describing the application of this system show the possibility to use home-made optodes for team not specialised in sensor chemistry. However, except for one study applying pH and O_2 optodes to aerobic soil, experiments were mainly carried out in a quartz-sand mixture, which is much more homogenous than soil [57,72,73,74]. Optode measurements were based on fluorescence

intensity which is the easiest approach but is also the most prone to drifts. Moreover, the optodes used were transparent meaning that roots and sand are visible behind the optode. This may cause fluorescence artefacts especially from roots as they could potentially emit fluorescence. This might be more pronounced in soil than in quartz-sand media due to higher heterogeneity background.

In contrast to Rudolph-Mohr approach, commercially available optodes from PreSens GmbH are non-transparent and consequently fully protect from background light scattering and heterogeneity. In rhizosphere studies, non-transparent optodes are preferable as they allow to monitor roots growing over time and to correlate oxygen and pH dynamics with roots morphology and activity. The study of Blossfeld (2013) highlights the importance of transparency to correctly identify the position of imaged roots [32]. In this study, commercial optodes (PreSens GmbH) were applied to monitor pH dynamics induced by intercropped plants in soil. These studies showed contrasting pH changes in the rhizosphere of chickpea and durum wheat. Figure 13 displays a time series of pH measurement, showing a strong acidification in chickpea rhizosphere and a slight alkalinisation around root of durum wheat.

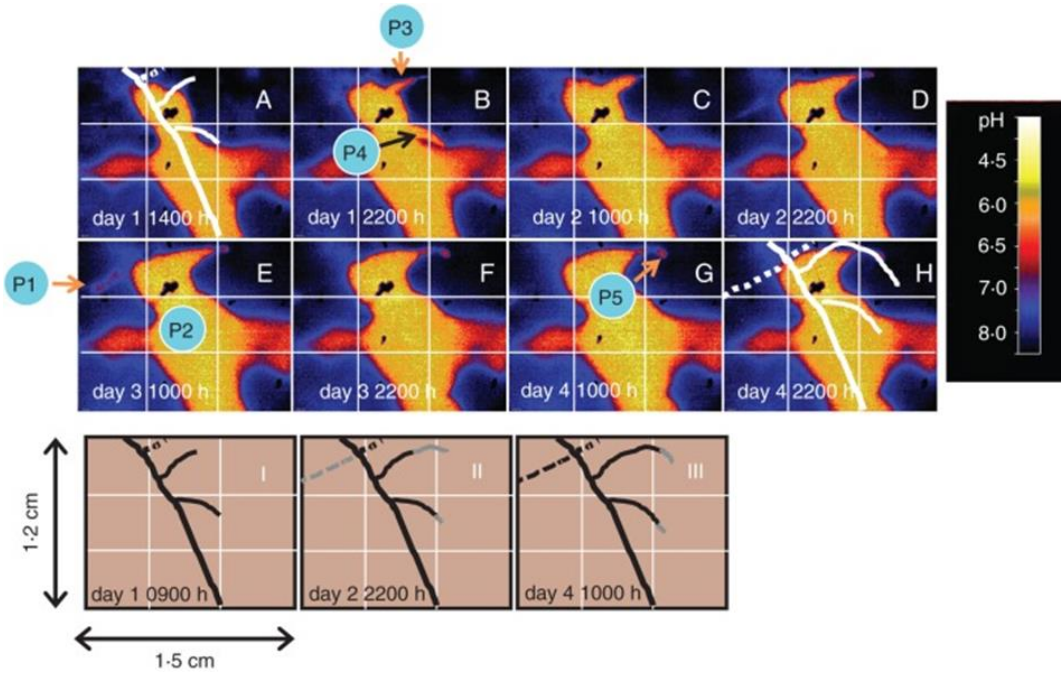

Figure 13: pH spatio-temporal dynamic in the rhizosphere of chickpea and durum wheat in intercropping. Solid lines are chickpea root and dashed lines are wheat root. (from Blossfeld, 2013 [32])

As the planar optode from PreSens are non-transparent, it was not possible to visualize roots growing and structures behind the optode during the experiment. Pictures of area of interest have to be taken before and after optode application, root growth during the application time can only be estimated. In addition, the discrimination between roots in intercropping experiments can be very tricky without any possibility to see roots during experiment. Moreover, this may lead to misinterpretation of the signal. Figure 14 presents a picture of the rhizosphere area imaged by planar optodes and the obtained pH map. It can be observed a cavity resulting in a heterogeneity of the soil structure. The signal measured was not due to roots but due to a water film between the optode and the soil cavity.

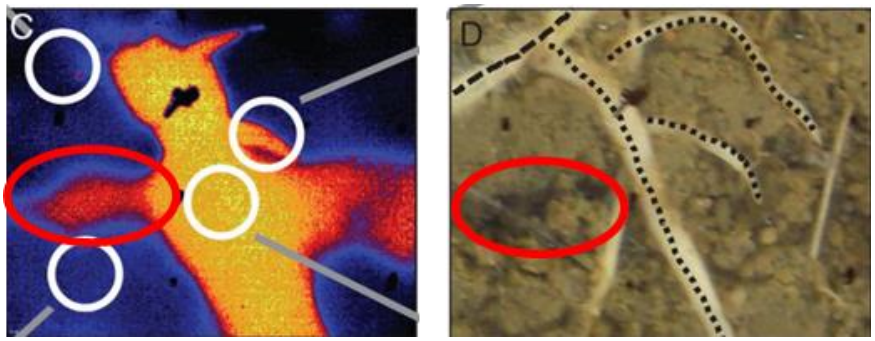

Figure 14: pH signal and soil cavities. pH map of chickpea and wheat rhizosphere (left). Picture of the corresponding rhizosphere area (right). Red circle shows a pH acidification due to soil structure heterogeneity. (from Blossfeld, 2013 [32])

While transparent optodes would facilitate accurate image interpretation, the excitation light will be guided through the optode and the transparent support towards the structure behind the optode. Soil-root environments are highly heterogeneous. Root structures can also emit light and its fluorescence properties can be used to distinguish dead and living roots [75]. Fluorescence emission from the sample can affect the signal emitted by the sensor itself and lead to an erroneous measurement of the concentration of analyte [76]. Optodes used in soil-root environments are either non-transparent, transparent but combined with a non- or semi-transparent membrane that is applied between optode and soil, or transparent without any optical insulation. In the case of spatial and temporal dynamics, which is the main interest of planar optode application in soil, the ability to detect structures behind the optode during the experiment (e.g. roots growth) is very useful and helpful to correlate structures with the dynamics of the target analyte. In one study using optodes to monitor oxygen distribution in soil amended with manure without any plant, a translucent silicone layer was coated on to the sensor layer [77]. The addition of a translucent layer is also used in sediment applications, with black carbon entrapped in the layer to reduce light transmittance of the planar foil [12]. This

key aspect has not been well documented until now. A relevant questions need to be addressed: is it possible to perform measurement with transparent optodes in soil-roots environment?

Imaging temporal dynamics of oxygen and pH requires to leave the optodes in place during the entire experimental period. Most of the applications in soil environment are conducted over a time periods ranging from a few hours to several weeks. Of the 18 publications identified, 12 involved imaging experiments lasting few days, and 6 were long-term experiments lasting up to 8 weeks. About half of the long-term experiments were conducted with a lifetime imaging approach. The others ones used the intensity and ratiometric imaging approach, like reported for most short-term experiments.

Only 5 studies carried out a calibration of applied optodes before and after the experiment. In the 8-weeks experiment conducted by Blossfeld and Gansert, it is noted that calibration curve after 8-weeks presented a small upshift, up to 0.4 pH units below pH 6.5 [4]. Also, in another 8-week optode experiment published by Blossfeld in 2011, dual O_2-pH planar optode was used with lifetime imaging approach [31]. As the optode presented drifts of signal over time, the calibration was performed before and at the end of the experiment. Coefficients were applied to the first calibration to compensate the shifts for each day of measurement. These publications are the only ones to quantitatively evaluate and correct, if necessary, the shift in the optode signal occurring during long-term experiments. More often, an end-calibration is not mentioned. To date, lifetimes of optodes when exposed to soil are poorly documented. Soil can be a tough environment rich in complex organic matter or pollutants with changing redox conditions. In addition, photobleaching and leaching of the probe can occur during long-term experiments. Even though fluorescence lifetime and fluorescence ratiometric measurements are assumed to remove artefacts caused by a variation in excitation light, heterogeneity of probe distribution within the optode, or photobleaching, shifts of the signal can occur over time as reported by Hakonen [29]. The authors proposed a calibration protocol taking account of the drifts over time when monitoring pH in sediment with fluorescence ratiometric approach.

Another aspect of the lifetime of the optode in soil is the incompatibility of the foil with some sample. As observed by Pradier [78], optodes can be irreversibly damaged by the sample and give signals which could be misinterpreted if optodes are not checked afterwards. In this study, optodes were applied on to *Eucalyptus grandis* rhizosphere in acidic soil. Acidification was observed around roots but when optodes were placed in a buffer solution after the experiment, the signal supposedly obtained from roots was still visible on the optode foil (Figure 15). The

optode was irreversibly stained probably by root exudates. This environment was clearly not adapted to optode application and the omission of an optode check at the end of the experiment would have resulted in the documentation of artefacts.

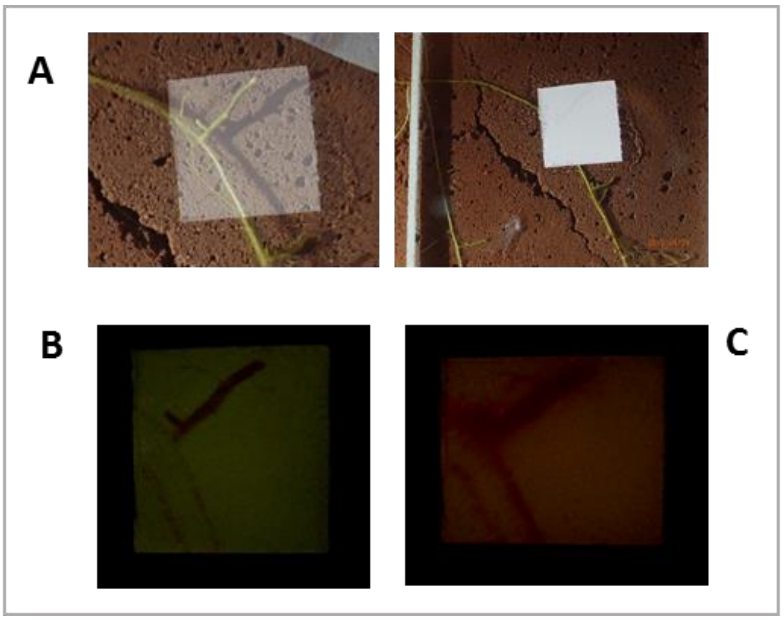

Figure 15: pH optode application on Eucalyptus rhizosphere. (A) Pictures of Eucalyptus roots and applied optode. (B) Optode signal from roots. (C) Optode signal in homogeneous buffer solution afterwards. (Adapted from Pradier, 2016 [78])

In contrast to sediment environments, most of soil studies are not conducted in waterlogged condition. Optodes are applied to rhizobox or transparent tanks. In most experiments, soil water content is fixed and controlled during experiment. A good contact between the sample surface and the sensor foil is a precondition to ensuring reliable diffusion of the analyte through the sensor matrix. Diffusion, especially for pH, also depends on water content. In dry conditions, the contact between soil and optode cannot be ensured and thus limit water diffusion towards the optode. In addition, pH optodes used in soil application are made of a hydrogel matrix which requires water to swell sufficiently for water diffusion through the matrix and react with fluorophore probe. Water content can also be an issue in terms of time response of the optode. Measurements at a water content close to the saturation limit of the soil can reduce the contact problem, but it can also be far from field conditions. This might explain why there are half as many publications that apply pH optodes in soil as there are on the oxygen optode application studies working under waterlogged conditions. In contrast to pH sensors, oxygen optodes can be used in both gas and liquid environment.

The majority optode applications in soil (11 of 18 publications listed) are carried out with custom-made optodes as it is often encountered in sedimentation application too. Planar optode are commercially available for pH, O_2 and CO_2 monitoring (PreSens GmbH) combined with a small USB camera and a dedicated software. These optodes are robust and a commercial system ensures the reliability of optode production and thus sensor homogeneity. However, custom-made optodes have emerged in research teams not specialised on sensor chemistry. The main advantage of a "home-made" optode is the ability to adapt the construction to meet specific needs. Also, the fluorescence ratiometric approach, most commonly used in soil studies, does not require expensive equipment. The most famous example, widely used since then, is presented by Larsen, who developed an oxygen optode and a pH optode based on fluorescence ratiometric RGB approach, coupled to a non-expensive DSLR camera [12]. This publication has opened new possibilities for non-specialist in optode construction, even though it is not trivial to produce reliable optode. Another advantages of the DSLR camera system is the field of view which is much higher than that of USB microscope camera from PreSens (typically 1.5 x 1.2 cm^2). However, this company has recently developed an improved optical setup increasing the field of view to 10 x 10 cm.

Even though several methodological issues in soil applications are still unresolved, optode technology provides interesting insights and is getting more and more used since few years. Optodes were not only used in rhizosphere studies but were also recently applied to soils with organic amendments. These application aimed to monitor temporal and spatial dynamics of oxygen after amendment addition to better understand N cycling and gas emission such as N_2O [34]. In summary, these studies demonstrate that optodes are adapted to study the heterogeneity of complex soil environments at a fine scale (infra millimetre) and help to get more information explaining larger scale phenomena. Finally, recent publications demonstrated the possibility to combine different *in situ* methods, like the combination of planar optodes and DGT to monitor elemental solubility (DGT) together with pH or oxygen concentration at exactly the same location [79].

Based on this context and needs of both research teams, the general objective of this work was to construct reliable oxygen and pH optodes, taking into account specific constraints of soil applications which to date are little documented such as the use of transparent optodes, the effect of soil water content as well as optode lifetime in soil.

Chapter II

Optode development

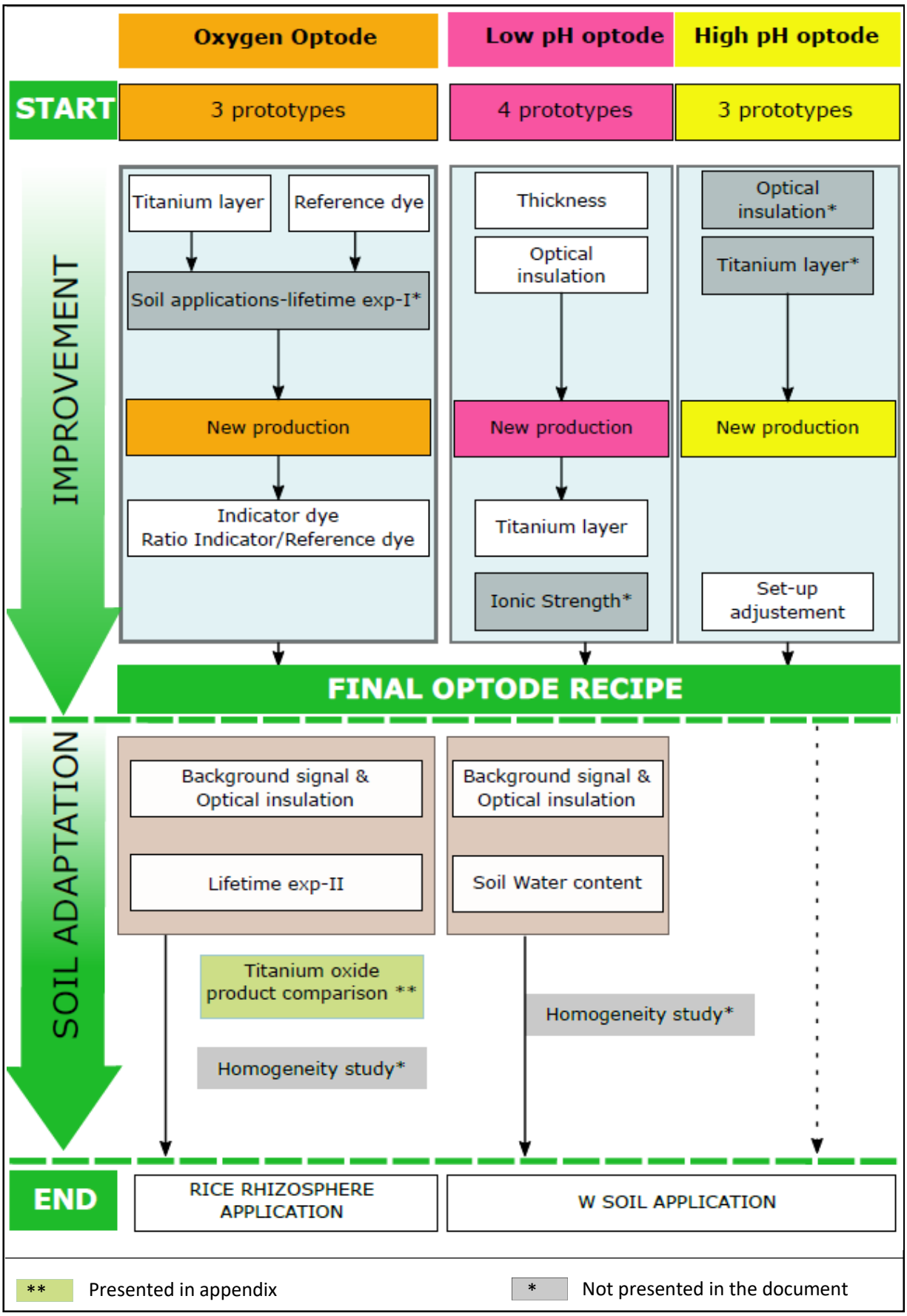

Figure 16: Overview of development work

1. Experimental design

1.1. General experimental plan

The first part of this work was carried out in close collaboration with Sergey Borisov, at the Institute of Analytical Chemistry and Food Chemistry, Graz University of Technology, who is an expert in sensor development. After discussing our aims, he proposed the production of pH and oxygen optodes with different properties in terms of fluorophore dye, brightness enhancement and thickness of the optode. All recipes supplied were in line with previous published work including some modifications [12,33,79]. Several recipes of oxygen and pH optodes were proposed to be tested. The experimental soils of our application project required an optode pH range from pH 5.5 to 8. As we expected pH variations during the experiment, a wider pH range would be preferable. Also, pH indicator dyes generally have a reliable pH response ranging ± 1.5 pH units from the apparent pKa'. Therefore, two pH optodes were studied: a Low pH optode (LO) and a High pH optode (HO), covering a pH range from 5 to 10.

Our main objective was to develop protocols to construct reliable optodes in a lab not specialised in organic chemistry or sensor development. In that context, the first step of my work was to test each sensor foil and improve the recipe if required. Based on obtained results, new optodes were then prepared to suit the needs for our research purpose in soil systems.

The tests of each optode were conducted in solution under standardized conditions. Then, optodes were investigated in soil conditions to specifically study: (i) soil and root auto-fluorescence and background interferences, (ii) optode lifetime in soil and (iii) influence of soil water content.

Figure 16 depicts an overview of the improvements and soil adaptation tests carried out for each optode. Experiments represented as grey squares in the flow chart will not be presented in this document. Experiments in green squares are presented in appendix. Using the first prototypes proposed by Sergey Borisov, tests in solution were carried out. For oxygen optodes (OxO), different reference dyes and brightness enhancements were explored. In parallel, these first prototypes were applied in flooded soil and a long-term experiment was conducted (results were presented in the EGU 2017, Vienna – abstract see appendix 1). Then, three new optode recipes were compared in terms of indicator dye as well as ratio between indicator and reference dye. Once the optode recipe was successfully improved, the optode was tested in soil conditions to study optical insulation and a second optode lifetime study in an anoxic soil system was carried

out. To finalise the optode production protocol, a study of different titanium oxide references was carried out as the reference used during the development part was not commercially available anymore (appendix 2). Consequently, it was important to be able to purchase a suitable new titanium oxide product. However, for consistency, the optodes used in the final application project were produced with the non-purchasable titanium oxide reference used during the development part. Finally, homogeneity of produced optode was studied in solution before project application.

Regarding pH optodes, two factors were first assessed for LO: thickness and optical insulation. Then, the second batch of optodes was produced to study titanium oxide effects and optode properties depending on ionic strength conditions. The soil tests were focused on root and soil reflectance, optical insulation and effects of soil water content. As for OxO, a homogeneity test was carried out before soil application project. Towards the end of the experimental work period, first optode property tests were also carried out for the HO, investigating the application of a titanium oxide layer and the optical set-up.

1.2. Optode foil preparation

Optode foils are composed of three parts, as explained in the diagram below (Figure 17):

- Support foil
- Sensor layer
- Supplemental layers
    - TiO_2 layer
    - Optical insulation layer

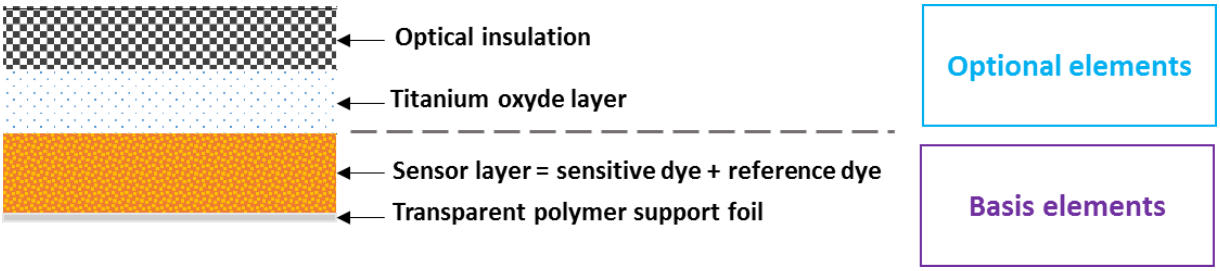

Figure 17: Planar optode scheme

The sensor layer is coated onto the support foil, a transparent 125-µm thick polyester foil (Melinex® 506). It is made of a mix of sensor and reference dye entrapped in a suitable matrix. Up to two supplemental layers were added on top of the sensor layer. The first one was a

titanium oxide layer to enhance the signal emitted by scattering light. The second supplemental layer was an optical insulation layer to avoid roots and soil reflectance and luminescence. Furthermore, it prevents signal interferences from heterogeneous background. This layer was prepared with black carbon entrapped in a polymeric matrix. An external optical insulation, a nylon membrane, was also investigated. Detailed information on chemicals and materials used for optode construction are provided below.

The mix of each individual layer was always freshly prepared and then coated on the support foil with a coating knife (Bar film applicator, BYK) as shown in Figure 18. The thickness of each layer was defined by the choice of the coating knife, 1 mil or 2 mils (1 mil is equivalent to a 25-µm thick wet film). The coating was prepared in a fumehood after a careful cleaning of the bench to remove dust. Also, prior to the coating, pieces of polyester foil were cleaned with ethanol and acetone. The second and third layer were coated once the sensor layer was completely dry. The specific composition details of each optode recipe tested are presented further below. After successful coating, the optode foil was stored in in the dark and protected from dust.

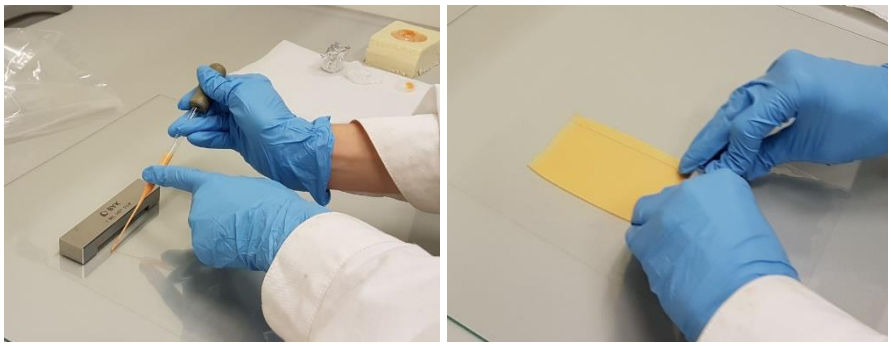

Figure 18: Sensor layer coating

1.2.1. Oxygen sensor preparation

The sensor layer consists of a reference dye and a sensor dye embedded in a polystyrene matrix. Two reference dyes were evaluated: (1) coumarin Macrolex® fluorescent Yellow 10GN (MY), commercially available and (2) Bu_3Coumarin (Bu_3C) produced and supplied by Sergey Borisov [24]. Both fluorescent dyes are non-sensitive to oxygen and are thus used as internal reference in the sensor. These dyes are also used in optodes as light enhancer as they transfer energy to sensitive dye and are therefore often referred to as antenna dye [80]. In addition, two

commonly used oxygen sensitive probes were studied, (1) porphyrin complex platinum(II)-tetrakis-(pentafluorophenyl)-porphyrin (PtTFPP) and (2) platinum(II)-octaethylporphyrin (PtOEP). Indicator dye, reference dye and polystyrene were carefully dissolved in chloroform by mixing with magnetic stirrer for at least 4 hours. The mixing was additionally supported by of repeated ultrasonification for a few minutes in between the stirring procedure.

A supplemental layer made of titanium oxide (TiO_2, UV-Titan P170, Merck) and silicon (Elastosil® E4, Wacker Chemie AG) dissolved in hexane was added to enhance luminescence of sensors for some optodes tests. The incorporation of titanium oxide directly in the sensor layer was also studied. Finally, a black optical insulation was coated. It was composed on black carbon powder (Flammruss, Kremer Pigmente) and silicon dissolved in hexane. The coating on the support foil was achieved with a 1 mil and 2 mils bar knife.

1.2.2. pH sensor preparation

Two pH optodes were investigated to reach our needs: A “Low pH” (LO) optode covering the 5-8 pH range, and a “High pH” (HO) optode with a pH range from 6 to 10.

The LO recipe was slightly adapted from Hoefer and al, 2017 [79]. Optodes with titanium oxide layer and black optical insulation as well as several thicknesses of each layer and a slight difference in terms of quantity of fluorophore were tested. The indicator dye was a derivative of lipophilic fluorescein, 2’,7’-dichloro-5(6)-N-octadecyl-carboxamidofluorescein (DClFODA) produced by Sergey Borisov [54]. This pH indicator dye was used in combination with the fluorophore Ziegelrot (Kremer Pigment) as reference dye. The dyes were mixed together in a 1:10 (w/w) sensitive dye / reference dye ratio and embedded in a hydrophilic urethane-based hydrogel matrix (Hydromed D4, AdvanSources Biomaterials) dissolved in ethanol. The titanium oxide layer was composed of titanium oxide, indicator dye, reference dye and hydrogel matrix. Optical insulation was made up of black carbon powder dissolved in hydrogel matrix. All the components were dissolved with ethanol. Both supplemental layers, i.e. titanium oxide layer and black optical insulation layer, contained also the chemical elements of the sensor layer (indicator and reference dye) to limit possible diffusion of the indicator and reference dye through optode layers. Each mix was coated using either a 1 mil, 2 mils or 3 mils bar knife.

The HO optode was made up of lipophilic 8-hydroxy-1,3,6 pyrenetrisulfonic acid trisodium (HPTS) as pH sensitive dye (modified by Sergey Borisov) [54] and Coumarin Macrolex® fluorescent Yellow 10GN as reference and antenna dye, based on Larsen et al. (2011) [12]. The dyes were mixed with Hydromed D4 matrix dissolved in ethanol. The mix was coated onto a polyester foil with the 1 mil bar knife.

Recipe details are presented together with each step of the development process further below.

1.3. Optical instrumentation

A versatile and non-expensive optical system was chosen as already described by Larsen et al. 2011 [1]. A digital single-lens reflex (DSLR) camera Canon EOS 1000D was used to measure changes in fluorescence emission of the sensor foils. It has an optical resolution of 3888 x 2592 pixels. The infrared filter NIR was removed and the camera was equipped with a macro lens (Sigma 50 mm f2.8 DG Macro). A long-pass emission filter was added to the macro-lens, 530 nm for oxygen sensors and 495 nm for high pH and low pH optodes (Edmund Optics).

The excitation light was provided by a set-up made of 7 blue LEDs with an emission wavelength of 445 nm (Royal-Blue, Luxeon) that was covered by a 475 nm short-pass filter (Edmund Optics). This set-up was used for both types of optodes: oxygen and pH. The camera and excitation light set-up was controlled and synchronized by a custom-made USB trigger LED box (http://imaging.fish-n-chips-de/) and controlled by the software Look@RGB. This controller enables the synchronization of the LEDs and the camera, the automatic image sequencing and recording in a chosen format, as well as light exposure time, focus, and lens aperture.

To capture the fluorescence emission of the sensor foils, three pictures were recorded at ISO speed 100, in RAW CR2 format and averaged automatically by the software. The RAW CR2 picture was split into the three primary colour channel Red (R), Green (G), Blue (B) images and saved individually as RAW TIFF, 12 bit. The size of the recorded RAW TIFF pictures was 1953 x 1301 pixels with a maximum theoretical pixel resolution of 11.4 µm * 11.4 µm. The R, G, B images were used for calculations depending on optode specificity in terms of reference and indicator dyes emission spectra. For example, the oxygen optode is emitting light at 650 nm and around 500 nm based on the properties of the indicator and reference dye respectively. In this case, Red and Green channel will be used to determine oxygen concentration.

Image processing was performed with the free software FiJi, a distribution of ImageJ (https://fiji.sc/). Calibration models were determined by the free software R (https://cran.r-project.org/).

1.4. Experimental procedures

Oxygen and pH optodes were investigated in solution for performance and sensitivity tests and in soil system to investigate different optical insulations and optode lifetime. All experiments were carried out in rhizobox filled either with solution or soil. These containers are commonly used to study rhizosphere process. They are made of a box with a transparent removable front window filled with soil and plants growing in it. Root growth is therefore visible and observable. In our work, the front plate was made of Perspex and fixed to the box with several screws. Despite its many advantages (robust, cheap, easy to clean), Perspex is prone to scratches, especially with soil or rough paper towels. The scratches may appear on the image resulting in artefacts that cannot be removed by image processing. Furthermore, it may scatter light. We used different rhizobox designs adapted to the planned application work. The rhizobox for the pH application project was a small one: 12 cm x 6 cm x 1.8 cm (H x L x l), with a 4-mm thick front plate; for the oxygen optode application project, the rhizobox was much bigger: 25 cm x 25 cm x 7 cm, with a 6-mm thick front plate.

The removable front plate was carefully cleaned with ethanol (technical grade) to avoid any dust when sticking the optode foil. Then, planar optode foils were fixed on the inner side of the front plate with black tape (Scotch® Super 33+) avoiding air bubbles between plate and optode foil. Then, the plate was screwed onto the box (Figure 19).

Figure 19: Rhizobox design with optode taped onto the removable front plate

For oxygen optode tests in solution, the rhizobox was filled with water that was mixed with N_2 gas to adjust oxygen content. Anoxic measurement in solution (0% air saturation) was reached with ascorbic acid (0.1 M) dissolved in a 0.1 M sodium hydroxide solution. The oxygen content was controlled with a dissolved oxygen luminescent probe (LDO 101, Hach Lange GmbH) connected to the multimeter HQ30d (Hach Lange GmbH) that was externally calibrated prior to the experiment. The temperature was kept constant during the calibration.

For the pH optode tests, the rhizobox was filled with buffer solution. Phosphate buffer solutions were prepared for Low-pH optode, from NaH_2PO_4 and Na_2HPO_4. Acid and alkaline stock solution were mixed to reach pH target. For High-pH optodes, TRIS buffer was better adapted to the pH range 6-10. It was prepared from TRIS-HCl and Trisma® base stock solution, mixed together. NaCl was used to match the ionic strength in all buffer solutions to the ionic strength of the individual soils. The pH of each buffer solution was measured prior to optode measurement with a pH meter (pH 730, WTW) and pH electrode (Sentix 41, WTW) externally calibrated with NIST calibration solutions. The pH check of the buffer solutions was made at room temperature according to optode measurement conditions.

The imaging set-up was adapted for each rhizobox design and the distance between camera and rhizobox was kept constant throughout all experiments (Figure 20). The implementation in both laboratories (University of Vienna and BOKU) was carried out based on the set-up conditions initially defined. Thus, experimental conditions were similar in both place.

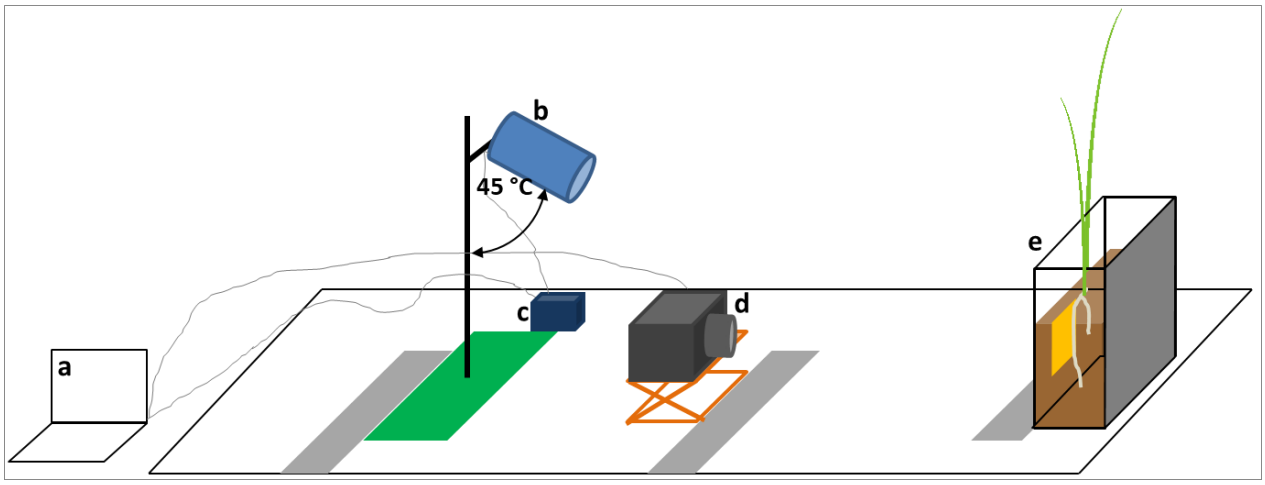

Figure 20: Experimental set-up.(a) computer (b) excitation light device (c) Trigger led box (d) camera (e) rhizobox

All imaging measurements were done in complete darkness to avoid any disturbance due to ambient light. Each measurement sequence started with a so-called “Black picture”. It is an image of the optode obtained without excitation light providing the camera sensor noise at the ambient light condition of the optode experiment. Then, this picture was subtracted from optode images. This procedure reduces the noise level of the optode images due to ambient light and camera sensor age.

Some investigations were conducted in soil conditions, in particular background and lifetime studies. For oxygen optodes, studies in soil were realised with a paddy soil (Italy, Rice Research Institute in Vercelli), in flooded conditions. Regarding pH optodes, soil experiments were conducted with a sandy soil (Siebenlinden, Austria), 2-mm sieved, with water content adjusted within experiment objectives. Soil pH was measured from soil solution obtained after centrifugation of wet soil (80% of maximum water holding capacity MWHC) and ionic strength was calculated from an empirical relation describing the relationship between measured electrical conductivity and ionic strength of soil solution [81].

2. Oxygen sensor (OxO)

2.1. Description and principles

OxO principles was based on intensity ratiometric approach. A combination of a reference dye not sensitive to oxygen and a sensitive dye was used. Two references dyes were compared in this study: Macrolex Yellow 10GN (MY) and a derivative of Coumarin (Bu3Coum). These two dyes belong to the class of Coumarins. They are not sensitive to oxygen. Their optical properties are similar and present an excitation peak around 450 nm and an emission peak around 500 nm [12,24]. The emission light of both reference dyes was dominated by green luminescence and hence recorded on the Green channel of the camera. The sensitive fluorophore dyes were the commonly used and commercially available platinum(II)-metalloporphyrin-based indicators, PtOEP (platinum(II)-2,3,7,8,12,13,17,18-octaethylporphyrin) and PtTFPP (Platinum(II)-5,10,15,20-tetrakis(-2,3,4,5,6-pentafluorophenyl)-porphyrin. In polystyrene matrix, they present excitation peaks around 395 nm/508 nm/540 nm and 383 nm/535 nm and emission peak around 662 nm and 647 nm for PtTPP and PtOEP respectively [23,82]. The luminescence was mainly recorded on the Red channel. The excitation of PtTPP and PtOEP around 508 nm and 535 nm is much less efficient than the excitation with UV excitation light [83]. To overcome this drawback, the reference dye was used as antenna dye as described by Mayr et al [80]. An

antenna collects light and transfers its energy to the acceptor. As there is an overlap between emission spectra of MY and absorption spectra of platinum indicators, MY is used as antenna dye and Pt based dye as acceptor. In that way, the fluorescence signal emitted by the acceptor is enhanced. Also, the capacity of MY to emit light and transfer it to Pt dye is not affected by oxygen concentration and can be used internal reference. With this ratiometric scheme, emission light from MY and Pt dye can be well separated, as we can see in Figure 21. It displays the emission spectra of a typical oxygen sensor with PtOEP as sensitive dye and MY as reference dye.

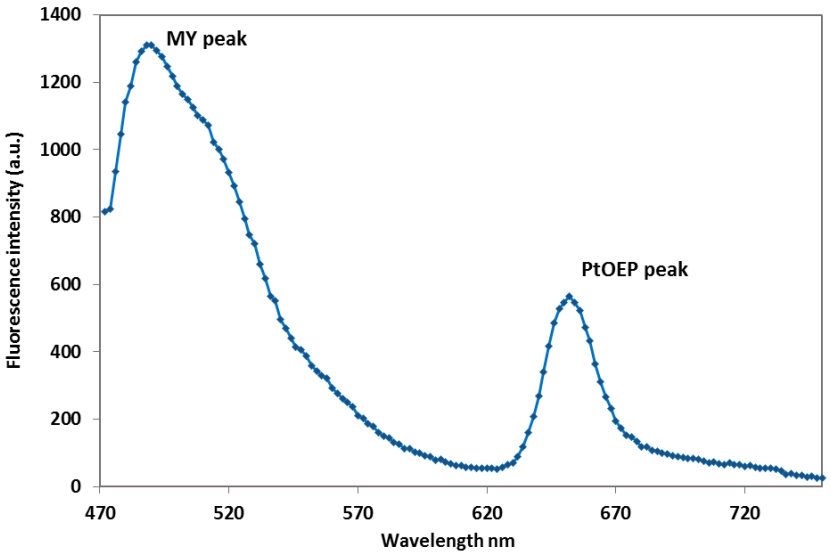

Figure 21: Emission spectra of a typical oxygen sensor (Macrolew Yellow as reference dye and PtOEP as sensitive dye), at 100% of air saturation. Excitation wavelength = 445 nm.

A second way used to improve brightness of the sensor was to add TiO_2 nanoparticles as scattering particles. Acting as scattering light centers, TiO_2 nanoparticles scatter light in many directions in the sensing film, improving the excitation process and increasing emission signals. TiO_2 nanoparticles of 14 nm in size were used in OxO preparation, either directly in the sensor layer or in a supplement layer on top of the sensor layer. The different OxO sensors were investigated in solution. Calibration curves of the optode foils were performed using a standardized procedure as explained above (section 1.4). Data were analysed with ImageJ software including a first step of image correction. So prior to ratio calculation, images from the Red and Green channel were corrected by subtracting the respective Red and Green channel

image of the black picture (i.e. picture taken previously to each measurement series without excitation blue light) as:

$$\boldsymbol{Red = Red(i) - Red(b)} \quad (6)$$

Red(*b*) is the pixel intensity of the red channel from the black picture. **Red*(i)*** is the pixel intensity of red picture of the sample. The black image correction was applied for all calibrations and measurements.

The signal from the indicator dye was mainly recorded in the red channel while the green channel was mainly impacted by the reference dye. As the reference dye is not sensitive to oxygen, it was used as internal reference. The calibration curve was calculated based on the ratio of pixel intensities of the red and green channel.

$$R = \frac{RED}{GREEN} \quad (7)$$

With ***R*** being the pixel intensity ratio, ***Red*** the mean pixel value of the red picture and ***Green*** being the mean pixel value of the green picture.

The oxygen sensor relies on fluorescence quenching of the indicator dye by oxygen and is described with a modified Stern-Volmer equation [46]:

$$\frac{R0}{R} = \left(\frac{1-\alpha}{1+K_{sv}\,.\,C} + \alpha\right)^{-1} \quad (8)$$

where ***R*** is the pixel intensity ratio, ***R0*** the pixel intensity ratio under anoxic condition, **α** the fraction of luminescence signal which is nonquencheable, $\boldsymbol{K_{sv}}$ is the Stern-Volmer constant and $\boldsymbol{C}$ represents the oxygen concentration, expressed in % air saturation.

The oxygen sensor calibration was carried out by taking optode measurements from a solution with O_2 concentrations ranging from 0-100% air saturation. Based on Eq 8, O_2 concentrations were fitted using the equation below:

$$C = \frac{R0 - R}{K_{sv}\,.\,(R - R0.\alpha)} \quad (9)$$

The oxygen sensor development was focused on:

(1) Study of two reference dyes, Macrolex Yellow and Bu3Coum,
(2) Brightness enhancement of the sensor,
(3) Study of two sensitive dyes (PtTFPP and PtOEP) and the ratio between reference and sensitive dyes.

These successive steps, presented in the following pages, led to an improved oxygen sensor recipe that was then applied in the soil adaption studies.

2.2. Reference dye

The objective of this experiment was to test the effect of two different reference dyes on optode sensitivity. The first one is Macrolex Yellow (MY), which is frequently used in optode sensing and commercially available [12]. The second one is Bu3Coumarin (Bu3C), a novel fluorophore dye produced by Sergey Borisov [24]. The Table 1 describes the detailed construction recipe of both optodes.

Table 1: Recipe of optode tested.

	MY		**Bu3C**	
Sensor layer*	Macrolex Yellow	3 mg	Bu3Coumarin	3.4 mg
	PtTFPP	1.5 mg	PtTFPP	1.5 mg
	TiO_2	300 mg	TiO_2	300 mg
	Polystyrene	200 mg	Polystyrene	200 mg
	Chloroform	3 g	Chloroform	3 g
Optical isolation	Carbon graphit spray		Carbon graphit spray	

*Coated with 1mil bar knife.

A calibration curve was performed in water with changing O_2 concentrations as described in section 1.4 and the ratio value R was calculated according to Eq 6 & 7.

Results

Pixel intensity of the red and the green image was plotted and is presented in Figure 22. It describes the luminescence intensity emitted and recorded on the Red and the Green channel

with changes of oxygen concentration. As explained earlier, the Red channel is mainly impacted by sensitive dye (PtTFPP) luminescence whereas the Green channel is dominated by light emitted by the reference dye (Bu3C and MY). Firstly, as expected, both reference dyes were non-sensitive to oxygen content as the signal from the Green channel was almost constant in the green image. Also, the pixel intensity from the Red channel images presented a decreasing signal with increase of oxygen concentration, corresponding to the quenching of PtTFPP by oxygen. A higher intensity for optode with Bu3C was observed, especially in the Green and Red channel at oxygen content ranging from zero up to 50% of air saturation.

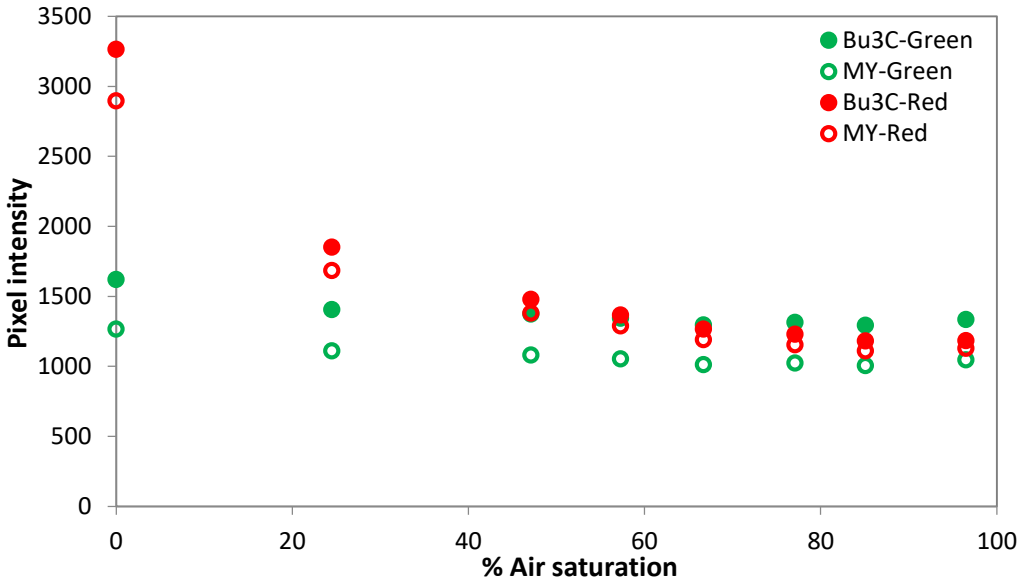

figure 22: Pixel intensity of the red and the green channel of Bu3C and MY optode

The pixel ratio Red/Green (R, Eq 7) was then calculated and plotted against oxygen content, describing the calibration curve of MY and Bu3C optode (Figure 23). Both optodes foils presented a typical calibration curve responding to the modified Stern-Volmer model (R^2>0.999). Another way to describe sensor reactivity for oxygen is to normalize the ratio by the ratio calculated in anoxic condition (R/R0) (Eq 8). It describes the quenching capacity of the sensor or its sensitivity. Displayed in Figure 24, it is called Stern-Volmer plot. The Stern-Volmer plot showed a slightly higher sensitivity of Bu3C optode, with $R0/R_{100}$ = 2.27 compared to that of MY optode with $R0/R_{100}$ = 2.13. The quenching efficiency was a little bit better for Bu3C optode. However, at low oxygen content (< 25% of air saturation), the sensitivity was similar for both optodes. Therefore, the Stern-Volmer constant K_{sv} was estimated at 0.043 and 0.042 for MY and Bu3C respectively.

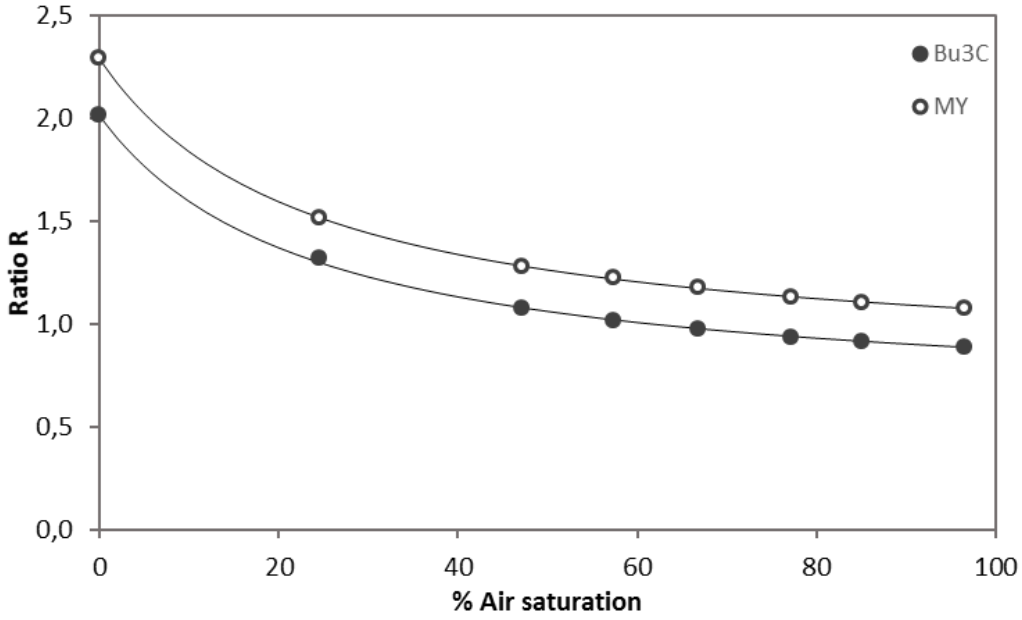

Figure 23: Calibration curve of Bu3C and MY optode. R value is mean pixel values with standard error. Errors bars are smaller than the symbol size (n = 39600 for MY and n = 43400 for Bu3C).

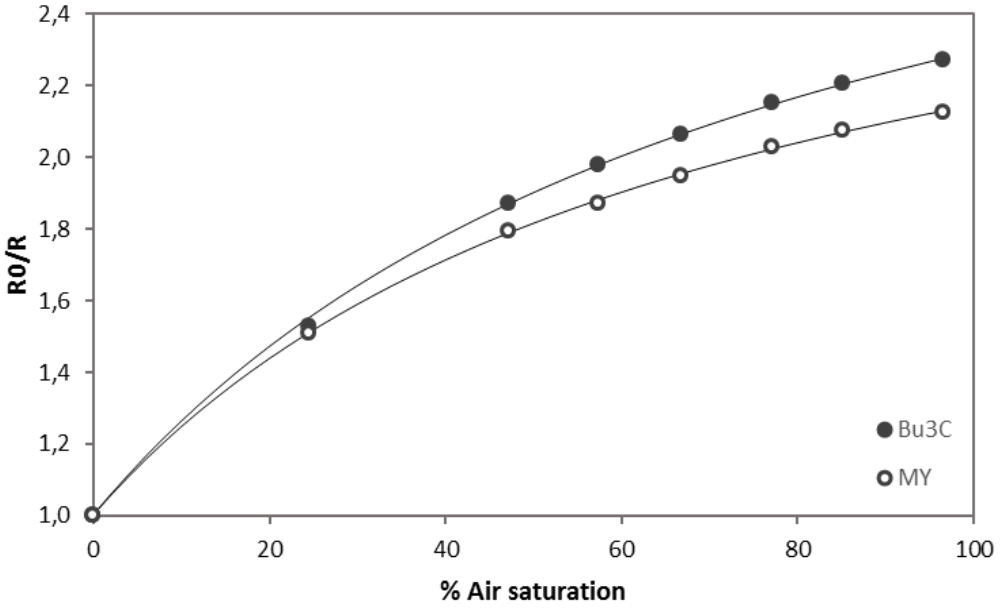

Figure 24: Calibration curve of MY and Bu3 presented as the quenching efficiency against oxygen content. (Calculated from the mean of R and R0 values.)

As the objective is to apply oxygen optode in low oxygen system, Macrolex Yellow will be used for the following of the study. This indicator dye is commercially available and fits well for our purpose.

2.3. Brightness enhancement

One of the relevant criteria in optode development is the brightness of the pictures obtained with the camera. A picture is composed of pixels. Each pixel is defined by the number of bits and the number of grey levels of the pixel. For example, a pixel of an 8-bits image can take 255 grey levels (number of grey level = 2^n-1, with n, the bit number). The pixel values determine the brightness and the darkness of picture areas. A pixel with a value equal to 0 is black whereas a white pixel has a value of 255. The histogram of an image is a plot of pixel values in x-axis versus the number of pixels in y-axis. It displays the brightness of an image.

The data used in optode measurement are the pixel values of the images from the Red and Green channels extracted from the RGB image. The luminescence emitted by the optode foil is recorded by the camera and transformed in pixel value, also called pixel intensity or brightness. When the fluorescence emitted by the dyes increases, more light is recorded in the camera sensor. Consequently, the image will be brighter. When too much light is recorded on the sensor, the image is very bright and the histogram is saturated as presented in Figure 25. At the opposite, when the fluorescence is low, the image is dark.

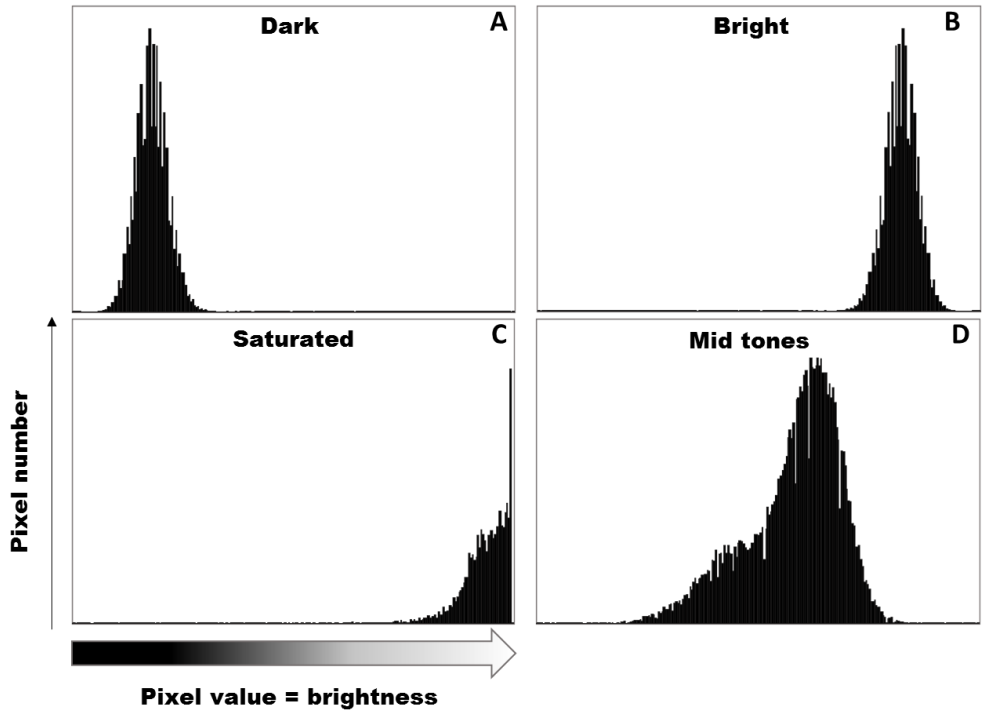

Figure 25: Image histogram. (A) Dark image. (B) Bright image. (C) Clipping image, saturated. (D) Middle tones.

For the oxygen sensor, the fluorescence decreases when oxygen concentration increase. It means that the brightest image is achieved at the lowest oxygen concentration. If the histogram is saturated at low oxygen content, a small change of oxygen concentration will lead to a small change in brightness which will be not discriminated by the camera sensor. The sensitivity is therefore reduced. Consequently, a saturated histogram should be avoided at very low oxygen concentrations. In contrast, a too low brightness at low oxygen concentration will lead to darker images and a poor sensitivity with increase of oxygen concentration.

As platinum-based oxygen indicators emit moderate light under visible light excitation, scattering light particles are used to enhance brightness of the optode. TiO_2 nanoparticles improve the efficiency of fluorophore excitation in scattering the excitation light in many directions in the sensor layer, and so, enhance the emitted signal [84]. Only a few studies presented addition of scattering light particles in optode preparation as TiO2 [84,85]. In these studies, particles were added directly in the sensor layer, mixed with fluorophore dyes and polystyrene. Another possibility was proposed in this work. A supplement TiO_2 layer was coated on top of the sensor layer, creating a white wall behind the sensor layer. To investigate the effect of the different ways to incorporate TiO_2 into the sensor, two different optode recipes were tested (Figure 26). The optode (a) contained a supplement layer made up of TiO_2 mixed with silicon dissolved in hexane. This layer was coated with a 2 mils bar knife on the dry sensor layer. Thus, the sensor layer contains a small amount of titan oxide. The optode (b) was prepared with titan oxide directly added to the sensor layer mix.

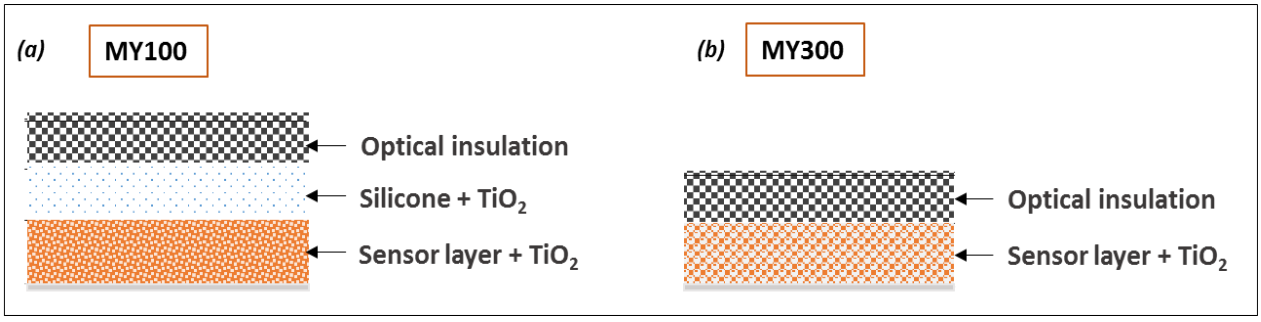

Figure 26: Optode construction with titan oxide. (a) With titan oxide extra layer (b) Titan oxide embedded in the sensor layer

The optodes recipe are presented in Table 2. Optode (a) and (b) are called MY100 and MY300 respectively.

Table 2: Composition of optodes MY100 and MY 300

	MY100 (a)	**MY300 (b)**
Sensor layer	Macrolex Yellow	
	PtTFPP	
	TiO_2 100 mg	***TiO_2 300 mg***
Silicone layer	***TiO_2 250mg***	**-**
Optical isolation	Carbon graphite spray	

Results

First, pixel intensity extracted from Red and Green channel presented in Figure 27 showed an increase of intensity in the Red picture (recorded mainly sensitive dye PtTFPP luminescence) for MY100. The silicone layer with TiO_2, acting as a white wall, strongly enhanced the luminescence emitted in the Red channel. The Green channel (luminescence of MY) was less impacted by this supplement layer. Actually, this could be explained by the role of antenna dye of MY. The energy emitted from MY is accepted by the indicator dye, PtTFPP. Its luminescence might be more harvested with the TiO_2 wall providing a stronger scattering effect.

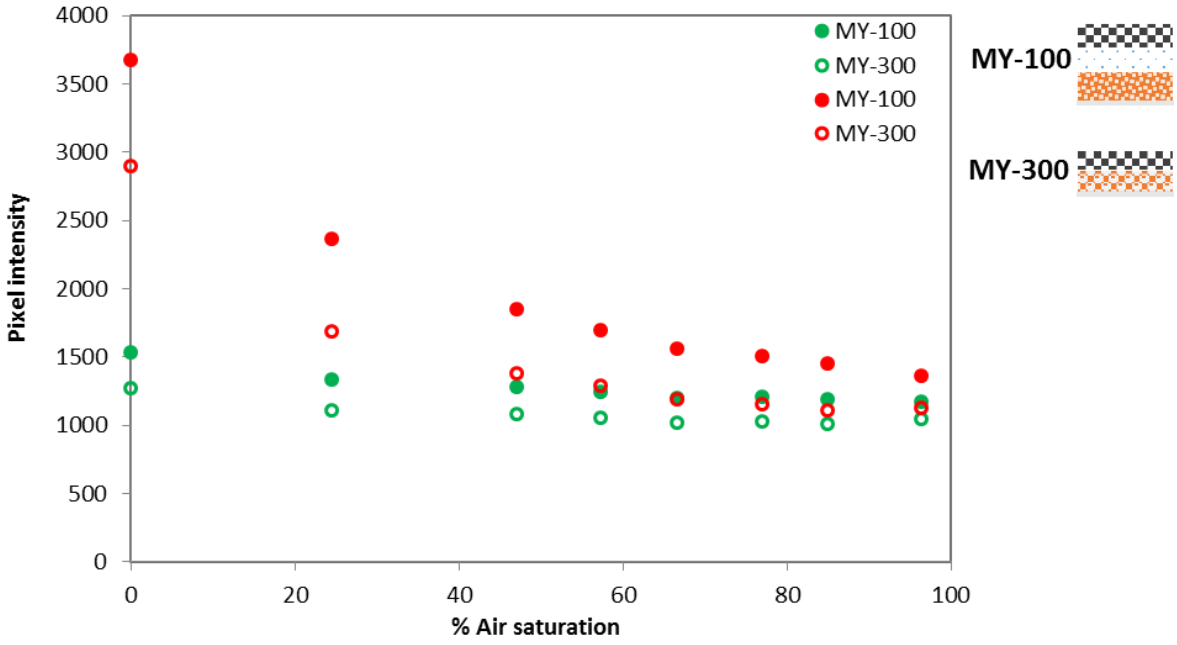

Figure 27: Pixel intensity of the Red and the Green channel of MY100 (sensor layer: 100 mg & separate insulation laver 250 mg TiO_2, filled symbols) and MY300 optodes (sensor layer: 300 mg TiO2 – no separate insulation layer, open symbols)

The histogram below (Figure 28) presents the brightness of the images from the Red channel in anoxic condition (0% of air saturation) acquired for MY100 (Figure 28.a) and MY300 (Figure 28.b). We can see that Red image of MY100 was over saturated whereas Red image of MY 300 was reasonably bright. It means that at low oxygen content, the signal variation of MY100 recorded by the camera will be low. The high pixel intensity observed in the Red channel in Figure 27 was actually saturated. This will negatively affect the sensitivity of the oxygen sensor.

Figure 28: Histogram of red picture in anoxic condition (0% air saturation). (a) Red channel of MY100 (sensor layer: 100 mg & separate insulation laver 250 mg TiO_2). (b) Red channel of MY300 (sensor layer: 300 mg TiO2 – no separate insulation layer)

The calibration curves of optode MY100 and MY300 are presented in Figure 29.A. Both of them were fitted with modified Stern-Volmer model (R^2>0.998). Figure 29.B displays the Stern-Volmer plot of MY300 and MY100, showing the quenching efficiency of the optode foils. As expected, the ratios of MY100 were higher than that of MY300 (Figure 29.A). At equivalent oxygen concentration, the more sensitive optode for oxygen is represented by a higher ratio R0/R. As shown in Figure 29.B, MY300 presented a higher sensitivity to oxygen especially at low oxygen content. This was confirmed by comparing the Stern-Volmer constant K_{sv} which was much higher for MY300 (K_{sv} = 0.043) than for MY100 (K_{sv} = 0.024). So, even though the TiO_2 wall of MY 100 improved the pixel intensity of the Red channel (Figure 29.A), it decreased the quenching efficiency (Figure 29.B). It might be due to the saturation of the picture to some extent. This hypothesis could be further tested by carrying out measurements with a lower time aperture of the camera, decreasing the quantity of light recorded on the camera sensor. However, this was beyond the scope of this work.

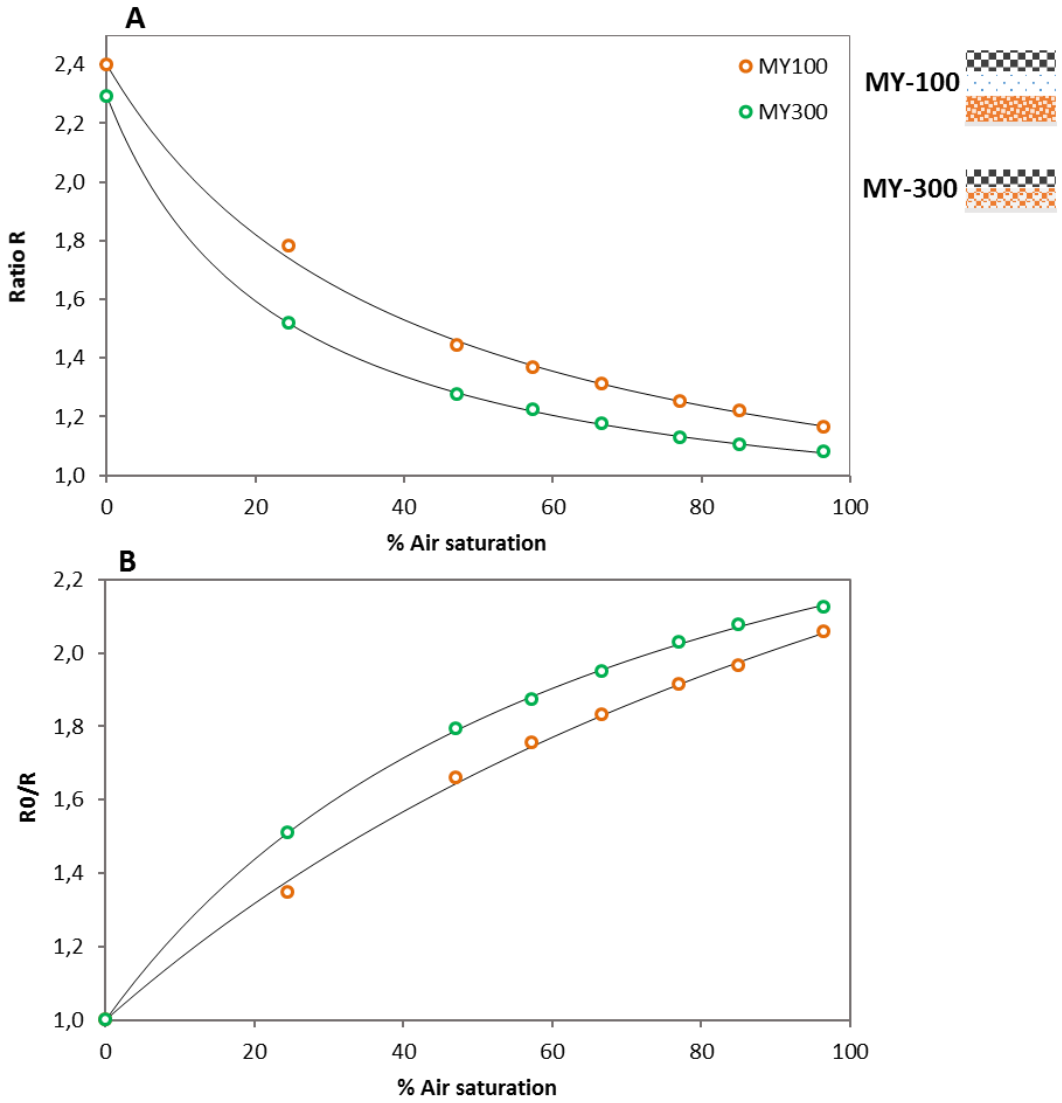

Figure 29: Calibration curve for MY100 and MY300 optodes. R value is the mean pixel value. Errors bars representing standard error are smaller than the symbol size. (n = 47740 pixels for MY100, n = 39600 pixels for MY300). (A) presents Ratio value against oxygen content. (B) presents quenching plot described by modified Stern-Volmer model (Eq.8)

To conclude, TiO_2 will be directly added to the sensor layer for the following studies as sensor with TiO_2 incorporated showed a higher sensitivity at low oxygen concentrations. This therefore also simplifies optode preparation with one less layer to coat.

2.4. Sensitive dye

Two commonly used oxygen indicator dyes were tested: PtTFPP and PtOEP. In addition, different indicator dye/reference dye ratios were also investigated in this study: 1 and 0.5 (Table 3). The factor was focused on MY concentration as it acts as antenna dye and its concentration

will have an influence on the indicator dye fluorescence. The objective was to choose the recipe showing the highest sensitivity in oxygen sensing. The Table 3 summarizes the recipes tested for this experiment.

Table 3: Details of optode recipe

Optode	PT-MY1	PT-MY3
PtTFPP	1.5 mg	1.5 mg
Macrolex Yellow	1.5 mg	3 mg
TiO_2	300 mg	
Polystyrene	200 mg	
Chloroform	3 g	
% Indicator dye (I)	0.75	0.75
% Reference dye (R)	0.75	1.5
Ratio I/R	1	0.5

Optode	PO-MY1	PO-MY3	PO-L
PtOEP	1.5 mg	1.5 mg	1.2 mg
Macrolex Yellow	1.5 mg	3 mg	1.2 mg
TiO_2	300 mg		/
Polystyrene	200 mg		120 mg
Chloroform	3 g		3 g
% Indicator dye (I)	0.75	0.75	1
% Reference dye (R)	0.75	1.5	1
Ratio I/R	1	0.5	1

In addition, the recipe already published by Larsen et al [12] was also tested. In this optode, the indicator and the reference dye are more concentrated in the polystyrene matrix and no TiO_2 was applied. For simultaneous calibration in water, small pieces of the different optodes were positioned next to each other on one front plate.

Results

Figure 30 displays the pixel intensity of the red and green picture respectively for each optode. PO-L showed the lowest intensity in both channels, three times less than the intensity of PO-MY. Even though the dyes were more concentrated in this optode, it did not improve the brightness. The other difference was the absence of TiO_2, which could explain the low signal intensity of PO-L. Potentially, this could be improved by changing the camera settings (exposure time, aperture or ISO) to get more light on the camera sensor.

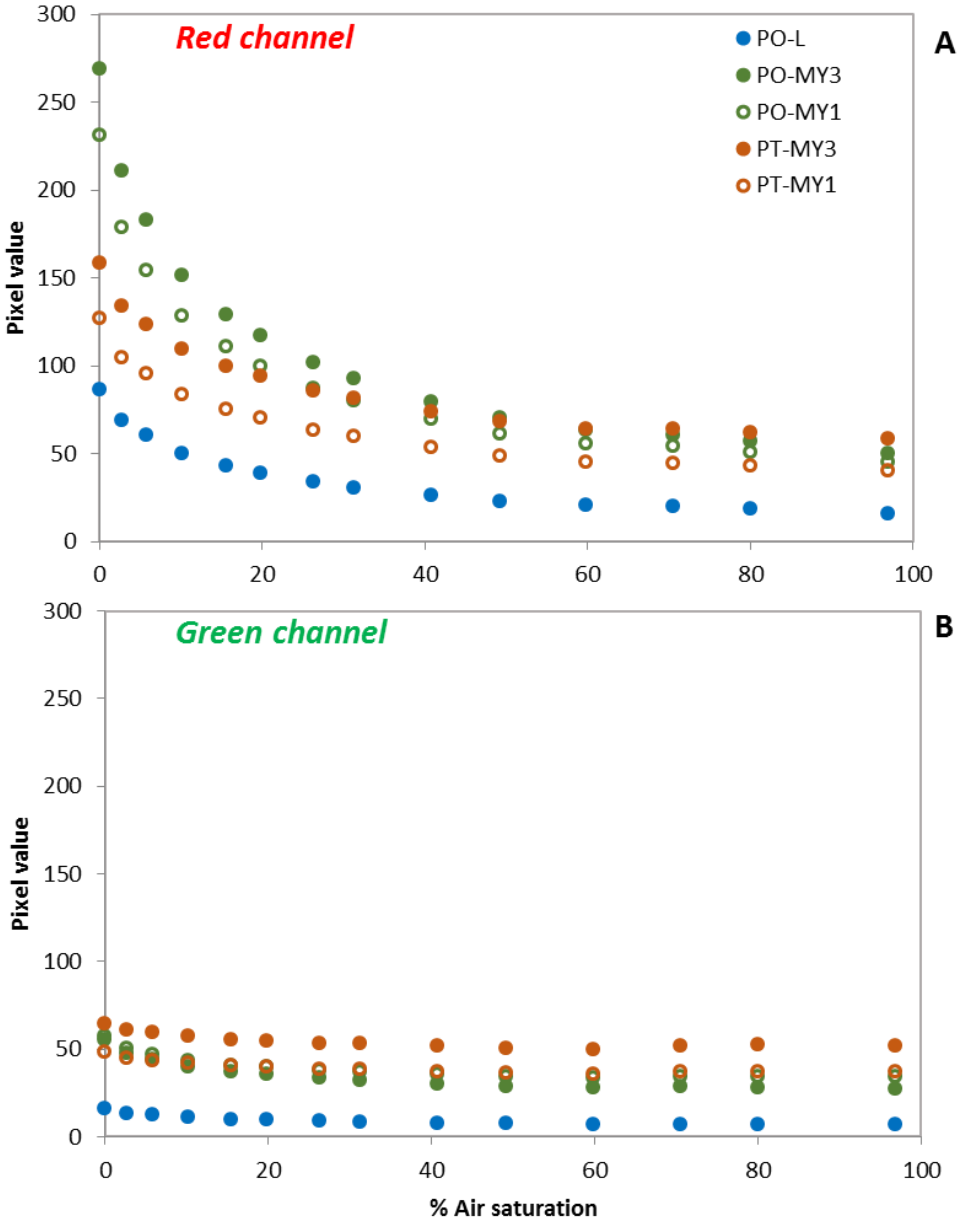

Figure 30: Pixel value y from Red (A) and Green (B) channel of of PO-L, PO-MY1, PO-MY3, PT-MY1 and PT-MY3.

Also, the pixel intensity of the red picture of PT optodes was almost half of intensity of PO optodes, irrespective of reference/indicator dyes ratio. The PO optodes showed a greater brightness than the PT optodes. The luminescence emitted by PO optodes was much higher (close to two fold) than PT optodes at low oxygen content. However, both indicator dyes reached a similar intensity at high oxygen concentration. The red picture (analyte sensitive channel, Figure 30.A) provides a first indication of the difference in sensitivity to oxygen between PO-MY and PT-MY. A higher intensity in the red channel for the lower indicator/reference dye ratio (I/R=0.5) was found for PT (+24%) and PO (+16%) compared to

PO and PT with I/R of 1. Macrolex Yellow is not only a reference dye (not sensitive to oxygen), but is also an antenna dye. It plays the role of light donor to an acceptor which is the indicator dye. This could explain the higher pixel intensity on the red picture for optodes with I/R of 0.5 as the reference dye was two times more concentrated. Finally, the pixel intensity of the green pictures indicates that the signal of optodes with 1.5% of MY was just slightly higher than that with 0.75% MY. The increase of MY concentration enhanced the indicator dye fluorescence, due to its capacity to donate energy.

The calibration curve of each optode are presented in Figure 31. The optodes were well described by the modified Stern-Volmer model (R^2>0.997). However, the shape of the curve of PO-L did not fit with the others optodes. This is not in agreement with Larsen and al [12]. The calibration curves were repeated three times and always gave the same pattern for each optode. The only difference between PO-MY and PO-L was a higher concentration of dyes. An explanation might be the start of aggregation of the dyes in the more concentrated PO-L. Potentially, an incomplete dissolution/mixing of the dyes during the preparation procedure could also be responsible. However, the same mixing time and procedure was applied to each optode recipe, consequently we consider this unlikely. The ratio R of PO-MY (particularly PO-MY1) decreased more strongly at low oxygen concentration than the ratio R of the PT optode, indicating a higher sensitivity at low O_2 concentrations. At 20 % air saturation, R of PO-MY1 was reduced by 37% while R of PT-MY1 decreased by 30%.

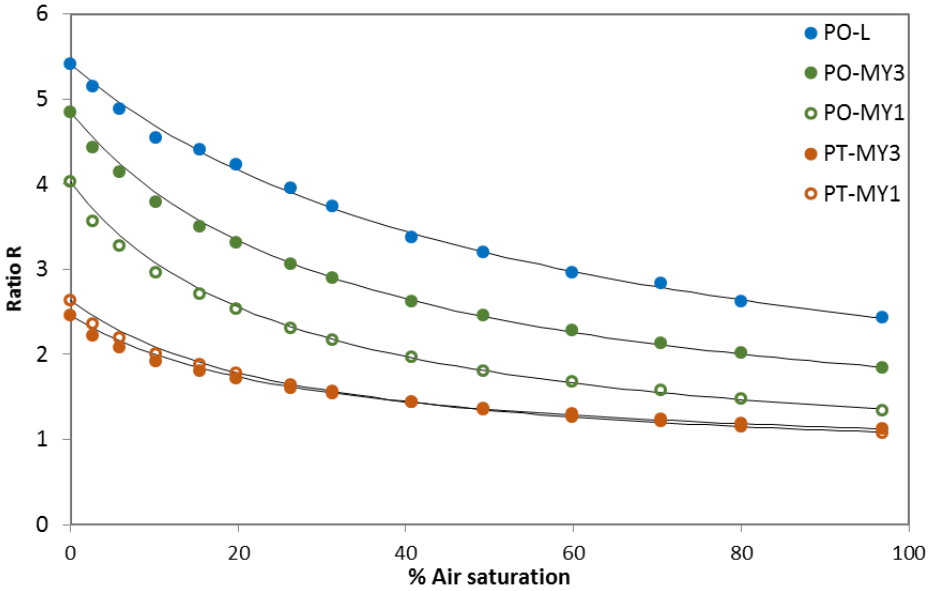

Figure 31: Calibration curve of PO-L, PO-MY1, PO-MY3, PT-MY1 and PT-MY3. Point are mean pixel values with error standard (n =12100 pixels). Errors bars are smaller than the symbol size.

This tendency was confirmed with the Stern-Volmer plot (Figure 32). This plot confirms that the highest sensitivity for oxygen was reached by PO-MY1 within the oxygen range studied. It can be noted that the sensitivity of the optode with the higher amount (1.5%) of Macrolex Yellow was lower compare to optode with 0.75% of MY.

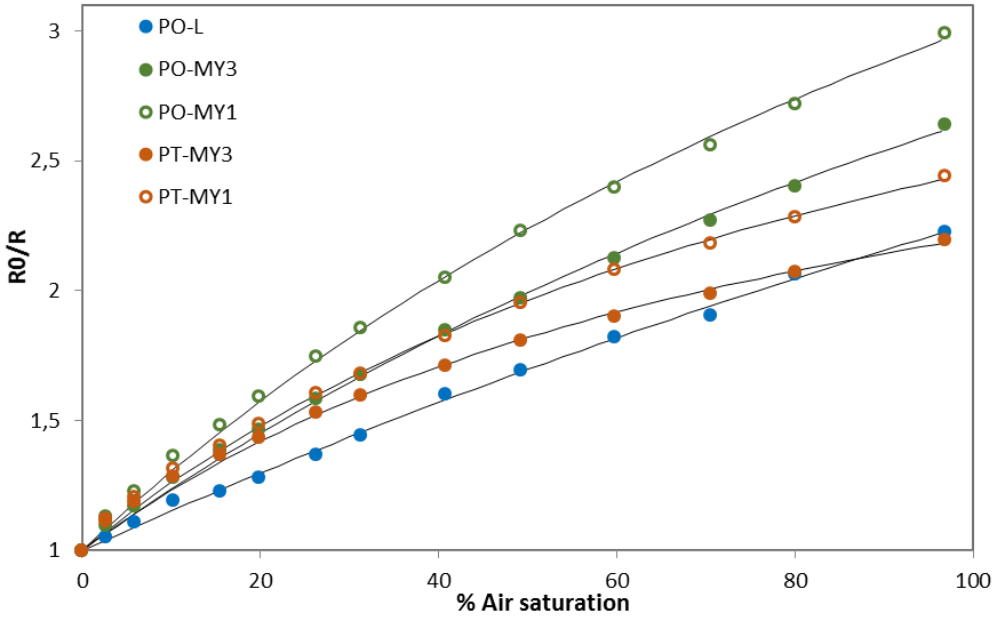

Figure 32: Stern-Volmer plot of of PO-L, PO-MY1, PO-MY3, PT-MY1 and PT-MY3.

The quenching constant K_{sv} was found to be the highest for PT-MY1 and PO-MY1 (Figure 33), with PT-MY3 also being in a similar range. This means that these optodes present a higher sensitivity for oxygen as K_{sv}^{-1} represents the concentration of quencher required to halve the initial fluorescence. Indeed, these two optodes show a similar sensitivity to oxygen at low oxygen content (<20% of air saturation). The quenching efficiency for PT-MY3 decreased with increasing oxygen resulting in a strong flattening of the calibration curve. This trend was reflected by the α coefficient (Figure 33), which represents the fraction of unquenchable fluorescence signal. As displayed in Figure 33, α of PT-MY3 was estimated at 0.25 for PT-MY3 and at 0.31 for PT-MY1. Also, Figure 33 shows a marked difference between PO and PT optode with α below 0.17 for PO and above 0.25 for PT optode. It seemed that the fraction of quenched sensitive dye is higher for PO regardless the quantity of reference dye. It could be assumed that PO could be used for a larger oxygen concentration range. Finally, whether for PO or PT optode, a higher concentration of antenna dye increased pixel intensity in the red picture but did not increase sensitivity to oxygen. This result was in accordance to Mayr et al

[80] who showed that the quantity of the antenna dye Coumarin C545T did not influence the sensitivity of PtTFPP to oxygen.

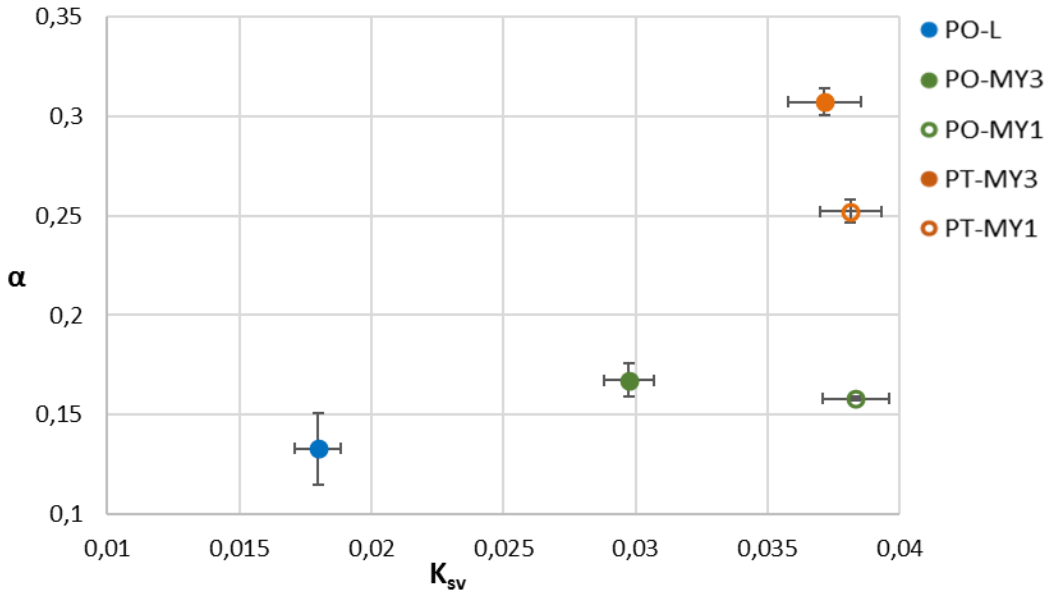

Figure 33: K_{sv} and α parameters estimated from Stern-Volmer model of of PO-L, PO-MY1, PO-MY3, PT-MY1 and PT-MY3.

To conclude, PO-MY1 was chosen for further experimentation. It presented a sufficient pixel intensity, the best balance between indicator and reference dye as well as the most efficient quenching at low oxygen concentration.

3. pH sensors

3.1. Low pH sensor (LO)

3.1.1. Description and principles

LO optode is based on a ratiometric approach. An indicator dye sensitive to pH was mixed with a reference dye which is not sensitive to pH. The reference dye used in this system was ziegelrot pigment with maximum emission at 595 nm, as shown in Figure 34. Consequently, its luminescence was mainly recorded on the red channel of the camera sensor. The indicator dye, DClFODA, a hydrophobic derivative of fluorescein, shows a fluorescence peak at 550 nm which was recorded on the green channel of the camera sensor. Under acidic conditions (pH 5.5), the protonated form of DClFODA does not exhibit any fluorescence. Under alkaline conditions, its deprotonation results in a high fluorescence emission.

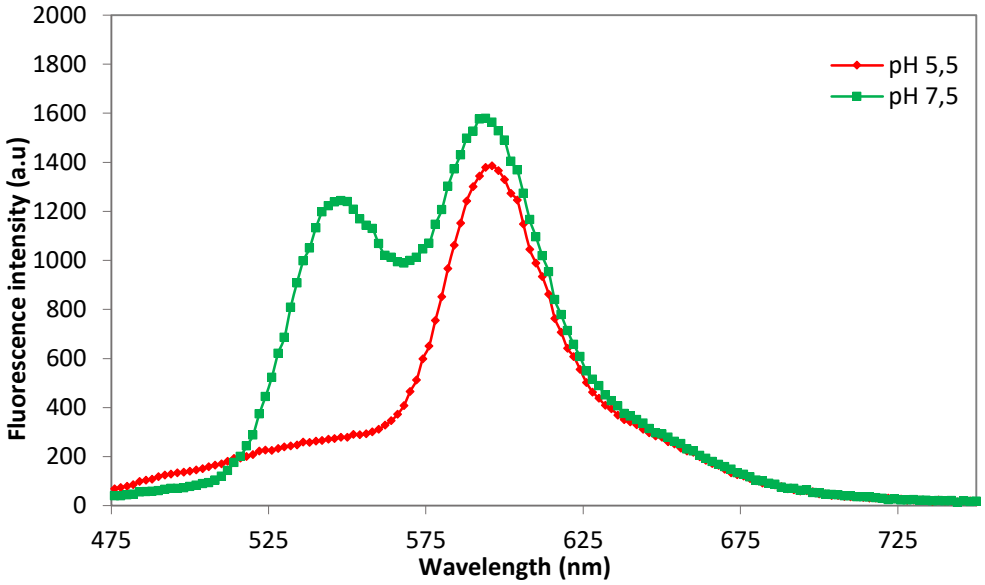

Figure 34: Emission spectra of LO (excitation wavelength = 445 nm)

To measure pH changes, Red and Green channels are analysed. First, the intensity ratios of both channels are calculated. The changes of the Green/Red ratio with pH follow a sigmoidal model as described in the equation below:

$$R = \frac{R_{min} - R_{max}}{1 + e^{\left(\frac{pH - pKa'}{dpH}\right)}} + R_{max} \qquad (10)$$

R is the corrected Green/Red ratio (corrected by Red and Green values of black picture), $\boldsymbol{R_{min}}$ and $\boldsymbol{R_{max}}$ are the maximum and minimum ratios (asymptotes of the curve), ***pKa'*** is the acid dissociation constant of the indicator dye in a specific system, ***dpH*** is the slope of the curve. By rearranging the equation (10), the pH value can be calculated as follows:

$$pH = pKa' + dpH.\ \ln\left(\frac{R_{min} - R_{max}}{R - R_{max}} - 1\right) \qquad (11)$$

Our LO sensor study was mainly focused on the thickness of the optode, especially on the thickness of each coated layer: sensor layer, titanium oxide layer and optical insulation. Each layer could change (i) optode time response (ii) level of fluorescence intensity (iii) and optode properties in terms of sensitivity and pH range. From the first batch of optodes, useful information about thickness and titanium oxide layer was extracted.

3.1.2. Optode thickness

The first batch of LO was made up of three layers: sensor layer, titanium oxide layer and optical insulation. The recipe was slightly adapted from Hoefer et al [79] by adding a titanium oxide and optical insulation layer. Each layer contained an indicator and a reference dye at 1/10 (w/w) ratio, embedded in hydromed D4 and was coated with different a coating knife: 1 mil, 2 mils and 3 mils. The thickness of 1 mil is equivalent to about 2.5 µm of dry film.

The Table 4 presents the different optode foil recipes tested for the effect of varying layer thickness and composition on optode sensitivity and performance.

Table 4: Thickness of each layer coated

Optode	Sensor layer (S)	TiO_2 layer (T)	Optical insulation (O)
A (S1-T2-O2)	**1 mil**	**2 mils**	**2 mils**
B (S1-T2-O3)	**1 mil**	**2 mils**	**3 mils**
C (S2-T2-O3)	**2 mils**	**2 mils**	**3 mils**
D (S2-T2)	**2 mils**	**2 mils**	**-**

Calibration curves and a time response study were carried out in phosphate buffer (10 mM) solutions at a fixed ionic strength (IS 30mM). For calibration, a piece of each optode was stuck on the same front plate position and then put in contact with phosphate buffer at varying pH for 15 min. For the time response study, the optodes were initially put in contact with phosphate buffer (5 mM, IS 60 mM) at pH 5.6 that was then replaced by a solution at pH 7.7. Thereafter, an image was taken every minute for 45 minutes.

Calibration

The Red and Green signals from the calibration pictures were plotted separately (Figure 35). The signal from the Red channel describes luminescence emitted mainly by the reference dye while luminescence emitted from the indicator dye is recorded on the Green channel. As expected, signals from the Green channel followed a sigmoidal model as described above (Eq 10), while signals from the Red channel was much flatter. The minimal variation of reference dye emission with changing pH (Figure 35) observed could be explained by the fact that the

luminescence emission peaks of indicator and reference dye overlap and some signal from the indicator dye is also recorded on the Red channel.

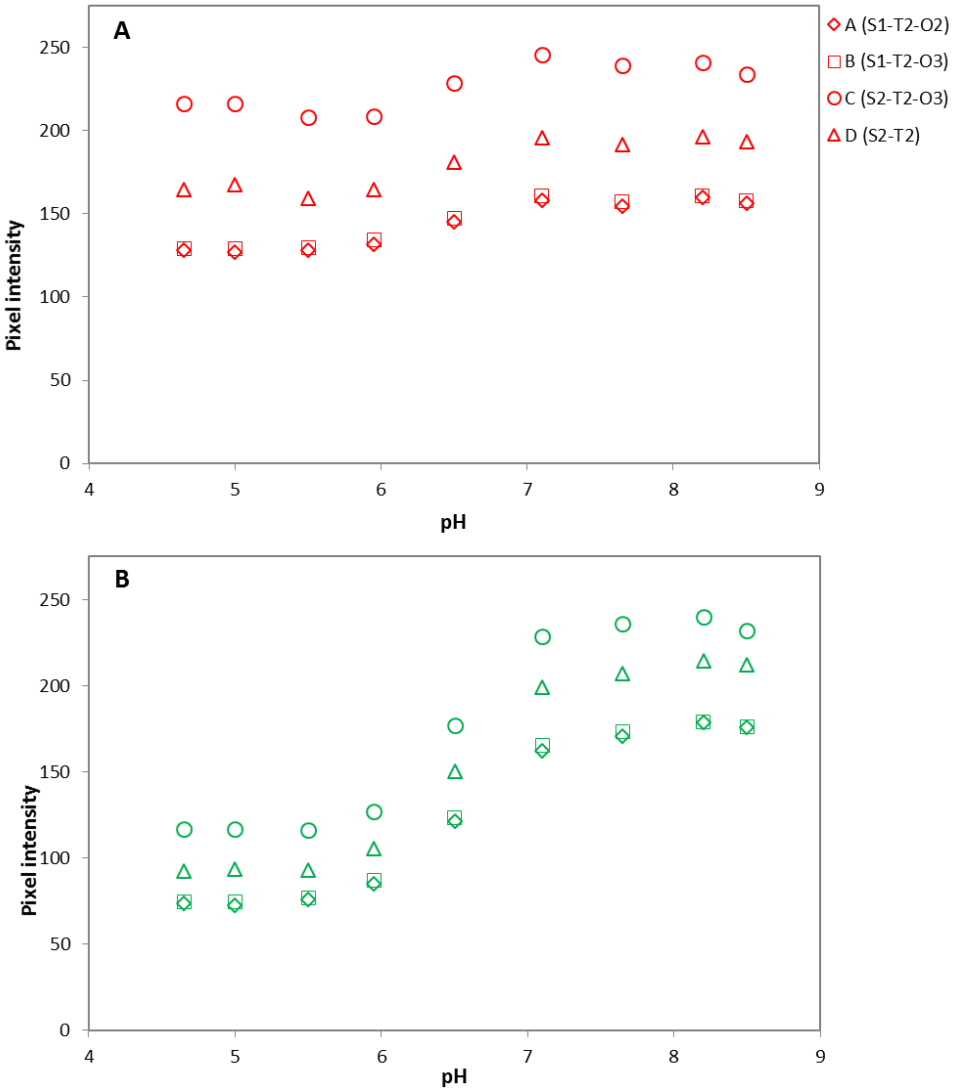

Figure 35: Pixel intensity of Red (A) and Green (B) image of LO optodes at various pH values. SxTxOx represents the thickness of each layer with S for sensor layer, T for titanium oxide layer, O for optical insulation.

As we can see in Figure 35, the thickest optode (C – S2-T2-O3) exhibited the highest intensity for both channels. Optode D (S2-T2) with a 2 mils thick sensor layer exhibited the second highest luminescence indicating a positive relationship between sensor layer thickness and signal intensity. Optodes A (S1-T2-O2) and B (S1-T2-O3) emitted the same luminescence intensity even though B had a thicker optical insulation than A. As mentioned earlier, indicator and reference dyes were also added to TiO_2 layer and optical insulation to minimize diffusion from the sensor layer. The Optode C (S2-T2-O3) presumably emitted more light than the other

optodes as it contains an overall higher amount of dyes. A 2 mils thickness of the sensor generally resulted in a higher signal intensity (C, D). In comparison, optodes A (S1-T2-O2) and B (S1-T2-O3) with a sensor layer of 1 mil showed less luminescence. Consequently, quantity of luminescence seems to depend more on the thickness of the sensor layer than on the thickness of optical insulation, which did not affect signal intensity (A S1-T2-O2 vs B S1-T2-O3). For the optical insulation layer, the hydromed D4 matrix was diluted twice in ethanol and black carbon was added at 30 % (mass % of hydromed D4). Optical insulation with 30% of black carbon was completely non transparent and absorbed light.

By calculating the ratio between Red and Green images, a calibration curve was fitted for each optode based on Eq 10. Displayed in the Figure 36, the calibration curves of each LO sensor fitted to the sigmoidal model (R^2>0.999) as described above and presented a dynamic pH range between 5.5 and 7.5.

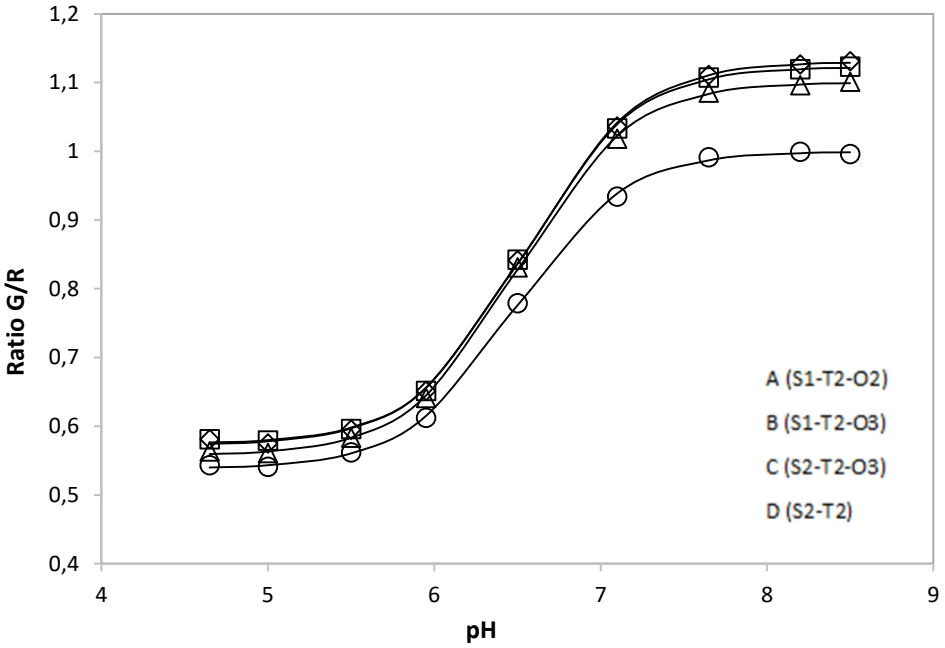

Figure 36: Calibration curve of optode A, B, C, D. Error bars (standard error) are smaller than symbol size. (n = 150 x 150 pixels)

The pKa' estimated from equation (10) amounted to 6.54, 6.53, 6.48, 6.50, for optodes A, B, C, D respectively, with a standard error below 0.015 pH units. The pKa' was only minimally impacted by the thickness of the optode but showed a tendency to be slightly lower for the thicker sensor layers. The pKa' of the four investigated optodes were in agreement with previous studies irrespective of thickness and optical insulation [54,79]. Contrary to individual channel analyses, optode C showed the lowest ratio values across the investigated pH range,

with a decrease in sensitivity at increasing pH. Optodes A and B with the lowest intensity levels reported by the individual Green and Red channels showed the highest ratio response to pH changes. A similar response was also observed for the optode D without optical isolation. The lower sensitivity of optode D might be explained by the inner filter effect that occurred in this thick foil. The reabsorption of the Green light emitted due to high quantities of indicator dye of this sensor may have resulted in an overlap between absorption and emission spectra of DClFODA under alkaline (pH >7) conditions [54].

Response time

As depicted in Figure 37, the optodes A (S1-T2-O2) and D(S2-T2) showed the fastest response time, with t_{95} (time to reach 95 % of highest signal) between 2 and 5 minutes while t_{95} of the thickest optodes B (S1-T2-O3) and C (S2-T2-O3) was 20 min. So, as predicted, a thicker coating decreased the reactivity of the sensor. Also, the response time curve of the optode D showed a slow decrease of the ratio over time. This trend was also observed for optode A. Optode D did not contain any optical insulation and that of optode A was 2 mils thick, while optical insulation of optode B and C was 3 mils thick. This suggests that either dyes leached over time decreasing the sensor sensitivity or that the optode was degraded by photobleaching with too much light received during the experiment. Titanium oxide particles have the properties to scatter light in the foil acting as light-scattering centres and bring more light to the sensor layer.

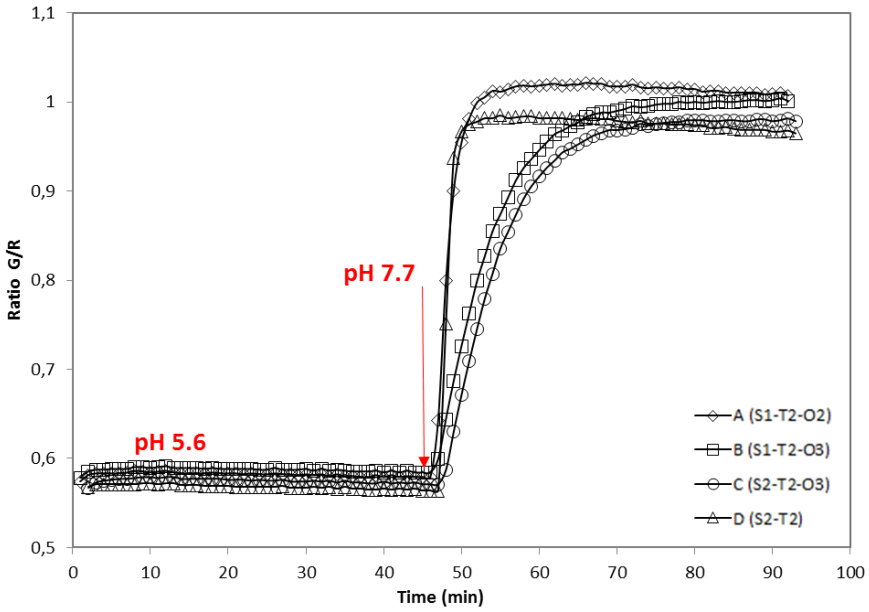

Figure 37: Response time curve. 45 min in phosphate buffer pH 5.6, then 45 min at pH 7.7.

3.1.3. Titanium oxide

To address the hypothesis of photobleaching, a new LO (E) was prepared with no titanium oxide and no optical insulation. If dye leaching would occur, this phenomenon should be more pronounced as the optode is thin (1 mil) with no protection. The sensor thickness was chosen as it showed the highest sensitivity in the optode recipe comparison. The response time experiment was carried out as previously described in a phosphate buffer solution (PBS) at pH 5.6 for 45 min that was then replaced with a PBS at pH 7.6.

The response time of the LO E is shown in Figure 38. Results indicated constant ratio values over time, contrary to the optode D with titanium oxide. It is reasonable to assume that the titanium oxide layer may have a photobleaching effect on the dye over time if it is not protected by a black optical insulation layer. In addition, the ratio change with pH was much higher without titanium oxide. Metal oxides can locally affect the pH in the surrounding environment due to surface protonation/deprotonation, and therefore change the sensor reactivity. Similarly, Hoefer et al showed the incompatibility between ZrOH and LO sensor with a constant luminescence with changing pH [79].

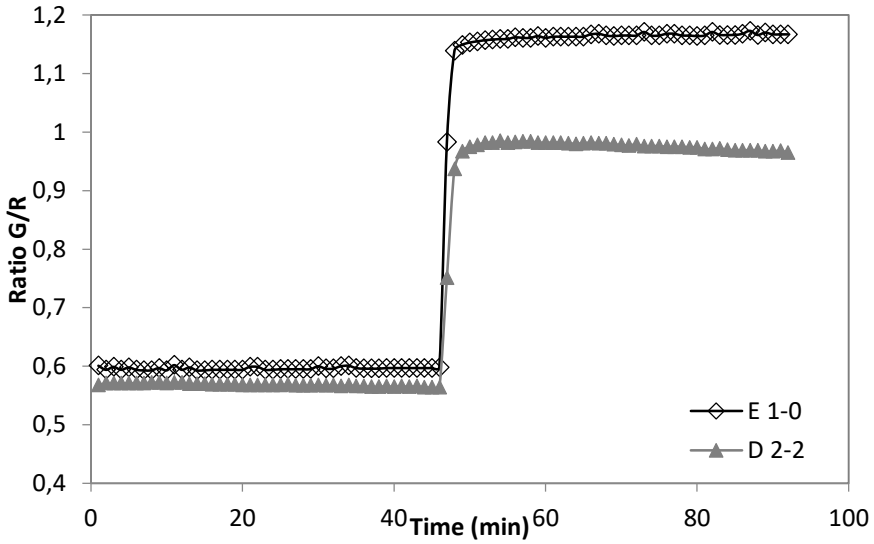

Figure 38: Response time curve of optode E, without titanium oxide.

To avoid early photobleaching due to the presence of titanium oxide and potential pH disturbance, we decided to continue the study with LO without titanium oxide, as our objectives was to obtain an optode reacting well to pH changes for longer time periods

3.2. High pH sensor (HO)

3.2.1. Description and principles

Like the LO sensor, HO optode was also based on a ratiometric approach. The indicator dye was the lipophilic derivative of 8-hydroxy-1,3,6 pyrenetrisulfonic, d-HPTS. HPTS is a fluorosensor commonly used in pH sensing [18,19,53]. This indicator was combined with Macrolex Yellow, as already applied for the oxygen sensor. The sigmoidal model used for LO was also applied to describe the response of the HO sensor to changes in pH.

The first batch of HO also contained a titanium oxide layer. Preliminary tests showed a slow response with pH change (not presented in this document). Consequently, HO sensors were constructed without titanium oxide. The HO development was then only focused on optical set-up adaptation.

3.2.2. Set-up study

Our main objective was to determine the applicability of HO within the conditions determined by our optical set-up. The ideal set-up in future projects would be to have one set-up for both LO and HO. It means using the same short pass filter (excitation) and long pass filter (emission) for both pH sensors. Thus, we could image pH changes in the same rhizobox with two optodes and only one picture. This objective implies ensuring the compatibility of HO with an excitation light at 445 nm combined with a 475 nm short pass filter and a 495 nm emission filter. In a previous study [12], HO was used with UV LEDs (405 nm) combined with a 405 nm band bass filter and 455 long pass emission filter. The indicator dye d-HPTS presents two excitation and emission peaks according to its acidic or basic form [54,86]. Also, spectral properties are modified depending on the matrix used. In polyvinyl chloride, excitation and emission wavelength of acidic form are 422 nm and 455 nm whereas the basic form present maxima at 521 nm and 548 nm [86]. In polystyrene beads, the acidic form presents maxima at 433 nm / 552 nm ($\lambda_{excitation}$ / $\lambda_{emission}$) as the maxima for the basic form is at 525 nm / 564 nm.

So, firstly, the emission spectra of the foil were obtained at two excitation wavelengths: 400 nm and 445 nm. Then a calibration curve was performed with our set-up in 10 mM TRIS buffer (60 mM ionic strength).

Emission spectra of HO are represented in Figure 39. The emission spectrum at 400 nm (Figure 39.A) was similar to previous study [12]. It indicated two emission peaks relative to Macrolex Yellow (MY) at 500 nm and d-HPTS at 558 nm as well as change of spectral properties with pH variations. At 445 nm excitation wavelength, the emission spectrum was consistent with the previous spectrum at 400 nm excitation wavelength. MY and d-HPTS showed the same maxima emission wavelength (Figure 39.B).

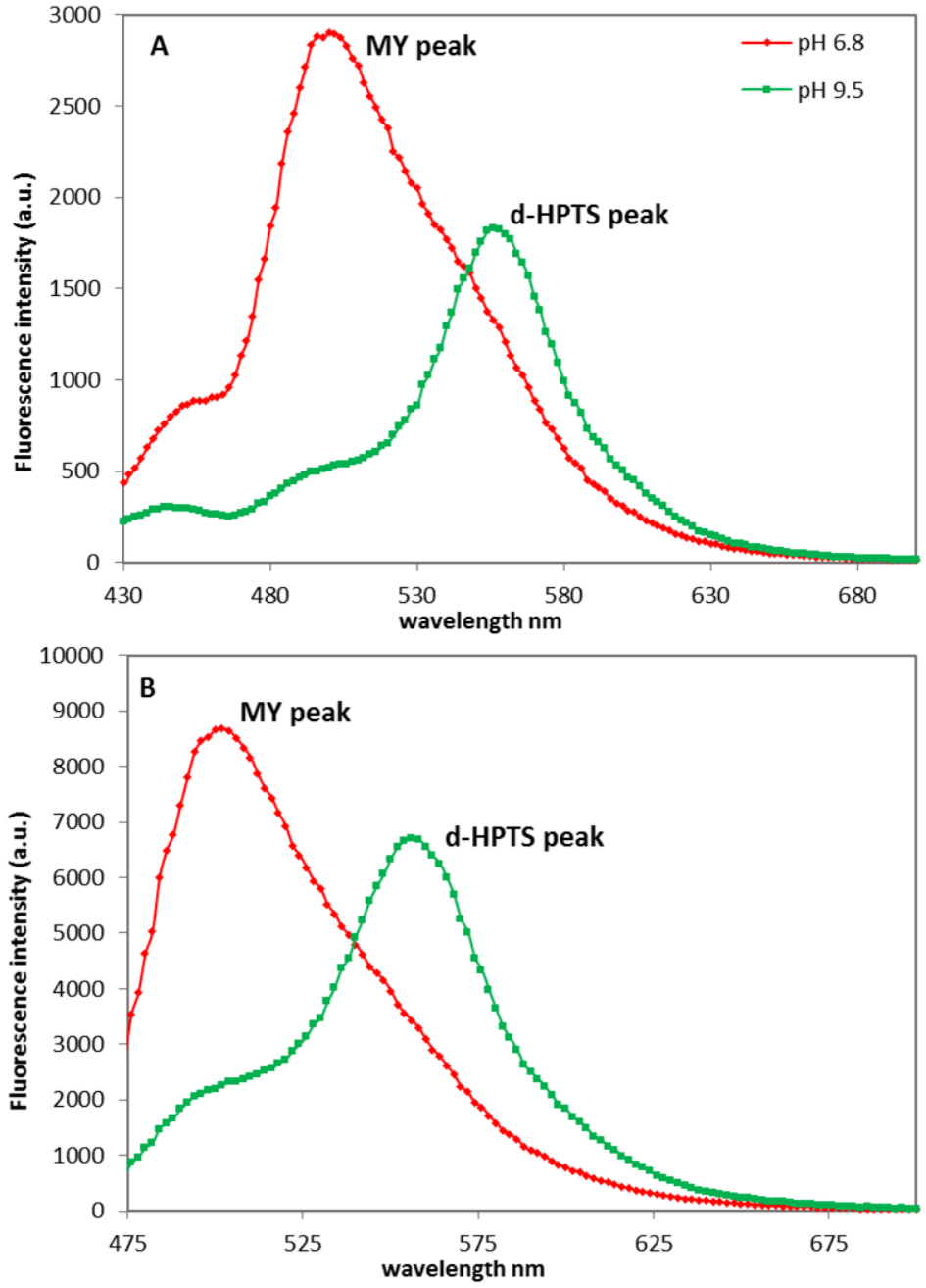

Figure 39: Emission spectra of HO. Excitation wavelength : 400 nm (A) and 445 nm (B)

Even though the emission spectra of MY and d-HPTS were discriminated they showed an important overlap, which was more pronounced at 400 nm excitation wavelength. Also, the luminescence intensity was increased by a factor of 3 for both dyes at 445 nm. As we can see in both spectra, luminescence intensity in the blue decreased with increasing pH whereas red and green light increased. At pH 6.8, blue light dominated strongly and then decreased at pH 9.5. In acidic conditions, d-HPTS presented a peak excitation wavelength around 430 nm and a maximum emission around 450 nm. This small emission peak can be observed in Figure 39.A. In contrast, at 445 nm excitation wavelength, MY emitted with a maximum at 500 nm and d-HPTS acidic form did not emit much light. So, under acidic conditions luminescence was dominated by MY. Under alkaline conditions, the amount of basic d-HPTS increased and it became an acceptor of the light emitted by MY acting as an antenna dye since excitation wavelength of d-HPTS basic form is around 520 nm. As a result, blue light decreased and red and green light increased mainly dominated by d-HPTS emission. These emission spectra suggest that it is possible to use a 445 nm excitation light for HO and moreover, it seems to improve response intensity. The results also demonstrate that the ratiometric intensity approach can be applied, even if there is a strong cross-talk between MY and d-HPTS signal in the green and red.

As we can see in Figure 40 displaying the intensity of Red (R), Green (G) and Blue (B) channels with changing calibration buffer solution pH, each channel presented a distinct trend of response to pH. G and R signals increased with increasing pH whereas the B signal decreased. It confirms the tendency observed in the emission spectra.

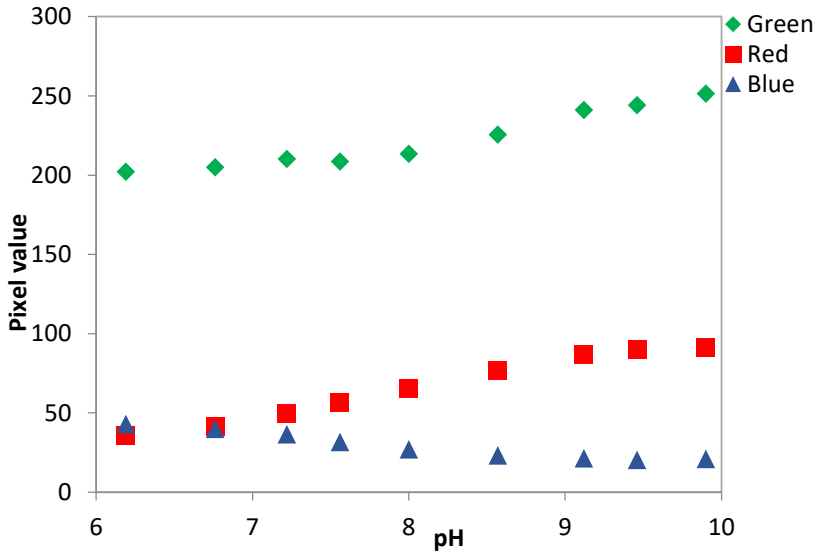

Figure 40: Pixel intensity of Green, Red and Blue image of HO, with pH changes

From R, G, B pixel values, calibration curves were built comparing three ratiometric approaches: R/B, R/G, G/B (Figure 41).

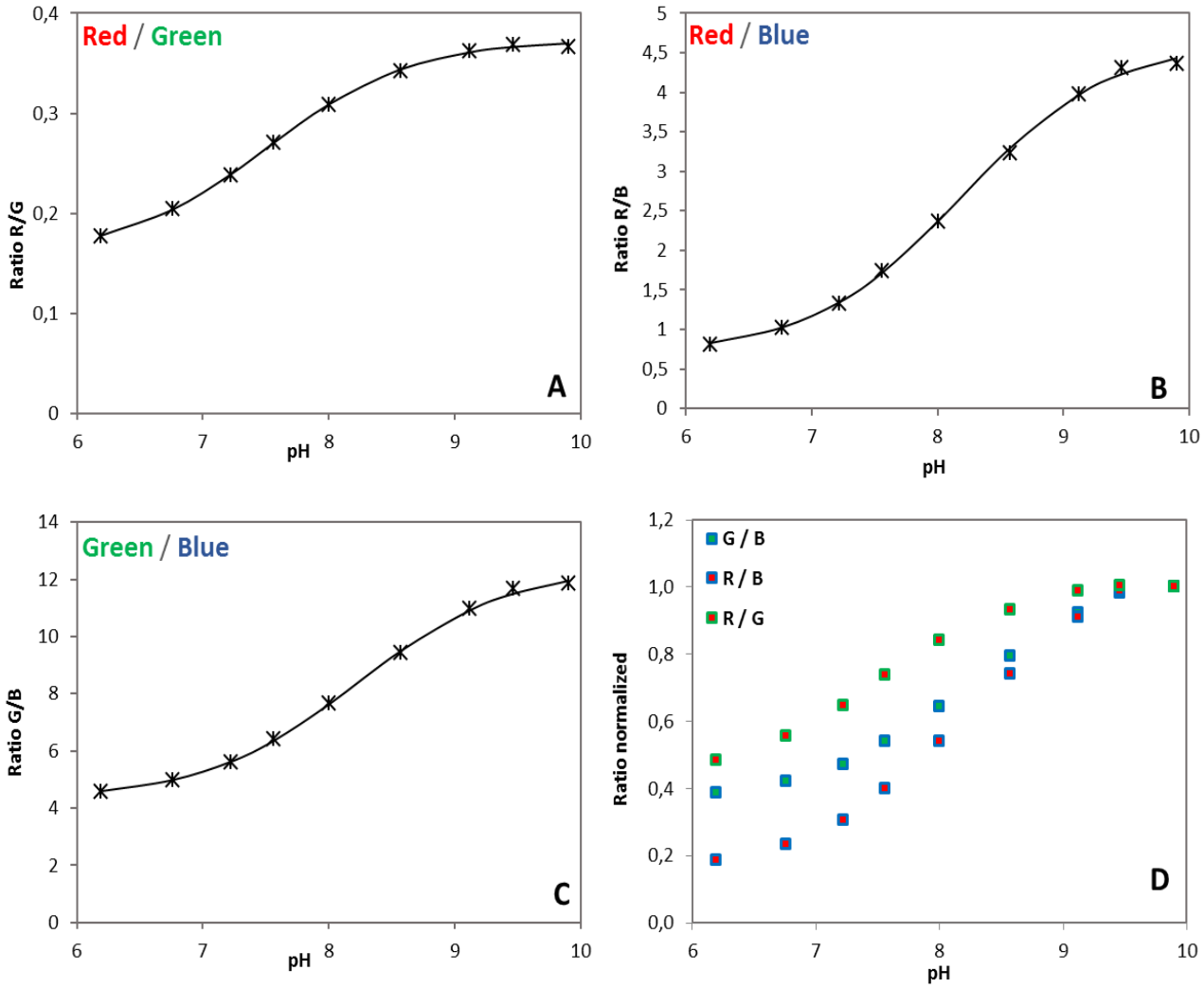

Figure 41: Calibration curve of HO. A, B, C represents ratio value of Green/Blue, Red/Green, Red/Blue respectively. D is calibration curve with normalized ratio value. Standard errors are below 0.002 (n=62500 pixels).

Whatever the ratio, the calibration curves fitted to a sigmoidal model ($R^2 \geq 0.999$) describing the relationship between ratio value and pH change. However, the comparison of each curve (Figure 41.D) showed significant differences between ratios in terms of dynamic pH range and sensitivity of the HO sensor. As expected, the ratio R/G appeared to be the least appropriate to describe HO response to pH changes. pKa' values estimated with the R/G ratio were more acidic than for the other ratio models (Table 5). It showed also a shorter dynamic range, between pH 6.2 and 8.6. Green channel as reference channel was also impacted by luminescence from

indicator dye. It could explain the lower sensitivity observed at high pH as Green signal also increased with pH. Blue signal as reference signal was found to be the least impacted by cross talk as the signal is mainly influenced by MY. Consequently, ratio calculated with Blue signal presented a broader dynamic range with a pKa' = 8.2, and a higher sensitivity. The ratio G/B showed a pH dynamic range of 6.8 to 9.5 similar to the R/B ratio (6.2 to 9.5). However, R/B ratio was found to be more sensitive to pH change with a 6-fold increase of the ratio over the investigated pH range. The pKa' estimated was much higher than those in previous studies published by Larsen [12] (pKa' = 7.47), Hulth [53] (pKa' = 6.4), Hakonen [19] (pKa' = 6.78) Zhu [18] (pKa' = 7.06) and comparable to that of Borisov et al. [54] (pKa' = 8.0). Also, the pH dynamic range of the sensor was similar to that of Larsen [12].

Table 5: pKa' of HO sensors. From normalized data (ratio at pH max = 1). SE = Standard error.

Ratio	pKa'	SE
Red / Green	7.51	0.03
Red / Blue	8.18	0.04
Green / Blue	8.23	0.04

Finally, calibration curve showed that the reliable pH range of the HO fitted with our purpose as we expected to cover a pH range not exceeding pH 9 for soil applications.

4. Adaptation for soil application

4.1. Soil-root system application: constraints

The objective of this optode development was to study *in situ* changes of pH and oxygen concentration in soil and in the rhizosphere. Soil is a complex medium with heterogeneities due to its texture and structure (e.g. more or less aggregated clayey or sandy soil), its organic and mineral composition, its water content and biotic properties. With respect to optode imaging, *in situ* measurements require good contact between the sensor and soil solution or soil particles. Experiments in rhizobox system were designed to meet this requirement with careful filling of the rhizobox with sieved soil being crucial to ensure a good contact between the front plate and soil particles and limit structure-related heterogeneities. Then, soil-sensor contact also depends on soil water content. Most environmental optode applications were carried out in marine sediments [30,50,53], saturated soil [32,72,87] and flooded soil [4,33,88]. In few studies only, pH optodes were applied to unsaturated soil with reported water content ranging from 19% to

60% [70,89,90]. Unlike O_2 optodes that can also be applied to gaseous phases, the water content during pH optode applications is relevant for two main reasons. Firstly, it could be assumed that the contact of pH optode foil with the soil and the reactivity of the sensor will decrease under dry soil conditions. Also, pH imaging could be influenced by the soil water content. As pH is defined as the activity of hydronium ions in solution, the soil water content will impact pH. At lower soil water content, protons are more concentrated, resulting in acidification. As optical pH sensors are based on the concentration of protonated and deprotonated forms of pH sensitive fluorophore dyes, a higher concentration of hydronium ions should change the fluorescence properties of these dyes and, thus, pH measurement [6]. No information is currently available about water content effect on pH measurements with planar optodes.

Secondly, the optodes used in this work were transparent. Structures as roots and soil can thus be observed through the optodes. This property is very useful to study root growth and its activity over time and to correlate spatial and temporal variation of pH or oxygen concentration to the structure. However, soil and roots could interfere with the optode signal by light scattering or reflectance. Also, a dark soil absorbs more light than water and roots. Finally, roots could also reflect light. In this case, we could have a signal on the image which is not caused by changes in pH or oxygen concentrations. The ratiometric approach can attenuate such an artefact if the fake signal is not wavelength dependant. Indeed, each channel will be affected by a signal of equivalent intensity which will then be suppressed by ratio calculation. However, reflection and scattering from background can also be wavelength-dependant meaning that one channel will be more impacted than the others. Consequently, ratio value will be biased [12]. It is well known that roots can emit fluorescence as this property has been used to study root elongation [75] or to distinguish alive and dead roots [91]. So if roots emit light in one channel specifically, it cannot be removed from the picture and will therefore change ratio value. Optical insulation has been used to reduce background interference and allows a constant background signal for all pictures. The most commonly used optical insulation approach is an extra layer containing black carbon at 1% entrapped in a polymeric matrix coated onto the sensor foil [12,24,26].

In our study, two optical insulation approaches were investigated. The first one is an extra layer with increasing concentrations of black carbon. The second one is an external insulation applied between the optode and the sample. This external layer has to be optically homogeneous and must not interfere with the dyes' luminescence. Also, it should not limit the accessibility of the

target analyte to the optode. The external layer used in this work was a white nylon membrane (Buisine SA) with a mesh of 1 µm and a thickness of about 100 µm. This membrane is cheap, homogeneous, easy to handle in rhizoboxes and permeable to soil solution. The different optical insulation approaches for soil environments were studied for LO and OxO sensors.

Finally, the lifetime of the oxygen sensor was also investigated in relation to optical insulation. Some information is available for long term application in water [22] and in sediment [29,53]. König et al [22] showed that the sensitivity of oxygen optode (based on ruthenium sensitive dye immobilized into a sol-gel matrix) was decreasing after few days in regards to dye concentration. Also, optode lifetime in soils has not been fully explored until now. Soil applications were mostly carried out over short time periods, few days [87], until two weeks [90,92]. Only a couple of studies have reported long-term experiment, from 3 to 8 weeks in flooded soil conditions [31,33]. As soil is a living medium containing many active (micro-) organisms, lifetime can be an issue for long-term imaging. Biofouling or sensor degradation may indeed appear during long-term deployment in biologically active environment [53].

To sum up, in the following part, the optical insulation issue was explored for LO and OxO sensors, including lifetime investigation for OxO and in flooded soil. Water content effect on LO sensor response was also studied.

4.2. Oxygen optode

The objectives of this work was (1) to evaluate the need of optical isolation to protect the optode signal from luminescence and scattering light from roots and soil particles, (2) to test - if needed - different optical insulation approaches, (3) to check the changes of sensor properties with each optical insulation, and (4) to evaluate the sensor lifetime with and without optical insulation.

4.2.1. Optical insulation

Materials and methods

The optical insulation was prepared with a mix of silicon and black carbon powder dissolved in hexane solvent. Increasing additions of black carbon were studied: 0.5%, 1%, 2 %, and 10% (w/w of silicon). The individual mixes were coated onto the sensor layer with a thickness of 2 mils. The layer with 10% of carbon was not transparent whereas carbon at 2% was translucent with a light transmission of about 30%.

◦ Background luminescence

To study reflectance, luminescence or scattering effects of soil and roots, foils without the sensor layer were prepared. The optical insulation layer was coated directly onto the polyester foil. These foils were then stuck onto a rhizobox front plate together with an uncoated polyester foil and a polyester foil covered with a nylon membrane. A white rice root was fixed with tape just behind the foil to ensure a good contact between the root and the foil. Then the plate was screwed on a rhizobox filled with flooded soil, as showed in the Figure 42.

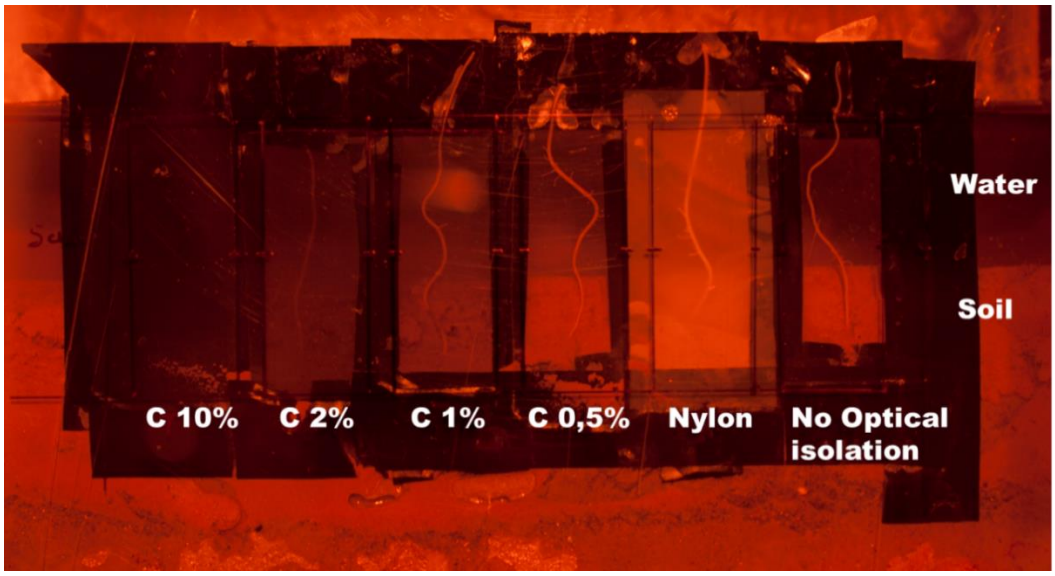

Figure 42: Image of foils stuck on the front plate screwed in the rhizobox filled with flooded soil

Due to the size of the front plate, two pictures were taken to ensure a homogeneous illumination of all optodes. Then, for better visualisation, pictures were combined and spatially adjusted with ImageJ. Foils were located at the soil-water interface and imaged with the same optical set-up as oxygen optode measurement (445 nm blue led combined with a 475 nm short-pass filter for

excitation and 530 nm long-pass filter for emission). In absence of fluorophore in the foil, the luminescence coming from background, polyester foil and optical insulation only was recorded by the camera. Then, data from Red and Green channels were extracted and Red/Green ratio were analysed as described above.

◦ Optode calibration

A second experiment was conducted to evaluate impact of optical insulation on optode properties. Optodes were prepared according to results from development part. PtOEP and MY were mixed in a ratio 0.75%:0.75% (% in weight of silicone) together with TiO_2 (300 mg) and dissolved in silicone matrix (200 mg in 3g of chloroform). This sensor layer was coated with a 1 mil bar knife on a polyester foil. Different optical insulation layers were then applied to the sensor layer as summarized in Table 6. The optodes were again taped to the front plate of the rhizobox. Then, sensor calibrations were performed in water with a mix of N_2 gas and O_2 as described above.

Table 6: Summarize of oxygen optodes prepared for optical insulation study.
**Carbon layer is 2 mils thick.*

Foil	Sensor layer	Optical insulation*
NoC	1 mil	-
Nyl	1 mil	Nylon membrane
C0.5	1 mil	Carbon 0.5%
C1	1mil	Carbon 1%
C2	1mil	Carbon 2%
C10	1 mil	Carbon 10%

Results and discussion

The Figure 43 displays the R/G ratio image for each foil. Despite the noise of the picture, no reflectance or scattering light from roots were visible even for the foil without optical insulation.

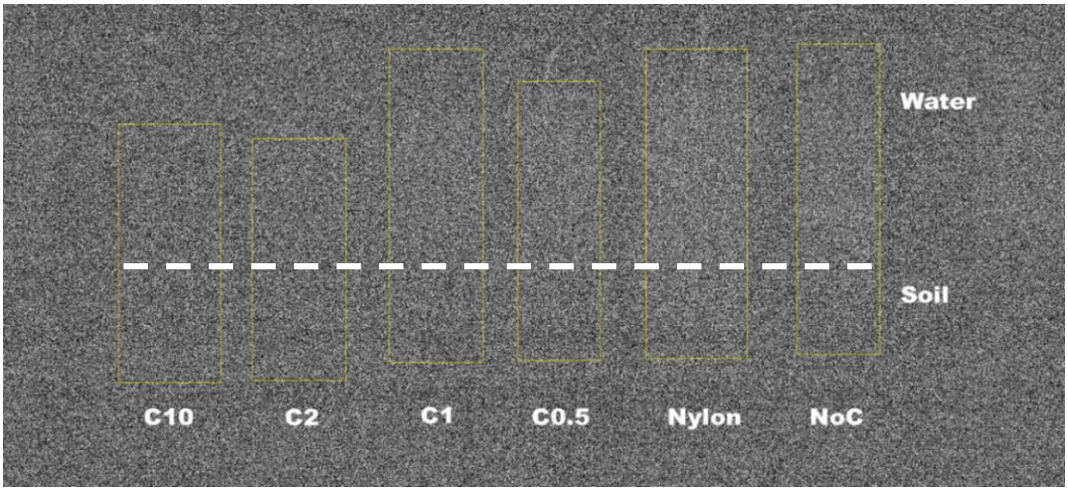

Figure 43: Image of Ratio Red/Green of each oxygen optode

Data were extracted from this picture and ratio values from soil and water part were discriminated (Figure 44). Due to the strong noise of the picture, it was not possible to extract the signal from roots. However, the ratio value from the soil area was much lower (up to 10-fold) than the signal from water (Figure 44). Soil absorbs more light whereas water with thin soil particles is more prone to scatter light. Also, as expected, the background signal was decreasing with carbon content in the silicon layer, even more so with water in the background. The silicon layer with 0.5 % of carbon emitted more light than polyester foil alone. This may be due to transparent silicon itself. The nylon membrane emitted the highest signal, similar to 0.5% carbon layer in water. However, it seems to better protect from the background heterogeneity than the 0.5% and 1% C layer as the signal difference between soil and water was reduced.

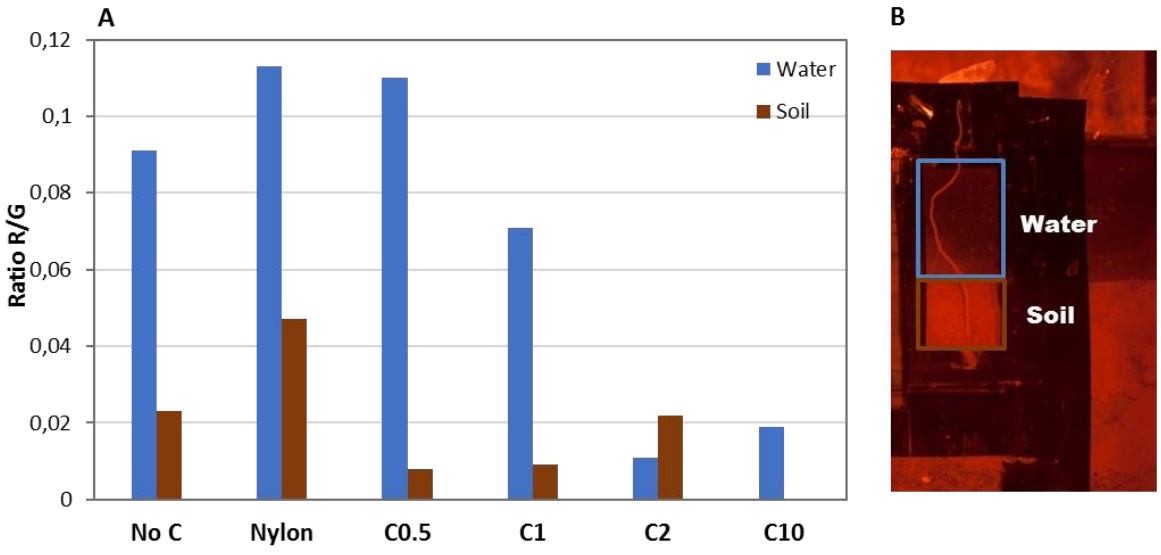

Figure 44: (A) Ratio R/G mean of water and soil area. (B) Drawing of water and soil area

The ratio value for each foil was below 0.12, whereas the calibration curve (Figure 45) indicated that the minimum ratio observed was around 1.5 at 100% air saturation. It means that the signal from the background was more than 10 fold lower than the lowest detected oxygen sensor signal. It was also noted that the calibration model curve was slightly impacted by optical insulation and all followed the Stern-Volmer model. In terms of ratio R/G used for calculation, values were similar regardless the optical isolation. However, we can see on the Stern Volmer plot (Figure 45.B) a shift of the quenching at oxygen content above 50% air saturation.

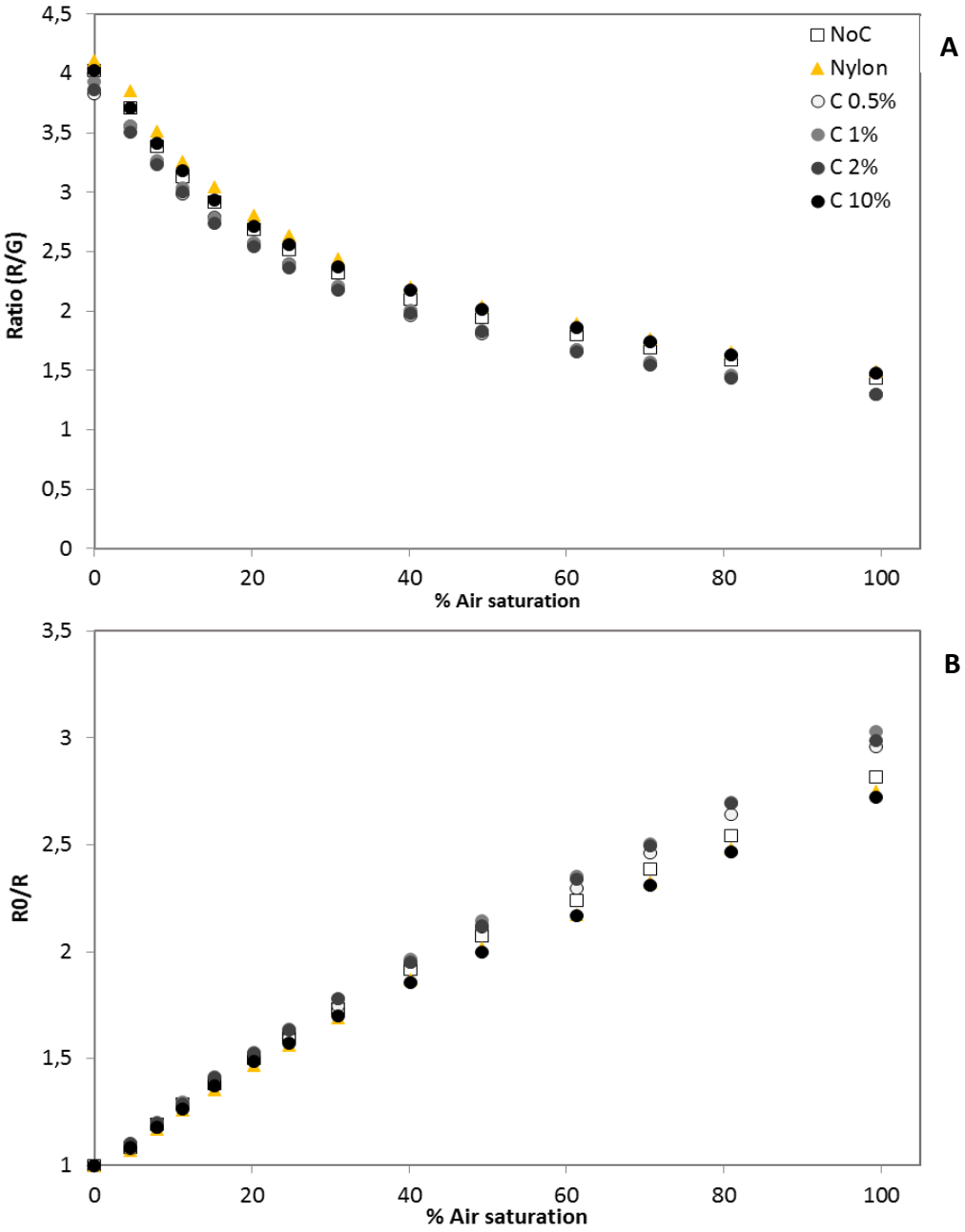

Figure 45: Calibration curve of optode NoC, Nyl, C0.5, C1, C2 and C10. (A) Calibration curve expressed from ratio Red/Green. (B) Stern-Volmer plot.

The shift was found to slightly influence the parameter α, but not the Stern-Volmer quenching constant K_{sv} (Table 7). Optode C0.5, C1 and C2 presented the lowest values of α and a more sensitive response to oxygen as shown by the Stern-Volmer plot (Figure 45).

Table 7: α and Ksv parameters describing Stern-Volmer model of optode NoC, Nyl, C0.5, C1, C2 and C10.

Optode	**NoC**	**Nylon**	**C0.5**	**C1**	**C2**	**C10**
K_{sv}	0.031	0.028	0.029	0.030	0.029	0.031
α	0.15	0.14	0.11	0.11	0.12	0.15

The standard deviation (SD) of the ratio value suggested a strong impact of optical insulation on signal homogeneity throughout the optode (Figure 46). Means and SD of R/G ratio were obtained with imageJ from a fixed ROI (Region of Interest) and the same size for each optode (42000 pixels). Nylon membrane presented the most homogeneous signal along the oxygen content increase, with a value close to the background signal measured in the previous experiment (R/G = 0.11 in water). Carbon coating at 0.5%, 1 % and 2% exhibited a higher SD. This might be of the carbon powder not being completely dissolved and therefore non-homogenously distributed during the mix preparation.

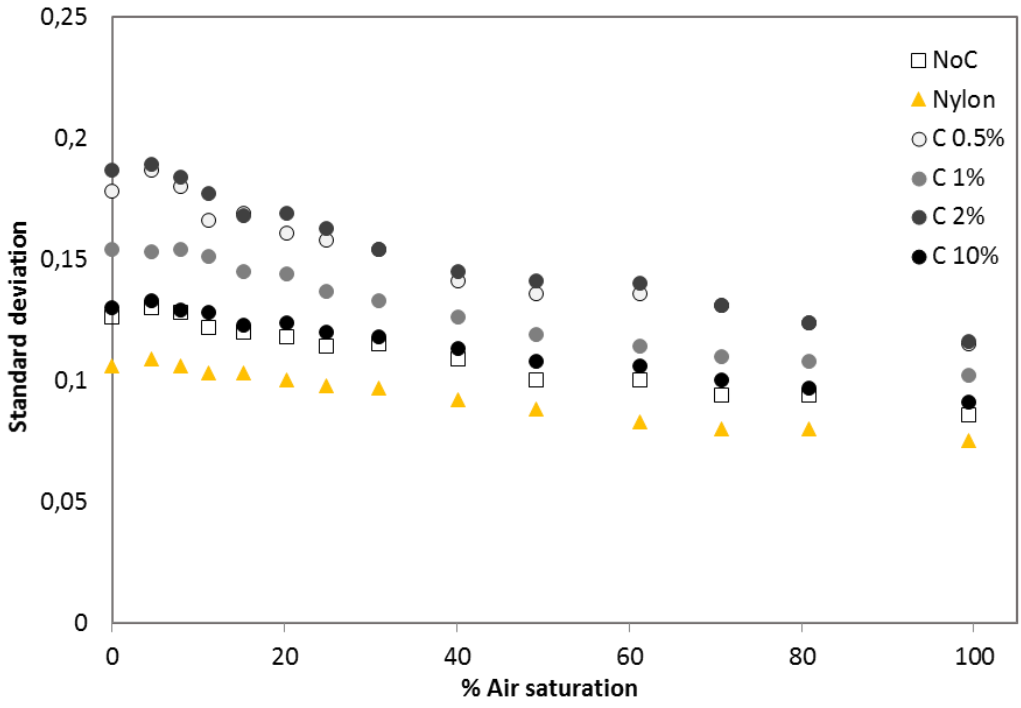

Figure 46: Standard deviation of ratio R/G values measured during the calibration.

These experiments gave us useful information about (1) background signal exhibited by roots, soil and water, (2) the requirement of optical insulation in this particular application, (3) properties of sensor foils combined with different kinds of optical insulation layer. The R/G ratio recorded from soil and water was low, at a similar or smaller level than the SD of optode signal. Consequently, the absence of an optical insulation might not be critical when optodes are used in such experimental conditions. However, depending on the structure of the sample behind the optode (e.g. soil) the background signal was quite heterogeneous. Therefore, a higher heterogeneity of the sensor (SD) was observed during calibration for optode with optical insulation at low carbon content. Even though nylon membrane emitted more light than other optical layers, it appeared to improve the homogeneity of the sensor. In addition, carbon coating might cause operator dependent artefacts for this application, as its coating on the sensor layer was not so reliable. Nylon membranes as an external layer can be easily applied in a rhizobox to ensure a better homogeneity of the background.

4.2.2. Lifetime in flooded soils

A lifetime study was conducted in rhizoboxes with flooded soil and the optodes were tested in combination with the previously tested optical insulation layers (NoC, Nylon, C0.5, C1, C2, C10). The objectives were (1) to determine how long an optode can be exposed to flooded soil without sensor degradation and (2) to investigate the role of optical insulation in protecting the optode from a potential degradation.

Materials and methods

The same optode/rhizobox setup as applied for the comparison of different optical insulations was used. After the calibration at day 0 in water, the front plate with optodes was applied on rhizobox filled with flooded soil during 28 days. The last day, the front plate was removed and optodes were gently rinsed with water to remove soil particles. Then a second calibration was performed. Between the first calibration at day 0 and the last calibration at day 28, a two-point control calibration was conducted in water at 0% and 100% air saturation once a week. For this purpose, the front plate with optodes was removed carefully and placed onto another rhizobox filled with water. After the two-point calibration, this front plate was re-applied to the soil rhizobox. Also, before removing the front plate from soil rhizobox, an image of optodes was taken. During the experiment, the rhizobox was covered with aluminum foil to protect the

optode from light exposure and avoid degradation by photobleaching of the fluorophores dyes. As for the previous experiments, two pictures were taken and then combined for analysis to ensure equal illumination of all tested optodes. Also, time series images were aligned to ensure analysis of a constant ROI (Region of Interest) over time. The workflow of the experiment is presented in the Figure 47.

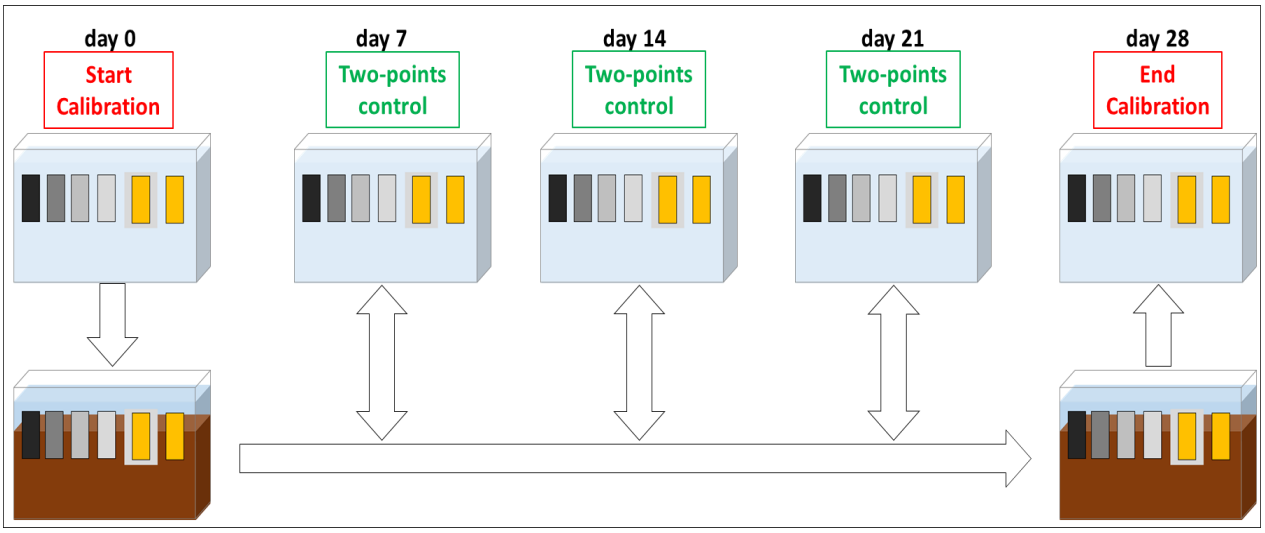

Figure 47: Workflow of oxygen optode lifetime study

Results and discussion

For each optode, the calibration model was determined at day 0 (model D-0) and day 28 (model D-28). From the model D-0, parameters α and K_{sv} were estimated. The model D-28 was fitted considering α being constant over time. This coefficient is dependent on optode construction and should be constant. For data analysis, we postulate that α is constant and evaluate optode lifetime based on the Stern-Volmer quenching constant K_{sv} variation after 28 days in flooded soil system. It means that the lifetime study was based only on variations of quenching efficiency as currently practiced in oxygen optode measurements even though optode degradation may affect theoretically the fraction of quenchable sensitive dye. Therefore, indicator and reference dyes may be degraded differently. Finally, the estimation error was also evaluated comparing oxygen estimation with the model D-0 applied to final calibration data (D-28).

The Stern-Volmer models from D-0 and D-28 calibrations were plotted for each optode (Figure 48). Two distinct trends can be observed. No shift of the curve was observed after 28 days for

optode without optical insulation and an external nylon mesh layer, in contrast to optodes with carbon coating at 0.5, 1 and 2%. The sensor with 10% carbon coating on the other hand did not present a shift after 28 days.

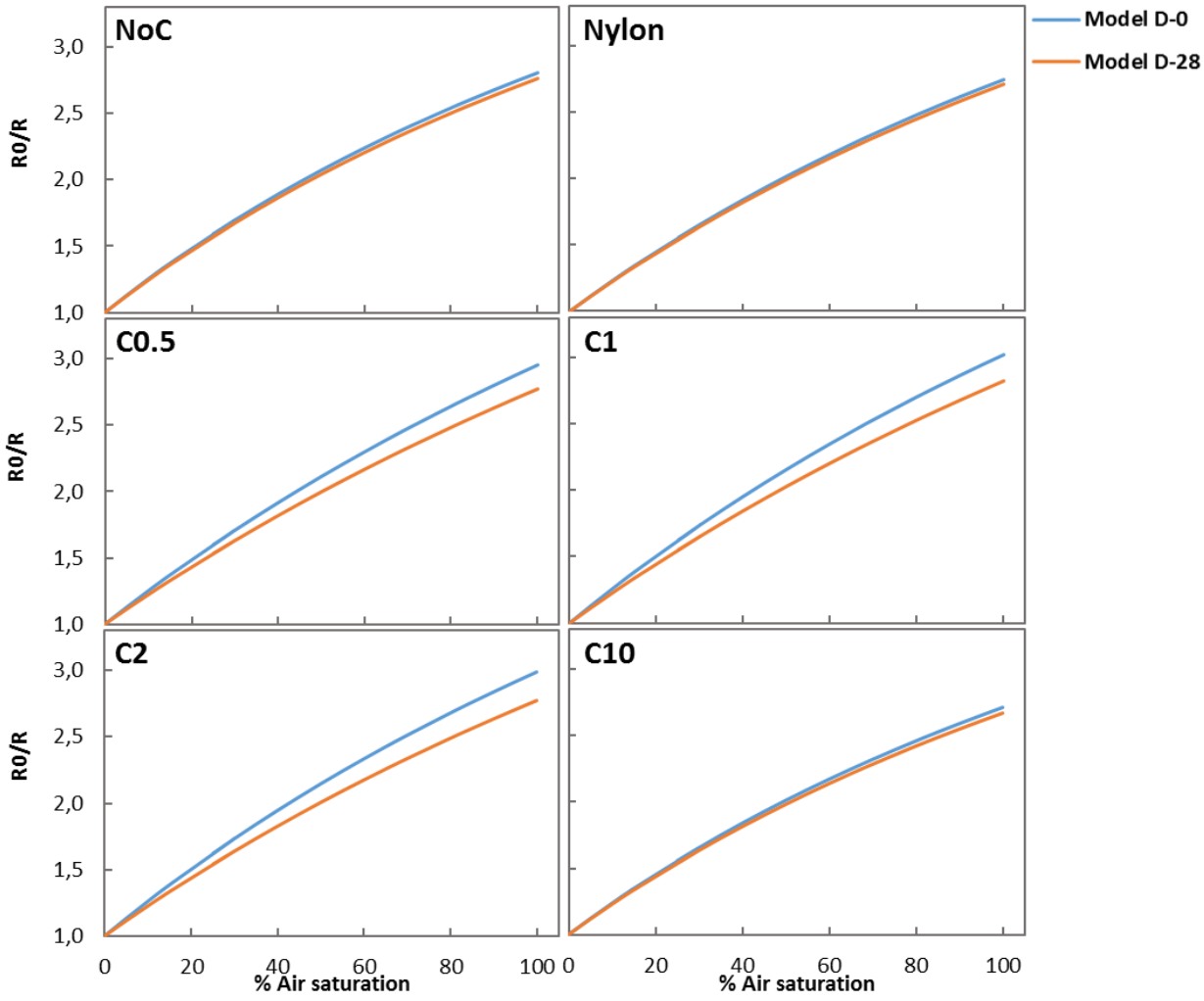

Figure 48: Stern-Volmer plot of NoC, Nylon, C0.5, C1, C2 and C10 optodes at Day 0 and Day 28 (R^2>0.998).

Quenching constant K_{sv} data plotted in Figure 49 confirmed the tendency observed above. A decrease of K_{sv} (up to 14%) after 28 days for C0.5, C1 and C2 can be observed whereas K_{sv} of NoC, Nylon and C10 presented only a slight decline (below 4%).

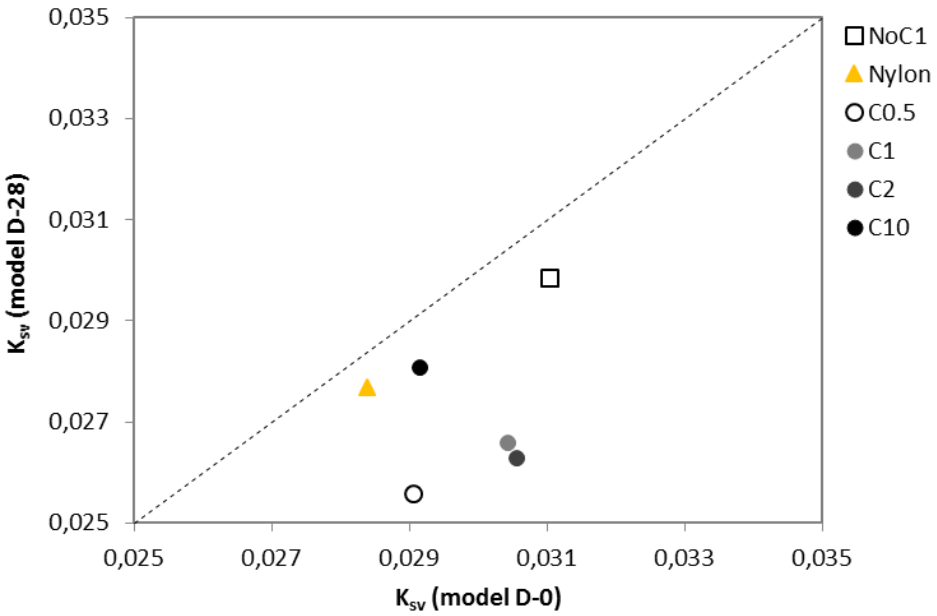

*Figure 49: Comparison of K_{sv} of model D-28 and model D-0. (Standard error was below 0.0008 for D-0 and 0.0002 for D-28***)**

Therefore, the estimation of oxygen concentration at day 28 with the model D-0 presented a negative bias as K_{sv} decreased (Figure 50). The accuracy error of oxygen concentration estimation at 28 days between model-D0 and model D-28 was found to be at 3.8%, 2.4% and 3.7% for NoC, Nylon and C10 respectively. The error was significantly higher for C0.5, C1 and C2 reaching 11.9%, 12.7%, and 14.1% respectively.

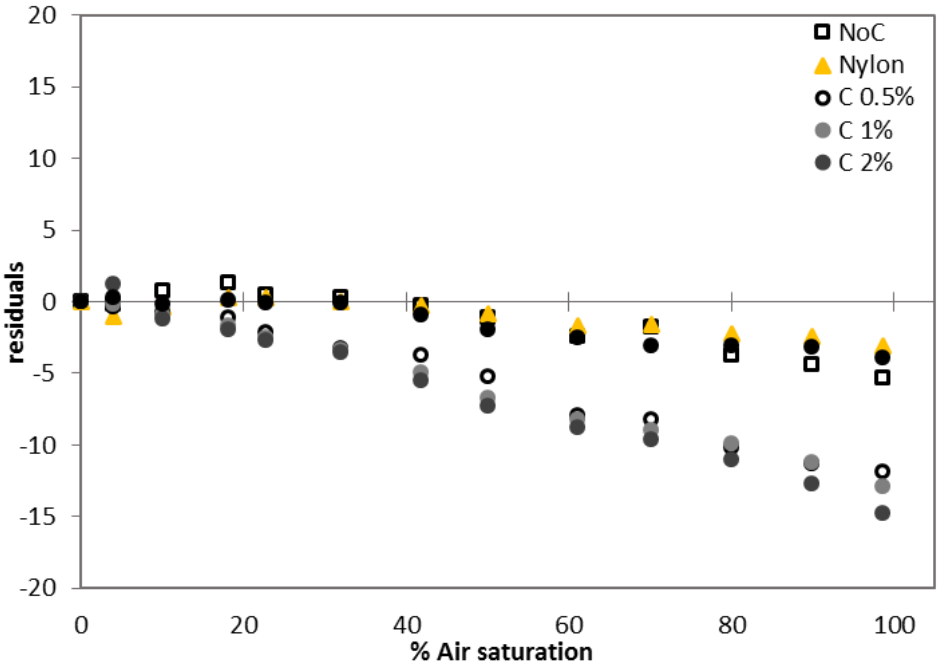

Figure 50: Residuals of % air saturation estimation with model D-0 after 28 days.

Finally, from the two-point control at 0 and 100% of air saturation, K_{sv} coefficient was calculated every 7 days (Figure 51). A major decrease of K_{sv} was observed at 7 days and at 20 days for C0.5, C1 and C2 optodes.

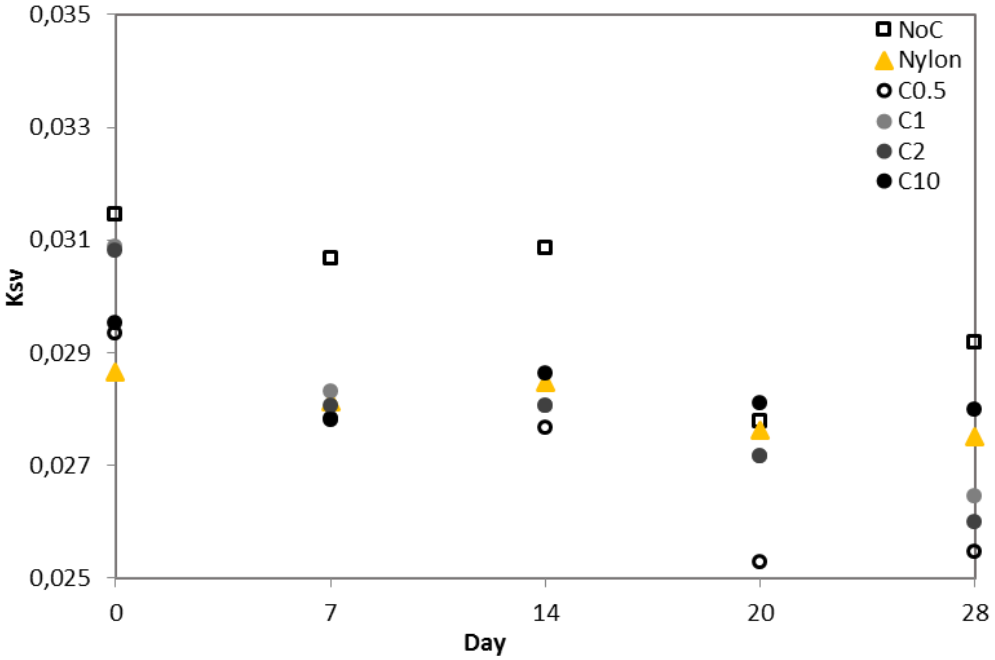

Figure 51: Temporal variation of oxygen quenching efficiency K_{sv}

To sum up, an optical insulation layer with 0.5 %, 1% and 2% carbon black presented a higher error of estimation after 28 days and a fast shift of K_{sv} (within few days). It led to an estimation error of oxygen concentration reaching up to 14%. Unexpectedly, the layer with 10% black carbon was less impacted compared to the optodes with low black carbon content. The absence of optical insulation did not lead to a strong degradation yielding only 3.8% of estimation error after 28 days which is similar to the optode with nylon membrane as optical insulation. A decrease of quenching efficiency can be due to optode degradation by photobleaching. However, C0.5, C1 and C2 were much more impacted than the other foils. In case of a too long light exposure time, each optode should be impacted more or less in the same way and even more for NoC and Nylon optodes. Another explanation might be the measurement environment. Soil is a living and complex media. In this experiment, the soil was in anoxic conditions and its carbon content was around 0.7%. Soil microbial activities might be enhanced at the surface of optode foil due to black carbon layer. However, this carbon was entrapped in silicon and should not be so easily available. Also, the 10% black carbon layer gave similar results as NoC and Nylon. Finally, it might be a combination of biotic and abiotic processes as well as biofilm formation as a thin film was observed on all foils after the experimental period. A previous

experiment carried out with a carbon graphite spray as optical insulation during 37 days in the same soil conditions showed a strong degradation of the carbon layer and thick biofilms on the foils (Figure 52). These degradations might modify biochemical processes close to the optode. The oxygen measurement was also much more impacted (data not shown).

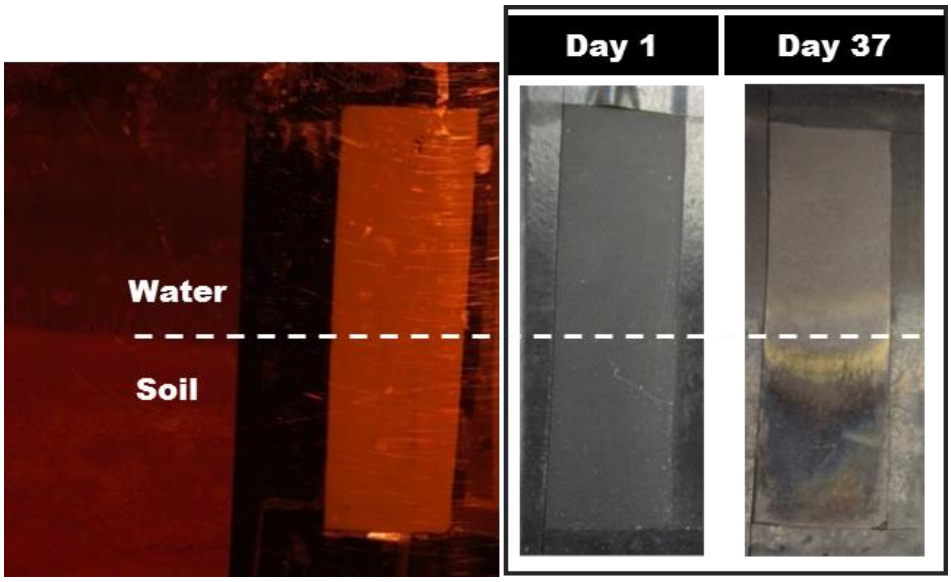

Figure 52: Picture of optode foil with carbon graphite spray layer, after 37 days in soils-water system.

To conclude, a long-term experiment in soil condition should be carried out with proper control of the optode performance over time. As the optode lifetime depends on its construction and on the measurement environment, it is necessary to evaluate a potential shift in the measurements over time in the same conditions as the experiment.

4.3. pH optode

4.3.1. Optical insulation

Materials and methods

The optical insulation of pH sensors was prepared with black carbon black mixed with sensitive and reference dyes dissolved in Hydromed D4 and ethanol. Fluorophore dyes were added to the optical insulation layer to avoid diffusion from the sensor layer to the optical layer. In gel matrices, dyes are physically entrapped and might slowly leach out. The mix was coated on the sensor layer with a 2 mils coating-knife. Black carbon black layers at 1% and 10% of Hydromed

D4 (w/w) were studied. Like for the oxygen sensor, the nylon membrane was also tested as external optical insulation.

◦ Background luminescence

To study the luminescence signal from soil and roots and the usefulness of an optical insulation, foils without sensor layer were prepared. Individual optical insulation layers only were coated onto the polyester foil. In contrast to the O_2 sensor, the optical insulation layers generally also contained fluorophore dyes. As the objective was to quantify luminescence only due to soil and roots, the optical insulations were prepared without fluorophore dyes. Thus, black carbon was dissolved in hydrogel solution and coated onto the polyester foil. Two levels of black carbon concentration were tested: 1% and 10%. Both foils were transparent to a different degree. The foils were stuck on a transparent front plate of a rhizobox together with two pieces of polyester foil. A nylon membrane, as external membrane, was applied on a piece of polyester foil. The other piece of polyester was used to mimic an optode without optical insulation (Table 8).

Table 8: Summary of foils tested for background luminescence study

Foil	Sensor layer	Optical insulation
NoC	-	-
Nyl	-	Nylon membrane
C1	-	Carbon 1%
C10	-	Carbon 10%

Behind each foil, a white rice root was carefully stuck with tape ensuring a good contact between root and foil. Then, the plate was screwed to a rhizobox filled with 2 mm sieved moist sandy soil (35% of gravimetric water content) (Figure 53).

The measurements were carried out by imaging with the optical set-up dedicated to the pH sensor (445 nm blue LED combined with 475 nm short pass filter and 495 nm emission filter).

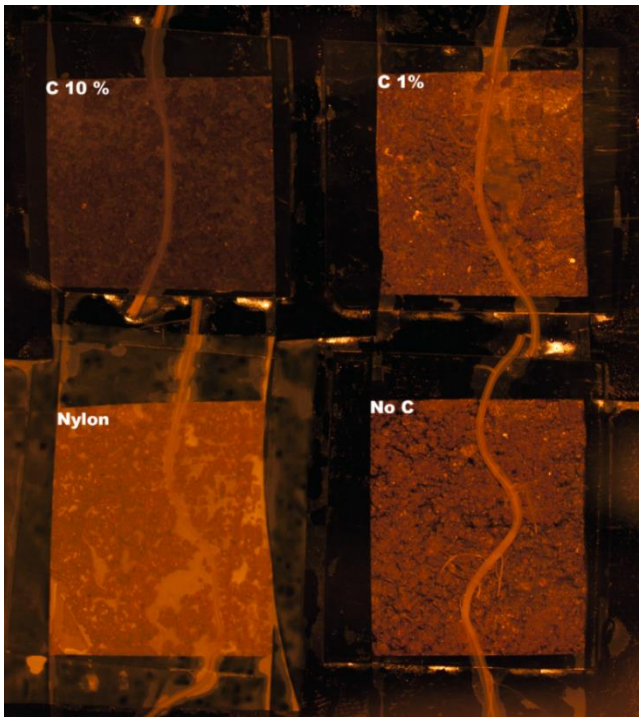

Figure 53: Foils without sensor layer, applied to soil and root.

◦ Optode properties with optical insulation

LO sensor foils were prepared with a 1 mil sensor layer according to the result of development part (pH probe DClFODA was mixed with ziegelrot in a ratio 1:10 and dissolved in hydrogel matrix) and a 2 mils optical isolation layer with carbon at 1% and 10%. One foil was also prepared without optical insulation layer. A piece of each foil was stuck onto the front plate as well as a piece of LO without optical isolation and one LO combined with nylon membrane (Table 9). Calibration of each foil was conducted in PBS (5mM, 60 mM IS).

Table 9: LO sensors prepared for calibration

Foil	Sensor layer	Optical insulation
No C	1 mil	-
Nylon	1 mil	Nylon membrane
C 1	1 mil	Carbon 1%
C10	1 mil	Carbon 10%

◦ Response time

Response time study was carried out with previous optode in PBS buffer (5 mM, IS 60 mm) during 45 min at pH 5.5 following by 45 min at pH 7.5. Imaging was performed every minutes.

Results and discussion

The Figure 54 and Figure 55 present the response time of LO for each optical insulation condition with details of Green and Red channels (Figure 55) and ratio values (Figure 54). The response time t_{95} was found to be around 3 minutes, regardless the optical insulation. So, the presence of a thin optical insulation or an external membrane did not seem to change the response time of the LO sensor. The short response time also fitted the needs for soil application.

As we can see in the Figure 54, the ratio value at pH 7.6 varied with optical insulation. Nylon foil presented the lowest ratio value at pH 7.6 while C10 reached the highest ratio values, fairly close to those of No C which was unexpected.

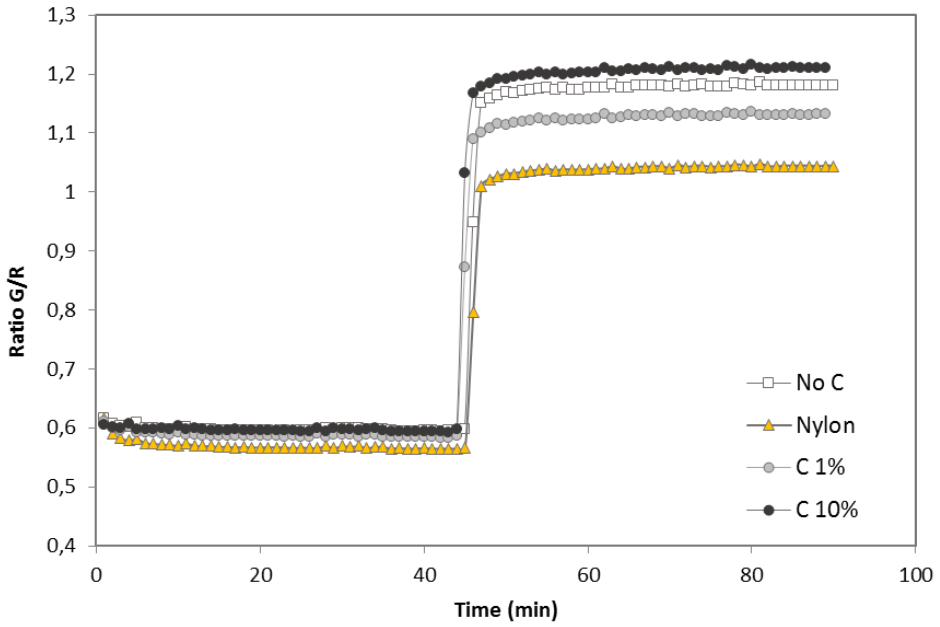

Figure 54: *Response time curve. Ratio value of G/R for each LO.*

Green and Red individual channel results (Figure 55) gave some interesting information about properties of each foil. Nylon foil emitted more light in both channel whereas C1 and C10 emitted much less in both channels. The foil without optical insulation was in between carbon coating and nylon membrane in terms of luminescence intensity. Black carbon could absorb

light emitted by the sensor layer or scattered by the buffer solution. High signal intensity of Nylon foil could be explained by the properties of light scattering of white nylon membrane.

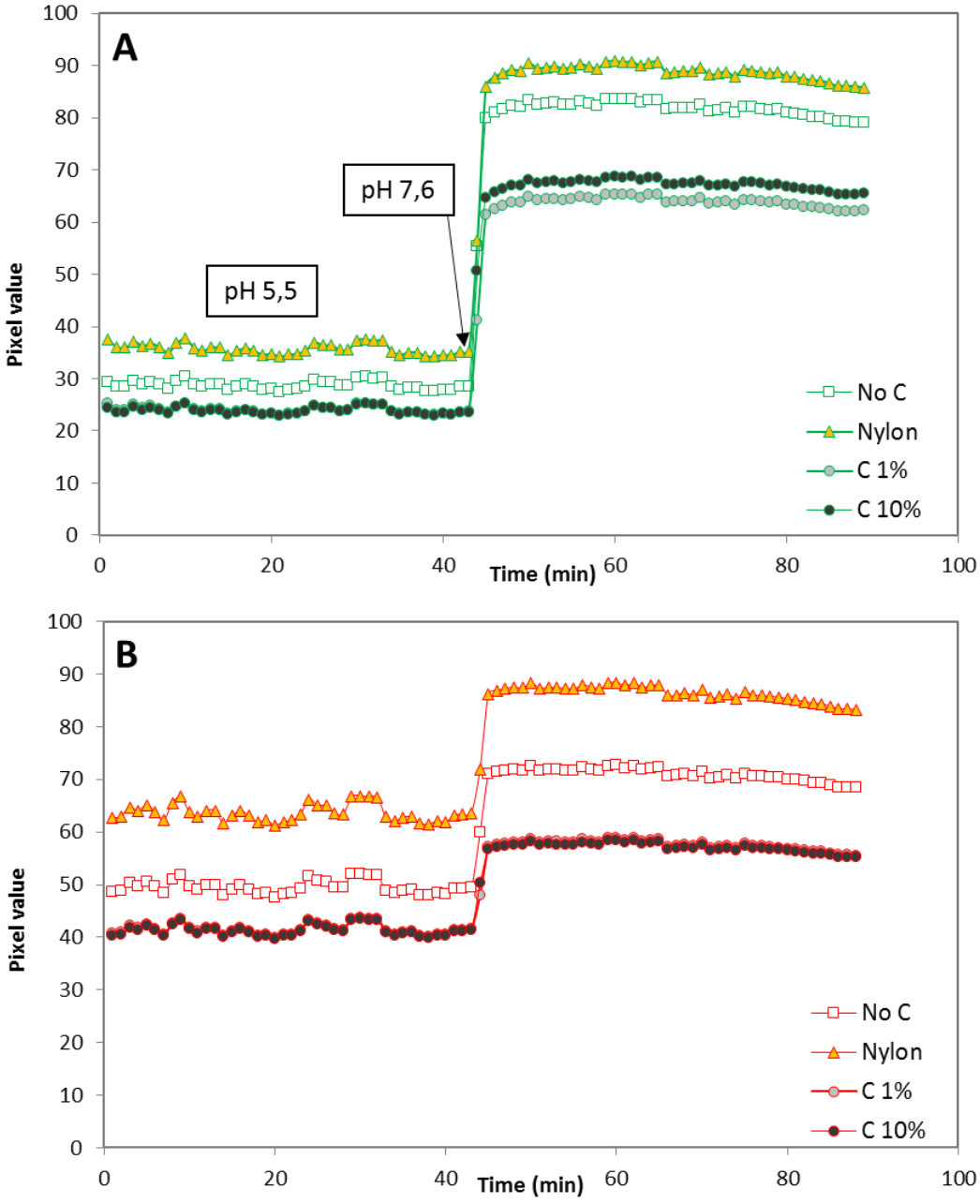

Figure 55: Response time curve. Intensity pixel of Green (A) and Red (B) image.

The calibration curve, displayed in the Figure 56 shows that whatever the optical insulation, the model fitted the Boltzmann equation (R^2>0.999). It confirms the difference of sensitivity observed in the time response study with pH increase. The asymptote at the highest pH (Rmax) was much lower with nylon membrane. However, the dynamic pH range, between pH 5.5 and

7.5, and pKa' was not affected by any optical insulation (Table 10). Each optode configuration could be applied even though the nylon membrane as optical insulation decreased significantly the optode sensitivity.

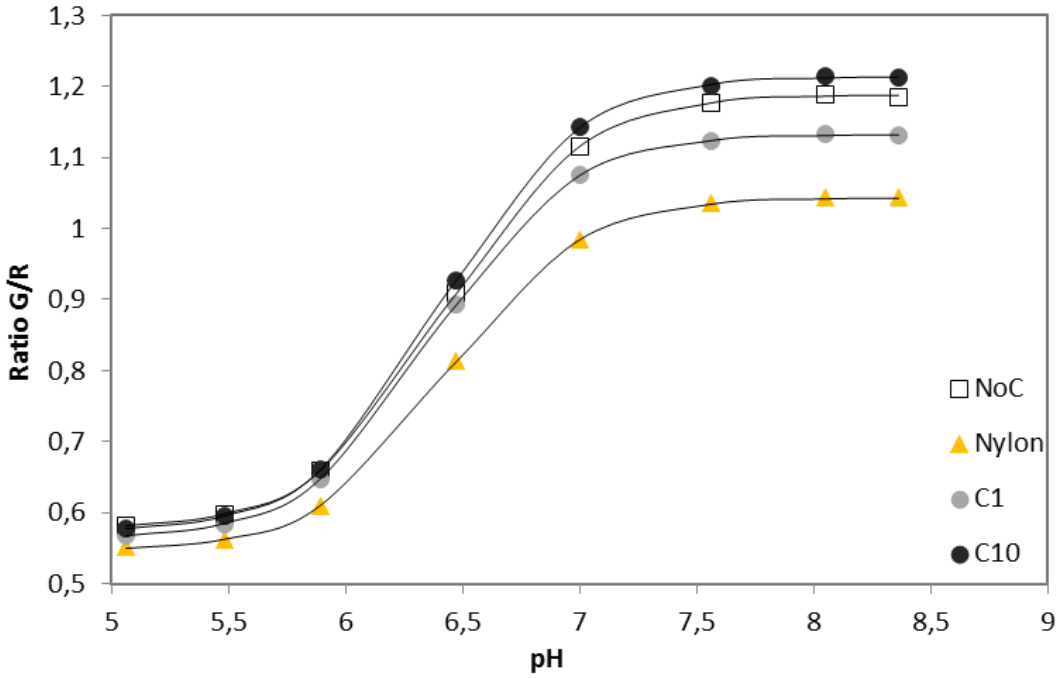

Figure 56: Calibration curve of NoC, Nylon, C1 and C10 foil. Error bars are smaller than symbol size (n = 52900 pixels for NoC, C1, C10 and 50600 pixels for Nylon)

Table 10: Boltzmann model parameters of NoC, Nylon, C1 and C10 optode. (errors standard of pKa' are under 0.004 unit)

Foil	pKa'	dpH	R_{max}	R_{min}
NoC	6.42	0.29	1.188	0.576
Nyl	6.43	0.28	1.044	0.544
C1	6.38	0.28	1.131	0.562
C10	6.41	0.28	1.214	0.572

The background luminescence study was carried out for soil and roots. Figure 57 displays the image of Green/Red ratios (G/R) of the optical insulation foils applied on soil and roots. As evident from this figure, white roots were visible for each optical insulation with a slight attenuation with carbon at 10%.

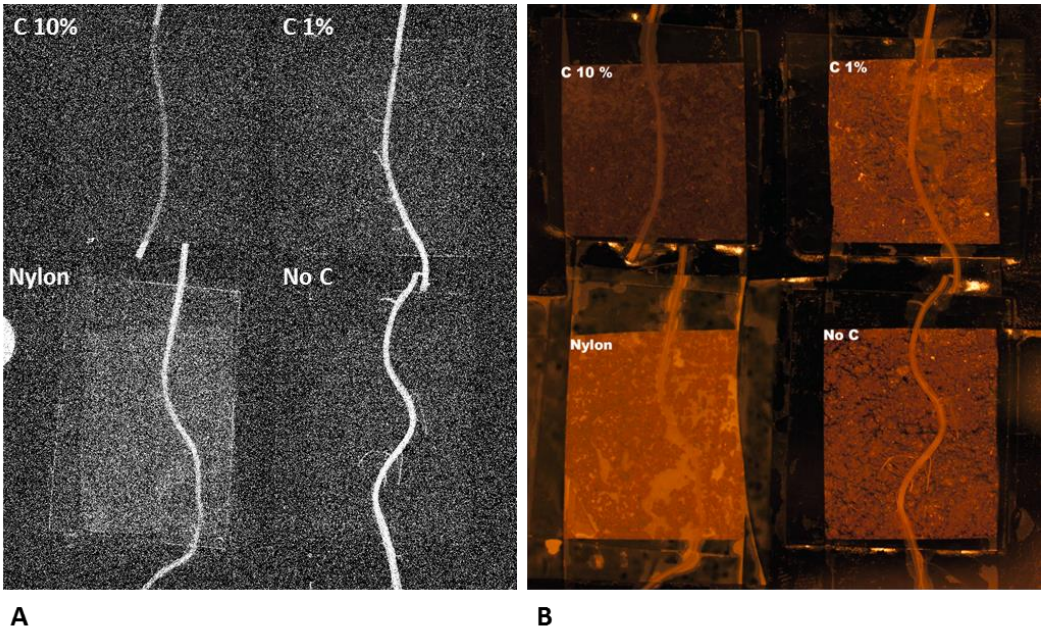

Figure 57: Background luminescence study. (A) Ratio G/R calculated picture. (B) Image of foil on soil-root system.

Ratio values were extracted from the picture with discrimination between root parts and soil parts. Data are shown in Figure 58. The signal from roots was up to 10-fold higher than soil luminescence. Also, the ratio value from roots was decreasing with increasing carbon content in the optical insulation layer. Signals from roots with nylon membrane were higher than carbon at 1% but lower than in absence of optical insulation

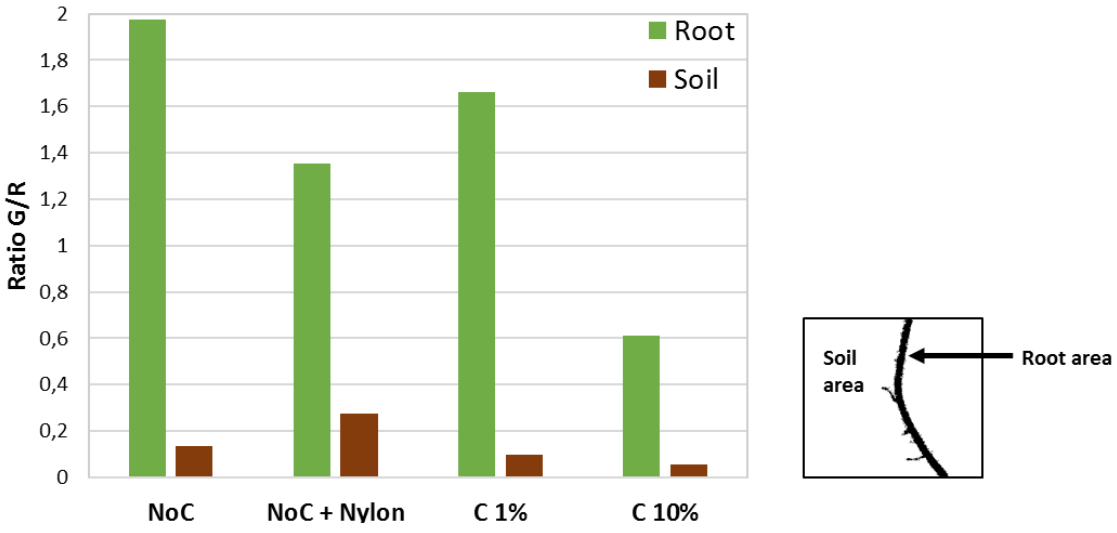

Figure 58: Ratio values of root and soil structures, extracted from ratio G/R picture with ImageJ by threshold.

Whatever the optical insulation, G/R ratio of root structure was above the ratio typically measured in buffer solution at pH 5.5. As a matter of fact, R/G ratios of the calibration curve generally ranged between 0.5 and 1.2; the ratios corresponding to the root part varied from 0.6 for 10% carbon to 2 without optical insulation. We can therefore expect a strong shift of pH only due to root luminescence during soil-root pH imaging. In contrast, luminescence from soil background was low, with a G/R ratio below 0.3 and a decrease with increasing carbon content. A higher ratio with nylon membrane was also observed, however it was still below the calibration range.

Our results show that none of the tested optical insulation approaches would efficiently protect from background heterogeneity and luminescence of root structures. Optical insulation with more opaque properties would be needed for experiments with roots as it might influence ratio values and, thus, obtained pH results. Nylon membrane and carbon at 10 % were not sufficient to limit background luminescence and its heterogeneity. To overcome this issue, two solutions could be applied. To suppress background signal, opaque optical insulation could be used. However, root visualisation would not be possible. Another possibility could be to change the ratio calculation from G/R to R/G as the background signal was much more pronounced in the Green image.

As observed in Figure 59, R/G ratio calculations drastically reduced background signals from roots and gave a value closer to soil, below 0.6. Nylon membrane presented a root signal similar to and a soil signal higher than that of the carbon layers. The difference between soil and root signals was the lowest with nylon membrane. The heterogeneity induced by roots was strongly reduced by nylon membrane. Even though luminescence of the background was strongly diminished, root patterns were still visible (Figure 59.A). Carbon coating at 1 % and 10 % did not yield to a homogeneous background signal. The use of nylon membrane combined with R/G ratio led to a slightly lower signal ratio from roots and above all was less heterogeneous between soil and root structures.

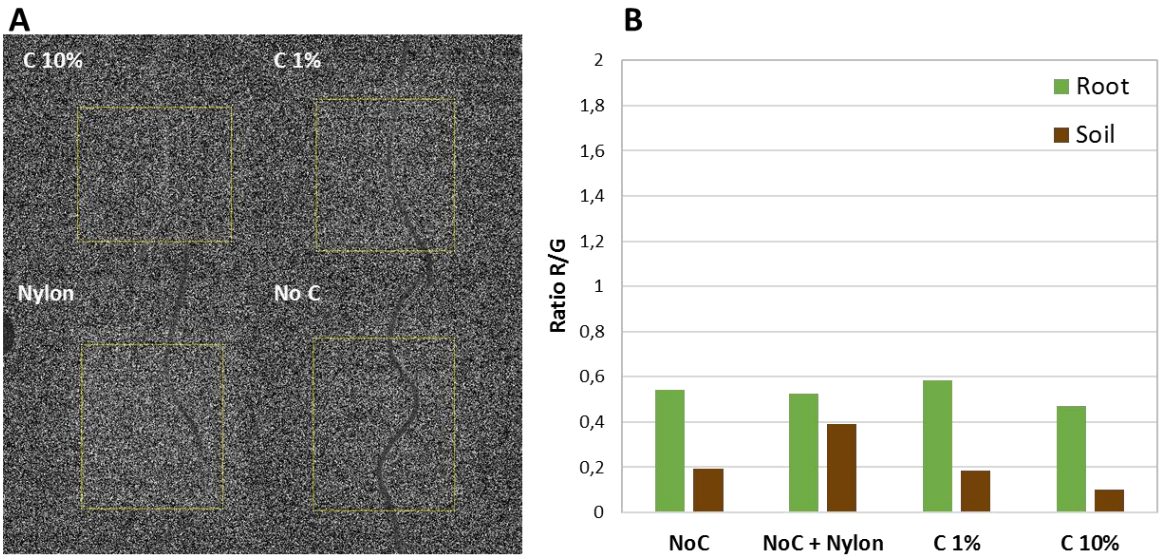

Figure 59: Application of ratio Red / Green. (A) ratio image (B) graph of R/G ratio values of root and soil structures

Then, R/G ratio was successfully applied to calibration data as presented in Figure 60. The relation between R/G ratio and pH was well described by the usual sigmoidal model (R^2>0.999). This calculation was found to mitigate the differences between the sensor combined with different optical insulation layers (Figure 56 vs Figure 60). Based on R/G ratios, carbon coating and NoC presented similar calibration curve. Also, the sensitivity of the Nylon foil was not impacted contrary to the calibration described from G/R ratio.

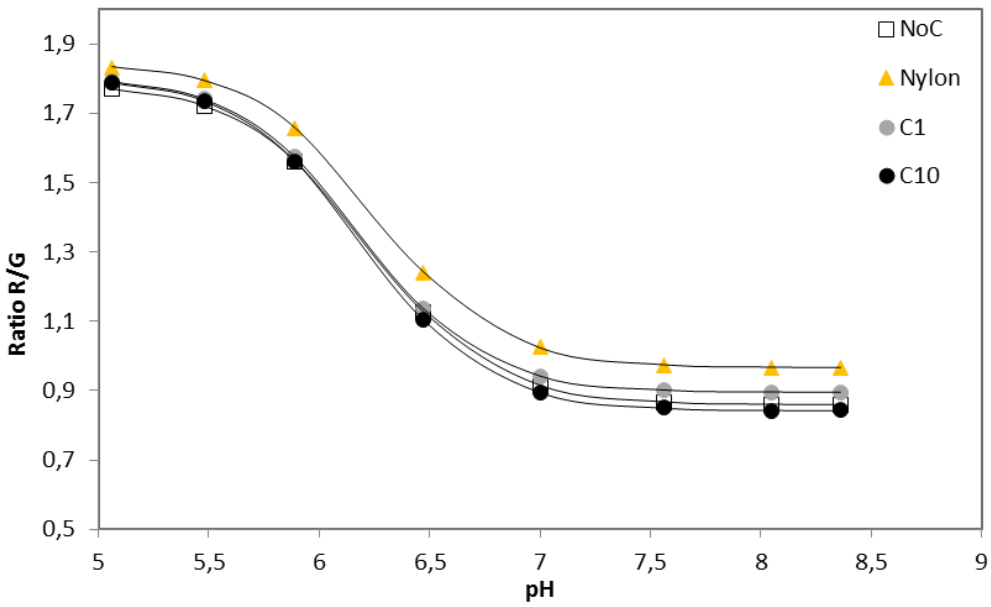

Figure 60: Calibration curve of NoC, Nyl, C1 and C10 foil expressed from Red/Green Ratio

Data in Table 11 suggest that pKa' were comparable between foils as it was observed for calibration from G/R ratio values. However, the calibration model from G/R ratio value estimated a more acidic pKa', with 0.2 unit of difference. This means that calibration curve presented a slight shift towards acidic pH values.

Table 11: pKa' value estimated from R/G and G/R calibration. (Errors standard are under 0.004 unit)

Foil	pKa' (R/G)	pKa' (G/R)
NoC	6.21	6.42
Nyl	6.25	6.43
C1	6.19	6.38
C10	6.19	6.41

Optical insulation study for LO sensor showed that roots might enhance the G/R ratio value and produce an unwanted heterogeneity. This will affect obtained pH results in soil-root experiments. As a result, optical insulation needs to be added to the sensor layer to avoid a significant background signal. None of the tested insulation layers (C1%, C10%, nylon) were sufficiently efficient to reduce root luminescence, reflectance or light scattering. An inverse calculation of the currently used pixel ratio was then applied to limit background effects. This G/R ratio calculation drastically decreased the luminescence signal from roots and attenuated the heterogeneity of soil and root structures. Even though it did not suppress the background signal, nylon membrane was found to produce greater background homogeneity, as well as a higher absolute luminescence intensity based on G/R ratios. This external membrane might be a good alternative to an opaque optical insulation for LO sensor, as for oxygen sensor.

Our results demonstrate that it is advisable to check the luminescence of the background before using transparent optodes prior to new experiments and adapt the experimental design if required. Finally, further investigations should be conducted to quantify the impact of reflectance and luminescence of roots on pH estimation.

4.3.2. Soil water content

The objective of this study was to determine the effect of soil water content on LO optode reactivity in terms of time response and signal quality.

Materials and methods

The experiment was conducted in rhizoboxes carefully filled with a sandy soil (Siebenlinden, Austria) sieved down to 2 mm. The slightly acidic soil was previously mixed with 2.5 $g.kg^{-1}$ of $CaCO_3$. Rhizobox were incubated for 9 days prior to optode application. Water content was controlled by weighing and adjusted by addition of water in to the rhizobox. One piece of optode (2 cm x 2 cm) was stuck with black tape onto the front plate and the soil was covered with a nylon membrane (Figure 61).

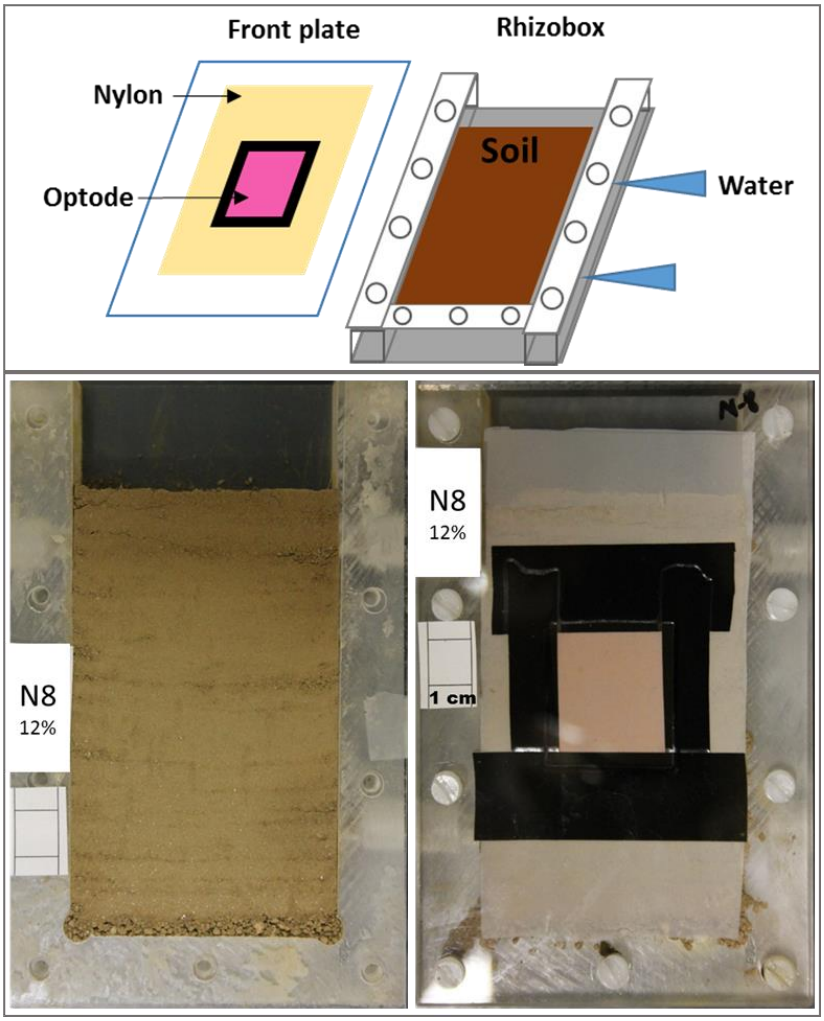

Figure 61: Drawing of rhizobox with soil and optode (upper diagram) and photograph of one rhizobox before measurement.

Optodes were imaged at 30 min, 1h, 2h, 4h and 21h after the application of the front plate. Rhizoboxes were protected from light and placed upside down in between the measurements to ensure a good contact between optodes and soil. Six levels of water content were studied ranging from dry soil to the maximum water holding capacity (MWHC, in weight content): 5%, 12%, 49%, 76%, 88%, 97% of MWHC. It is important to note that it was not possible to study the full range of water content in one experiment due to technical problems. Measurements of 88% and 97% of MWHC were conducted in a second experiment under the same experimental conditions. However, the soil mixed with $CaCO_3$ was incubated longer for the second experiment prior to rhizobox filling. The first experiment will be noted as Exp I and the second one as Exp II.

Results and discussion

To perform image analysis, pictures of each time series were aligned beforehand and the same size of ROI was analyzed (250 x 250 pixels equal to 3 cm^2). Images with pixel values were transformed to pH images using calibration parameters (data not shown). Figure 62 displays images of the time series in pH values measured at various water content.

First, it can be observed that black pictures were obtained for 5% of MWHC (equivalent to 2% of gravimetric water content). At this very low water content, more than 95 % of pixel values were outside the calibration range and could not be transformed in pH value. This can be attributed to the dryness of the soil. At a such low water content, the contact between optode and soil is likely to be very limited. The hydrogel requires water to swell which is a prerequisite for proton diffusion across the sensor layer. Images with a higher water content (> 12% of MWHC) suggest a water content dependent change in obtained pH signal over time. Significant pH differences were observed between water content levels, up to 0.5 pH unit at t = 1h. We found an increase of pH with increasing water content and over time. Even though signal homogeneity seemed to improve with the contact time, the RSD (calculated on 62500 pixels) was below 3% for Exp I and 5% for Exp II and was constant over time.

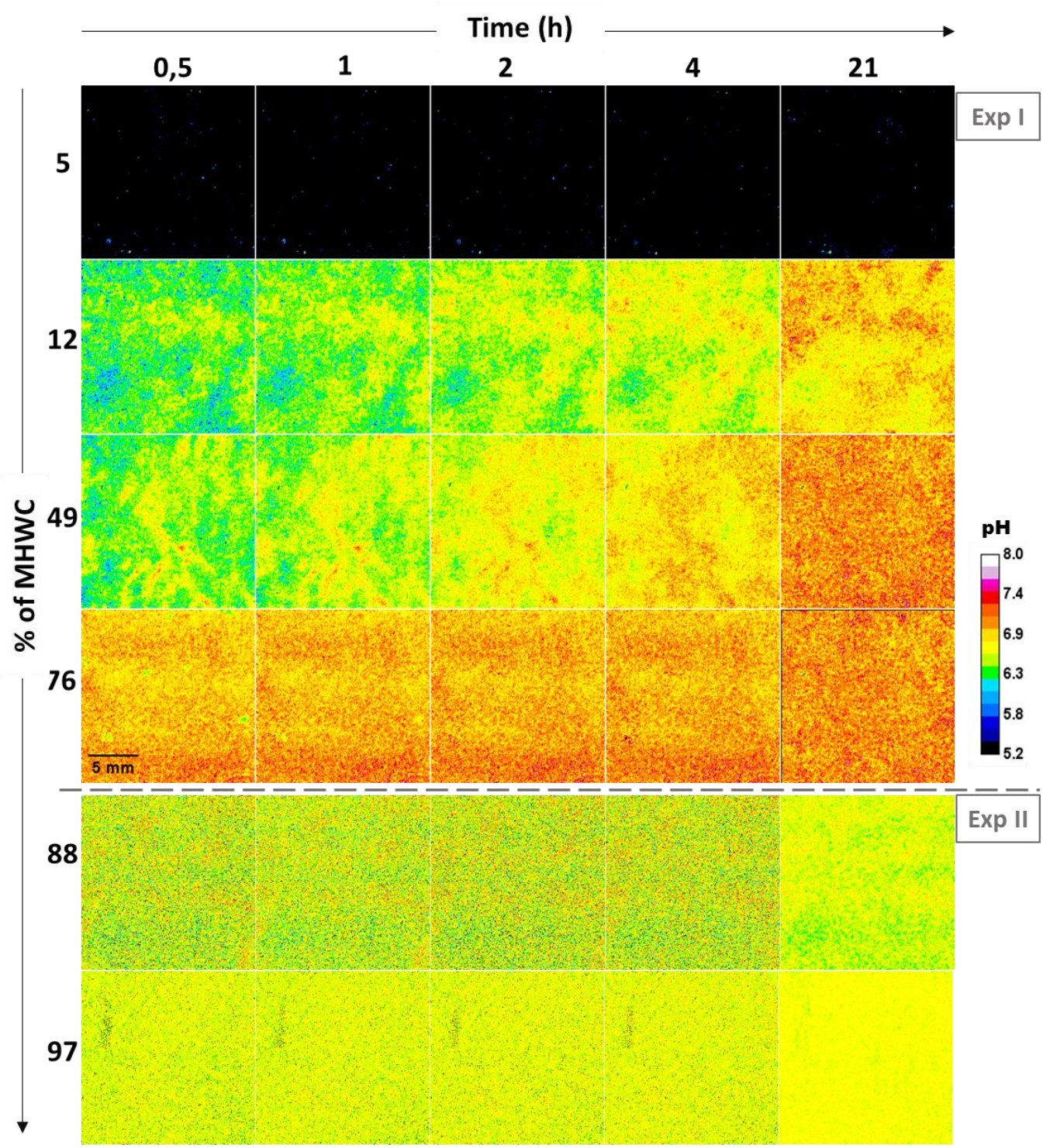

Figure 62: Time series of pH images of Exp I, from 5% to 76% of MHWC, and Exp II (88% and 97% of MHWC)

In Figure 63, pH results (mean ± SD) of each picture were plotted against contact time. Values from Exp I and Exp II were represented separately as they were not conducted together at the same time.

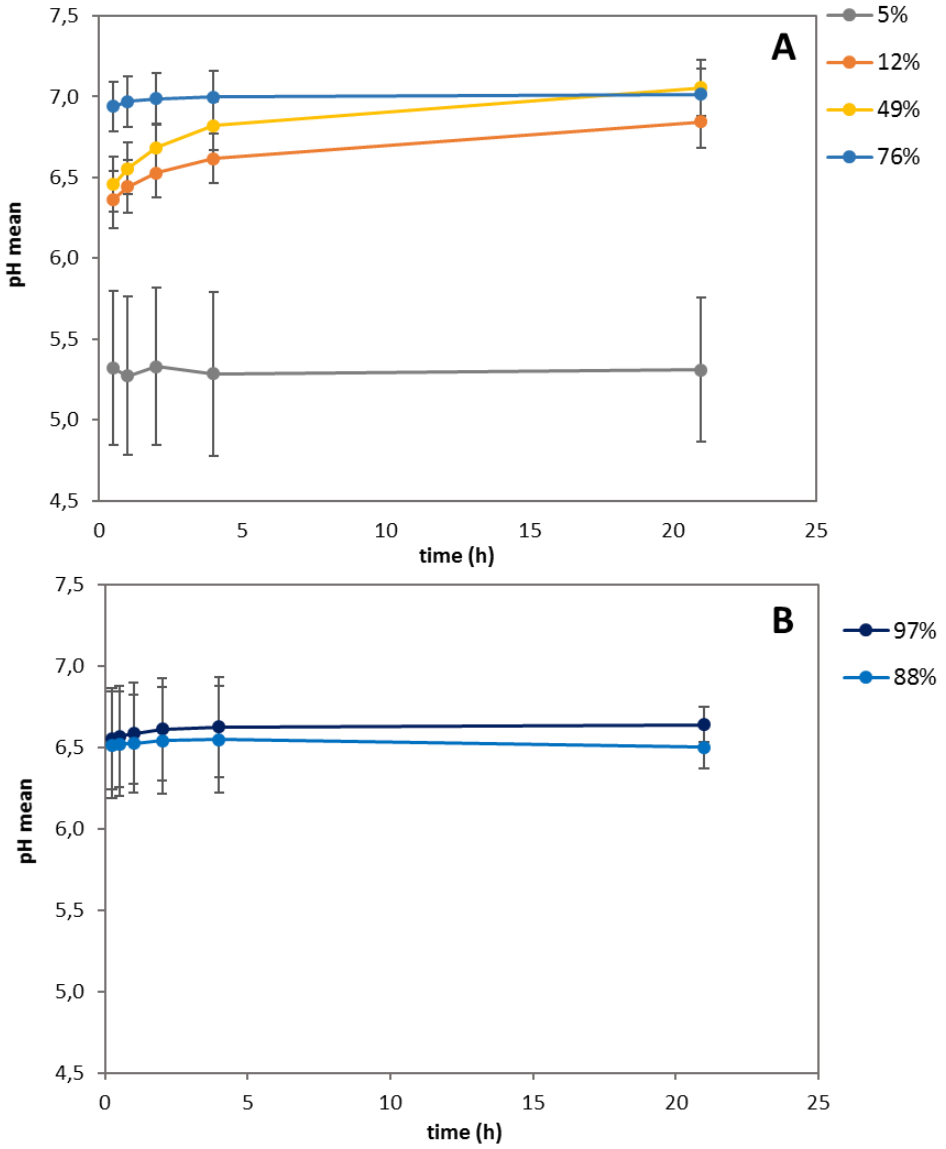

Figure 63: pH changes over time, for each water contact. (mean of 62500 pixels, with SD). (A) Exp I: 5% to 76% of MWHC. (B) Exp II 88% and 97% of MHWC.

These data confirm the observations in the images, with pH increasing with increasing water content and over time. An increase of pH with water content (Exp I) might be explained by a lower concentration of protons as H^+ released in the soil solution are more diluted at higher water content. Alternatively, this could be due to an indirect effect of water content on microbial activities responsible for soil pH changes. Also, it can be noted that a shorter time to reach stability was needed at a MWHC above 76% (Exp I and II). Above this threshold, the averaged

pH was stable after 30 min, with an absolute pH change less than 0.1 pH units. At 49% of MWHC, the pH change between 30 min and 21h amounted to 0.6 pH units. Finally, after 21h, the measured pH means were 6.85, 7.06 and 7.01 for 12%, 49% and 76% of MWHC respectively. This experiment suggested that optode measurements at changing water content in soil may lead to inaccurate pH results for short term application times and results may not be comparable. The contact time before measurement should be fixed and similar for all optodes applied in a given experiment. This also means that a strong change of water content during a long-term experiment might induce artefacts in obtained pH results. Finally, optode application is not possible at very low water content, far from soil saturation.

This experiment can be considered as an interesting preliminary study which gave us useful tips about application conditions of planar optodes in soils. However, it might be relevant to repeat it, covering the full range of water content with replicates in a single experiment to confirm these results. Also, this trend might be different for soils with different properties (e.g. clayey or sandy soil).

5. Optode development: conclusion

The objective of this development work was to design reliable protocols for oxygen and pH optode construction for soil system application. Based on the initial optode batch produced by Sergey Borisov, we were able to improve the recipe when needed and to produce a finalized protocol.

Oxygen sensor

First, we investigated two references dyes from the Coumarin class, a novel one Bu3Coumarin (Bu3C) and the commonly used Macrolex Yellow (MY). Bu3C presented a higher luminescence compared to MY. However, the quenching efficiency was similar for both optodes especially at low oxygen content. MY was then considered fully adapted for our further applications as it is commercially available. In a second development step, the addition of titanium oxide as brightness enhancer was studied. Titanium oxide was either added directly to the sensor layer or applied as a silicone supplement layer coated on top of the sensor layer ("white wall"). Both applications worked well. The supplement layer brought very bright

images, with an increase of luminescence on the Green and Red channels. However, the channels were oversaturated whereas embedding titanium oxide into the sensor layer gave us more balanced histograms of obtained images (see section 2.3). Also, the quenching efficiency was strongly reduced for optodes with a "white wall". Consequently, titanium oxide was used as an addition to the sensor layer which also facilitates the optode construction procedure as only one layer needs to be coated. Finally, sensitive dyes and sensitive/reference dyes ratios were explored. Two luminescent metalloporphyrin-based oxygen probes were compared, PtTFPP and PtOEP. They were combined with MY at 1:1 and 1:2 ratios (w/w of sensitive dye/reference dye). All combinations worked well and could be used as oxygen sensor. However, PtOEP presented higher luminescence intensity as well as an improved sensitivity for oxygen compared to PtTFPP, at both sensitive dye/reference dye ratios. Therefore, equal concentration of reference and sensitive dye was found to be a good balance as the ratio 1:2 did not improve the sensitivity of the sensor but requires more fluorophore, which raises construction costs. Thus, the final oxygen sensor recipe was a combination of PtOEP (oxygen sensitive dye), MY (reference dye) and titanium oxide nanoparticles embedded in polystyrene matrix. The detailed protocol is presented in appendix 3. Also, important information about titanium oxide are given in appendix 2, as additional experiments revealed that not all commercially available titanium oxides are suitable for optode applications. A supplement test with two different titanium oxide products showed a strong impact on optode luminescence (Appendix 2).

Oxygen optode adaptations to soil environments were firstly focused on the importance of optical insulation. Carbon layers at 0.5%, 1% ,2% and 10%, and an external white nylon membrane were studied. Autofluorescence of roots and soil was low compared to optode luminescence intensity. In addition, it shall be stressed that light scattering from water resulted in a signal ratio increase up to 10-fold to that of soil. As expected, the increase of carbon content in the optical layer led to a decrease of background signal ratio. However, signal from water and even more so from soil was low compared to optode luminescence intensity without optical insulation. The absence of optical insulation might thus not be critical. Nevertheless, nylon membrane was found to improve homogeneity of the signal ratio from the background and to keep optode performance unchanged while still being semi-transparent and allowing the observation of root growth. Ultimately, optode lifetime was studied in the absence and presence of optical insulation (carbon layers 1%, 10% and nylon membrane). The optode with nylon membrane was the least impacted by a four-week exposure time to flooded soil, similar to what

was observed in the absence of optical insulation. In contrast, optodes with low black carbon content coated in an additional silicone layer onto the sensor layer showed a greater decrease in sensitivity. This lifetime study demonstrated that long-term optode measurements in soils require a careful quality control of optode performance during the experiment.

pH sensor

pH sensor development was focused on two fluorophores with a different pH range. Starting from a first batch proposed by Sergey Borisov, further investigations and modifications were carried out.

The Low pH sensor (LO) was based on a modified fluorescein pH probe (DClFODA) combined with a non-sensitive dye ziegelrot. It presented a reliable pH range from 5.5 to 7.5 with a pKa' at 6.5. We tested the impact of the thickness of optode's constitutive layers (i.e. sensor layer and optical insulation layer) on response time, varying from 2 minutes to 20 minutes. Also, the increase of sensor layer thickness did not lead to an increase of signal ratio. Therefore, the thickest optode presented the lowest sensitivity to pH changes. Like for the oxygen sensors, titanium oxide was tested as a brightness enhancer. We observed that titanium oxide could lead to photobleaching in absence of a black optical insulation supplement layer. It might also interfere with obtained pH results as the optode without titanium oxide presented a higher ratio change with changing pH. LO sensors were finally prepared with a 1 mil thick hydrogel sensor layer containing DClFODA (sensitive) and ziegelrot (reference dye) at a 1:10 ratio with no titanium oxide added.

LO optode adaptation to soil applications was first focused on the importance of optical insulation. A supplement carbon layer (1% & 10% black carbon) and an external nylon membrane were tested as optical insulation. We found that the background signal from roots was higher than optode luminescence applied. None of them proved sufficient to reduce the background signal from roots to an acceptable level, below the lowest luminescence signal of the sensor. To avoid the use of non-transparent black optical insulation, another ratio calculation was applied reducing the impact of the high signal observed on the Green channel. The application of Red/Green instead of Green/Red drastically lowered the background signal and the background signal heterogeneity. When applying the new ratio calculations (Red/Green), nylon membrane presented the most homogeneous signal as optical insulation layer. The shape of the calibration curve was not influenced by the application of nylon membranes; however,

the new ratio calculation was found to slightly change the optodes' pH range towards more acidic pH values, from 5 to 7.5, instead of pH 5.5 to 7.5. Our results highlight the importance to check the background luminescence intensity before every experiment when applying transparent optodes.

In a second step, the influence of soil water content on pH optode measurements was studied. This preliminary study gave us some interesting guidelines for non-saturated soil optode applications. It was possible to apply optodes on soil at low soil water content when the soil-optode contact time exceeded 20 hours prior to the first measurement. Also, a constant signal was generally reached faster with increasing water content, with 21h contact time at 49% of MWHC being reduced to 0.5 h at 76% of MWHC. Our results clearly showed that optode measurements should be carried out at a constant water content and after a sufficiently long and fixed contact time when applying optodes to non-saturated soils.

High pH sensor (HO) trials were mainly focused on camera set-up adaptation. Comprising a lipophilic HPTS pH probe combined with MY in a hydrogel layer, this optode presented a useful pH range from 6.2 to 9.5. The first batch of HO optode was initially prepared with titanium oxide. Initial test however (not shown in this document), presented a low response to pH changes. Removing TiO_2 improved the sensor response to pH changes. In a next step the applicability of the set-up used for LO measurement was studied. The objective was to check the possibility to use one set-up for LO and HO imaging simultaneously. The analysis of individual Red, Blue and Green channels showed that pH changes could be recorded by the LO set-up and that the ratiometric approach could be used. We found that the Red/Blue ratio described the pH changes with the highest sensitivity. Consequently, HO and LO could be used with the same imaging set-up, allowing both optodes being applied and imaged simultaneously.

After this development and soil adaptation steps, optodes were then applied to image oxygen and pH in two projects.

(1) The oxygen sensor application project focused on imaging spatio-temporal changes of oxygen concentration in the rhizosphere of rice growing in flooded conditions.
(2) The second application project aimed at monitoring pH gradients in soil around tungsten beads as a heavy metal pollution source.

The chapter III presents the context, methodology and results of these application projects.

Chapter III

Application projects

1. Imaging oxygen in rice rhizosphere

1.1. Context

This experiment was carried out in collaboration with Dr Hannes Schmidt, University of Vienna. His research focuses on investigating identity, diversity and activity of N_2-fixing microorganisms associated to lowland rice (*Oryza sativa*). About 75% of rice are grown in flooded soils with O_2 depleted conditions (i.e. lowland or paddy field rice) [93]. In anoxic environments, rice develops aerenchyma tissue to maintain root function. Aerenchyma allows the efficient transport of oxygen from leaves to roots [94]. Oxygen is then released by roots, a phenomena called radial O_2 loss (ROL). ROL creates an oxygenated zone around roots, protecting the plant from reduced toxic chemical elements as H_2S and Fe2+ [95]. In addition, this root-induced change in redox conditions modifies biological and chemical processes in the rhizosphere of flooded plants. Low oxygen concentrations in root environments of waterlogged paddy soils may provide suitable niches for N_2-fixing microorganisms. However, ROL may affect nitrogen fixation by N_2-fixing microorganisms located at the soil-root interface as high concentration of O_2 can inhibit the nitrogenase reductase, key enzyme of nitrogen fixation [96]. Spatially resolved oxygen concentrations in the rhizosphere of wetland rice are currently missing to test the hypothesis of a link between the oxygen hotspot around roots due to ROL and activity of N_2-fixing microorganisms.

The work presented here was a preliminary experiment to apply the oxygen optode previously developed to monitor oxygen in rice rhizosphere growing in flooded condition. Combining O_2 optodes with microbiological techniques in the future shall allow to gain a better knowledge of N_2-fixation associated with wetland rice.

1.2. Material and methods

1.2.1. Soil and plant conditions

The experiment was conducted in waterlogged rhizoboxes filled with soil from Italy, Rice research institute in Vercelli. Rice seeds (*Oryza sativa*, cultivar IR 64) were pre-germinated on tissue papers in beakers filled with autoclaved water for 10 days in the dark at 22°C-28°C in the greenhouse. One seedling was then planted into each rhizobox. The plants were grown for 8 weeks before oxygen measurements.

1.2.2. Optode preparation

A batch of optode foils was prepared according to the recipe previously developed. Briefly, sensitive dye PtOEP and reference dye Macrolex Yellow were mixed at 0.75% / 0.75% (w/w) of polystyrene dissolved in chloroform (0.2 g / 3 g). TiO_2 was added to the mix at 10% (w/w of chloroform). The mix was then coated onto polyester foil with a 1 mil bar knife. The detailed protocol is presented in appendix 3

1.2.3. Optode calibration

Foil calibration can be carried out in different ways. The first one is to calibrate the piece of optode used for measurement directly at the same position as in the soil measurements. The second one is to calibrate a small piece of optode foil and use another piece from the same foil for measurements. The two procedures are presented in Figure 64. In both cases, the calibration model is defined from the signal ratio mean of a selected area.

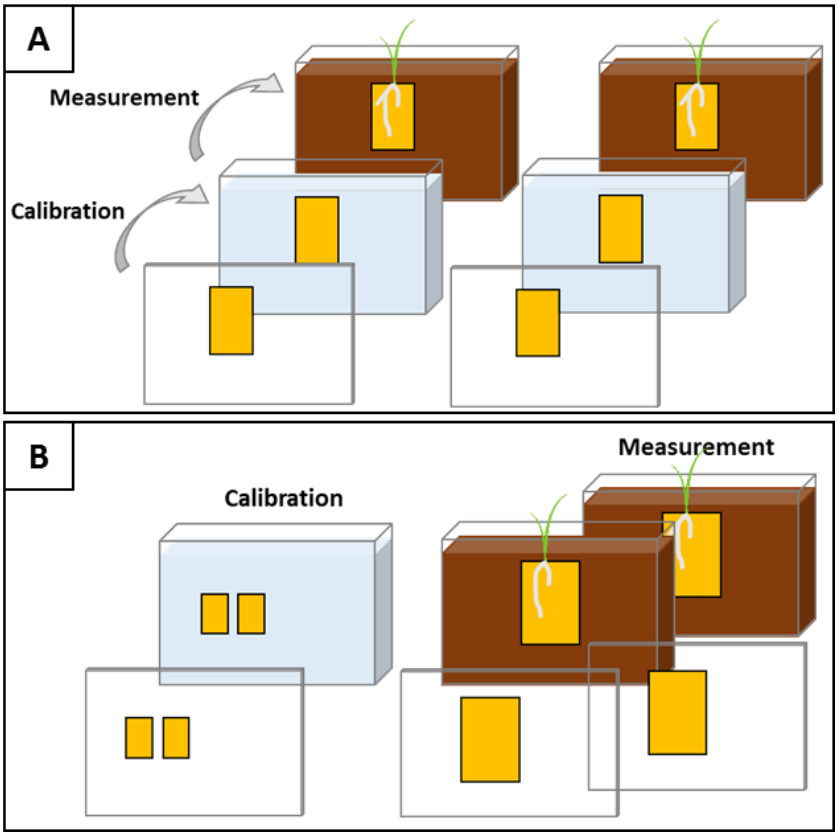

Figure 64: Optode calibration procedure. (A) Calibration of optodes that are then directly used for measurements. (B) Calibration of small pieces of an optode foil with bigger pieces from the same foils used for measurement.

The second way (Figure 64.B) is the easiest to perform as it is possible to calibrate several pieces of optodes at the same time. However, this approach requires that the piece of optode used for calibration is representative of the overall optode and the signal ratio is homogeneous throughout the optode foil. The first solution is more accurate as the calibration model is determined for the very piece of optode used for measurements. However, each piece of optode foil applied has to be calibrated separately beforehand, which is very laborious and time consuming. In this study, the rhizobox volume was 4 L. The production of N_2-purged water and the aeration of such a volume of water was a long process, particularly when homogeneous oxygen concentration had to be ensured throughout the rhizobox.

Optode foil homogeneity test

Prior to the calibration procedure, a 40-cm^2 optode foil was taped onto a front plate and put in contact with water at 0% of air saturation. One picture was taken and analysed. The objective was used to evaluate the signal heterogeneity across the foil. In anoxic conditions (0% of air saturation), the standard error (SE) of the signal ratio for a 40-cm^2 foil was found to be ± 0.00023 (n = 338560 pixels). Also, the big area was virtually cut into 1-cm^2 areas. The SE of the ratios between 1-cm^2 sub-area was calculated to be ± 0.00383. These calculations were performed for the least homogeneous optode foil of the batch. So, we considered that the signal across the foil was sufficiently homogeneous. Consequently, for the rhizobox application experiment, optode calibration was carried out for a small piece of each foil.

1.2.4. Rhizobox experiment

Each piece was stuck onto a rhizobox front plate and a 2-cm^2 area was used for calibration data analysis. Figure 65 illustrates how optode foils were used. Calibration was performed at room temperature in a rhizobox filled with N_2-purged water. Oxygen level was then increased with ambient air bubbling and monitored using an oxygen luminescent probe (LDO 101, Hach Lange) connected to a multimeter (HQ30d Hach Lange). Anoxic conditions (0% of air saturation was reached by adding ascorbic acid solution (0.1 M in NaOH 0.1M). Images were taken in the same conditions as for measurements.

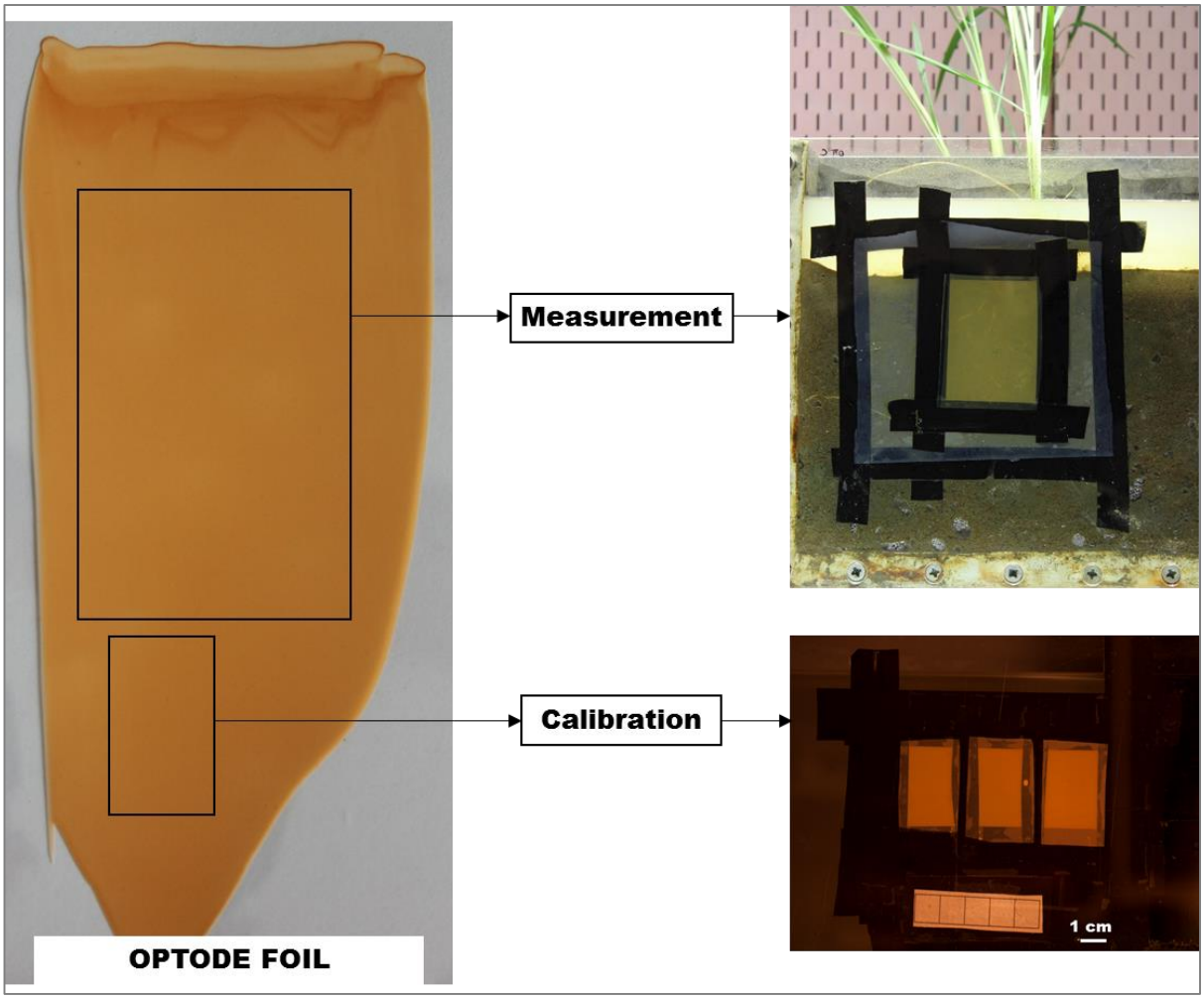

Figure 65: Illustration of use of optode foil : a small piece for calibration and a big part for measurement

1.2.5. Oxygen imaging

Optodes for oxygen monitoring of rice rhizosphere were taped three days before the measurement allowing an equilibrium of the system after disturbance during optode sticking. Rhizobox were carefully opened and optodes were taped onto the clean front plate. Nylon membrane was then carefully fixed to the plate covering the optode and avoiding air bubbles between the optode and the membrane. The front plate was screwed onto the rhizobox (Figure 66). Optodes were protected from light with aluminium foil and rhizoboxes were kept in the greenhouse until measurement.

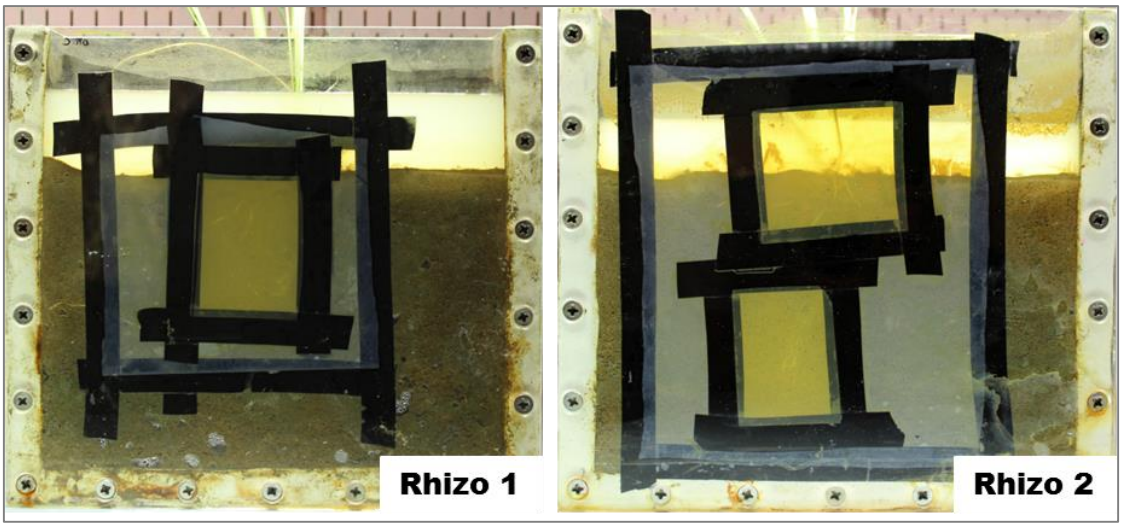

Figure 66: Pictures of rhizobox with optode in place.

Optode measurement were carried out in a lab next to the growth chamber using a portable black box ensuring constant light condition. The rhizobox was put in the black box just before measurement to avoid plant physiological changes as a response to long darkness periods. Larsen et al [33] showed that the oxic area around roots and mean oxygen level decreased quickly when rice was placed in darkness over longer time periods (1 hour) especially at the basal root zone and at root tips.

Imaging set-up was kept in place during the entire experiment (calibration and measurement). As for previous work, pictures in a black area were taken prior to oxygen monitoring. Two measurements were taken at 24-hour intervals. Finally, pictures of the optode applied onto the rice rhizosphere were taken using a normal DSLR camera as the transparent nature of the optode allowed to capture the rice root system.

1.3. Results

1.3.1. Optode calibration

Data analysis was achieved on 2-cm^2 optode area equivalent to 20000 pixels. Changes of signal ratio R/G with increase of % air saturation of each optode was well described by the modified Stern-Volmer model (R^2>0.999). A representative calibration curve is presented in Figure 67. Parameters α and K_{sv} were determined for each foil (Table 12) and then applied to oxygen measurements.

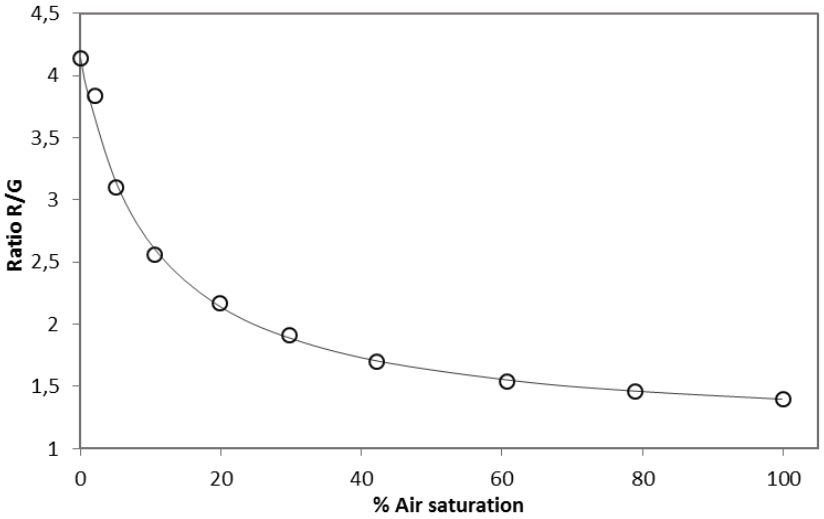

Figure 67: Calibration curve of optode A (Rhizobox 2)

Table 12: Parameters α and K_{sv} of optodes

Optode	K_{sv}	α
A-R2	0.098	0.27
B-R2	0.098	0.28
C-R1	0.104	0.27

Equation parameters were similar between optode foils showing homogeneity of optode preparation process. From calibration data, an accuracy profile was constructed to evaluate accuracy and uncertainty of the overall optode batch prepared for this experiment. For each of the three foils applied in this experiment, the area used for calibration analysis was virtually cut in 4 equivalents parts. Oxygen concentration was calculated for each sub-areas and uncertainty profile was constructed according to Feinberg et al [97]. Results provided an evaluation of the global uncertainty for each oxygen concentration. At 2% air saturation, the uncertainty was ±0.4% of air saturation which was equivalent to 18% of relative uncertainty. From 5% to 100% of air saturation, the relative uncertainty ranged between 9% and 1%.

1.3.2. Oxygen imaging

Optode images were transformed in O_2 maps using the calibration parameters of each optode. Figure 68 depicts typical oxygen gradients around rice roots and corresponding root pictures.

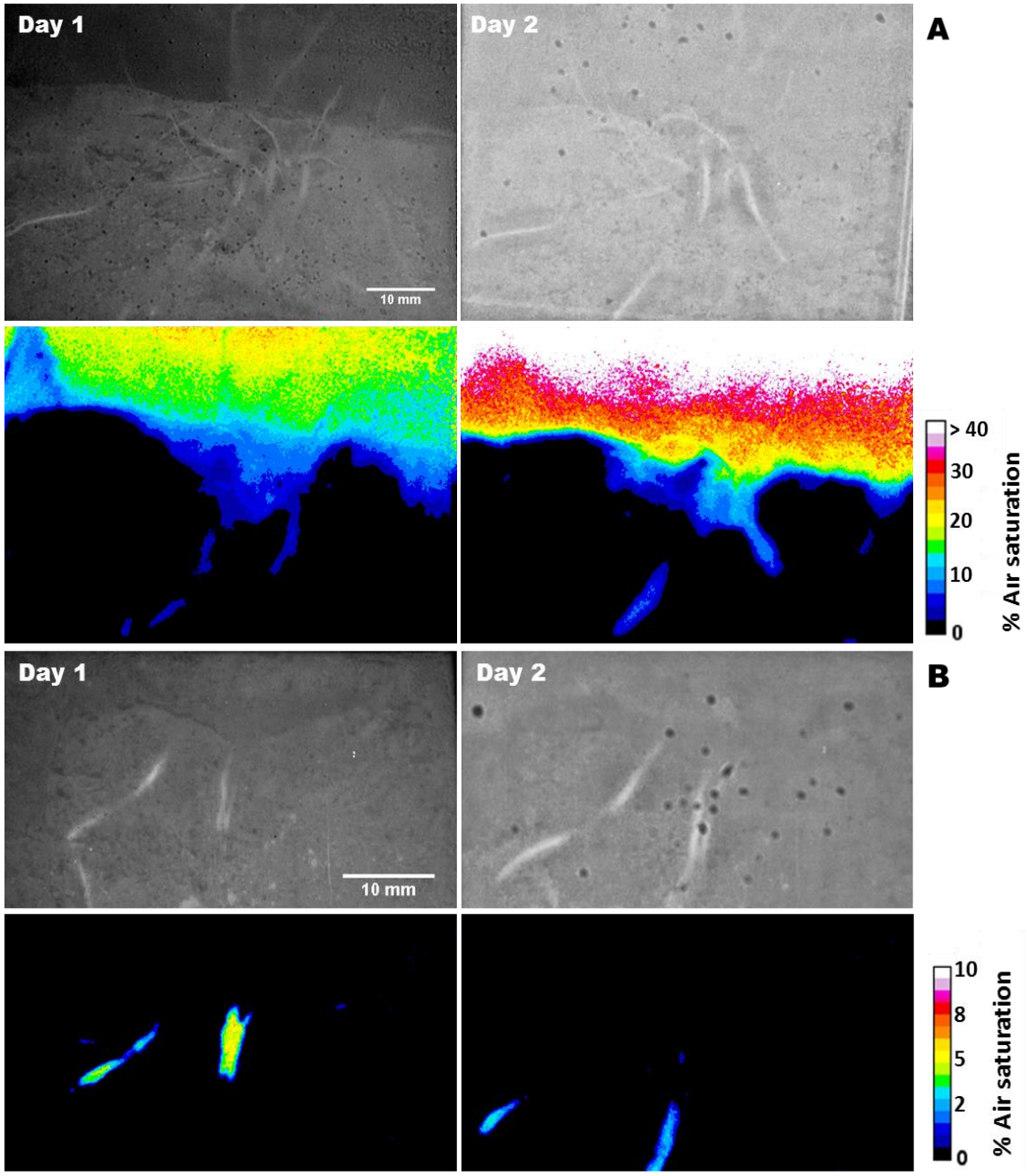

Figure 68: Two-day imaging of oxygen concentrations in rhizosphere of rice (color picture) and corresponding DLSR picture (gray scale). (A) Soil-water interface images (Rhizobox 2). (B) Rice rhizosphere images (rhizobox 1).

Anoxic and oxic zones were well distinguished, with a zone of high oxygen concentration at the soil-water interface (Figure 68.A). Also, the basal part of the plant roots presented a higher oxygen concentration. In addition, the oxic spots observed corresponded to root tips (Figure 68.B). Images taken at 24-hours interval time showed a temporal variation of oxygen concentration around roots. Typically, as shown in Figure 68.B, oxygen concentration around roots tips changed with root growth.

In addition, in-depth spatial information was extracted from the image that displays spatial distribution of oxygen concentration in the rhizosphere. For example, Figure 69 shows the changes of oxygen concentration with increasing distance from root tip. Oxygen concentration were then extracted along the root axis and plotted against the distance from root tip (Figure 69.A). We observed an increase of oxygen concentration from root tip to basal root. Observed oxygen gradients from the base of the root towards the tip are in agreement with Larsen et al [33] reporting a similar pattern in the rhizosphere of young rice roots grown under flooded conditions. This could be explained by a longer O_2 transport distance from soil surface to root tip.

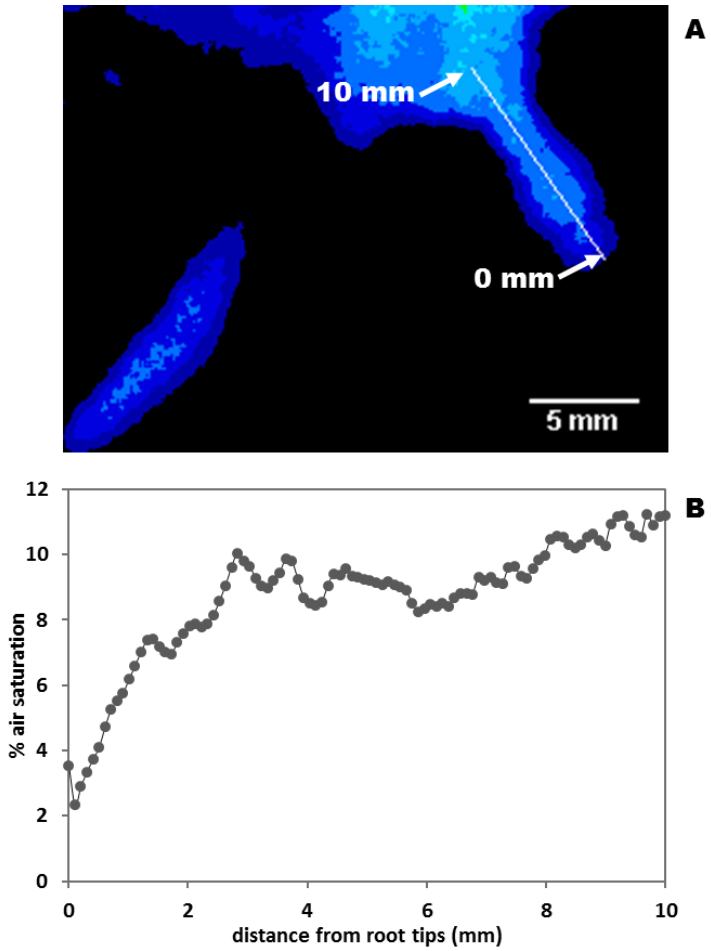

Figure 69: Illustration of oxygen concentration changes along root.
(A) Oxygen map. (B) Spatial variation of oxygen concentration along root.

Also, temporal analysis can be implemented together with a spatial analysis as displayed in Figure 70. Oxygen concentration values along a root (Rhizobox 1) were extracted at day 1 and 2 and changes of oxygen concentrations of growing roots were observed. An oxygen concentration hotspot was localised at the root tip and elongation zone at day 1. After 24 hours, a hotspot of oxygen was only observed at the root tip. Towards the basal part of the root, O_2

leaking along the root was spatially different. Changes of root morphology and the formation of a barrier to ROL along the elongation zone over time most likely resulted in the observed oxygen dynamics.

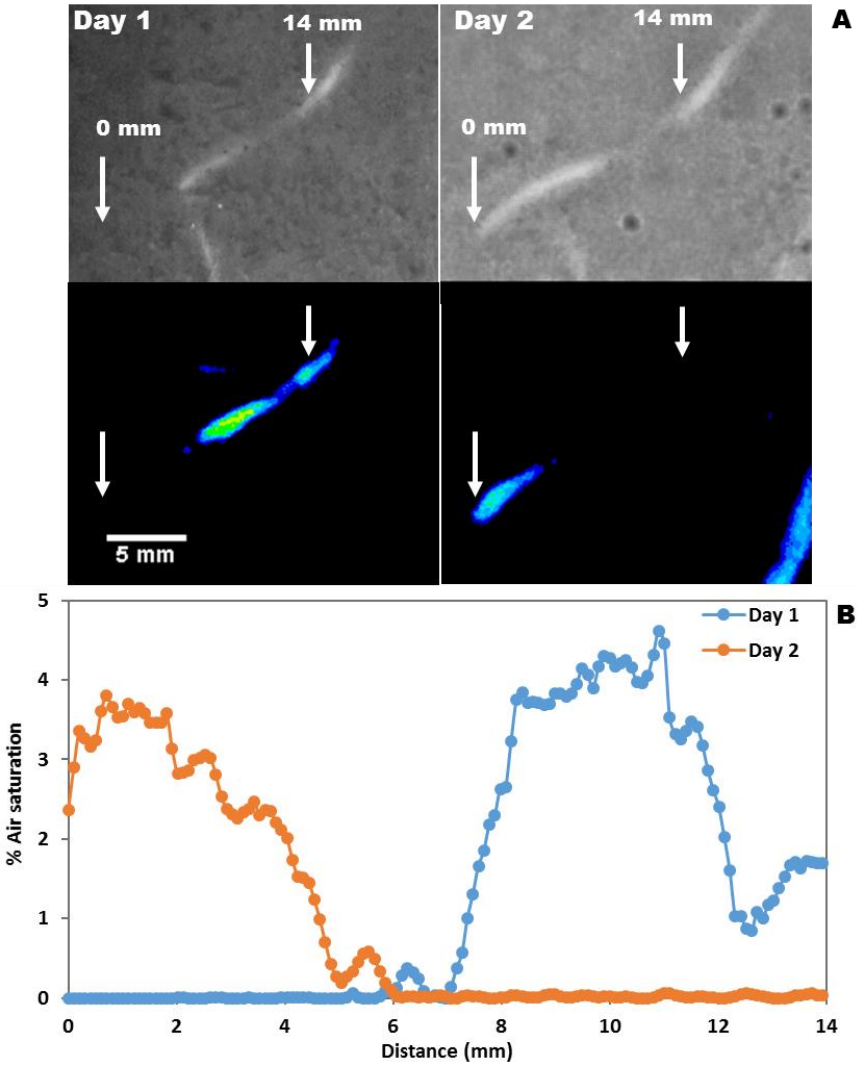

Figure 70: Illustration of spatio-temporal variation of oxygen concentration along root tip. (A) Picture of root area in grey and corresponding oxygen map (in color) at day 1 and 2. (B) Graph of oxygen concentration changes with root growth.

1.4. Conclusion

Image homogeneity tests revealed a reliable optode preparation process producing optodes with a low standard error of signal ratio within the optode foil. In addition, this experiment was used as preliminary experiment to apply accuracy profile concept to this *in-situ* analytical method. It might be used as a validation procedure to get a better knowledge of optode analytical characteristics. The rhizobox experiment demonstrated the applicability of oxygen planar

optode in flooded soil systems. It was possible to monitor oxygen concentration in the rhizosphere of paddy field rice and observe dynamic changes of distinct oxic and anoxic areas around growing roots. Oxygen concentration hotspots at root tips were also well imaged.

Our results showed that planar optode are well suited to monitor spatio-temporal changes in oxygen concentrations in the rhizosphere of rice in flooded condition and allow to visualize oxygen hotspot at the soil-root interface.

2. Imaging soil pH around tungsten input

2.1. Project overview

Tungsten (W) is a transition metal with remarkable chemical and physical properties such as a high melting point, high density and resistance to corrosion. Tungsten has been used in a wide range of applications: metalworking, mining and construction industries, household products as lamp filaments, television sets. It has been recently used in fishing weights, hunting and military ammunitions in substitution to lead. Being considered as a green alternative to lead, W consumption for ammunition is rising significantly in the past decades [98]. However, reported clusters of childhood leukemia in United States were correlated to W pollution in drinking water demonstrating a negative impact of elevated W concentrations on human health [98]. High W concentrations were repeatedly reported in soils close to mining activities and war areas [98]. Despite an increasing number of studies, detailed knowledge of transport and ecotoxicology of W in environmental systems is still scarce [99]. In particular, it was found that W was toxic to earthworms and bacteria [100].

In the environment, W occurs mainly as oxyanion, tungstate (WO_4^{2-}). In acidic conditions, W oxyanions can polymerize with each other or with others ions to form polytungstate components. Polymeric tungsten was found to be more toxic than monomeric tungstate [99]. In contrast, in alkaline conditions, depolymerization and dissolution of tungstate was observed [101]. Different W forms interact differently with the soil matrix and therefore W speciation strongly affects W mobility, bioavailability and toxicity [99].

The experiment presented here has the objective to visualize pH changes around different metallic tungsten sources in soil differing in pH. Two W sources were applied: tungsten ammunition (bullets containing W and alloying metals) and metallic tungsten powder.

2.2. Material and methods

2.2.1. Soil and rhizobox preparation

The experiment was conducted in rhizoboxes with sandy soil (acidic Cambisol, World Reference Base of Soils, FAO, sandy loam) form Siebenlinden Austria (N 48° 40.513', E 14°59.933'). The soil was sieved down to 2 mm and aliquots were limed by adding $CaCO_3$ at 0.25 $g.kg^{-1}$ and 2.5 $g.kg^{-1}$ to get three pH levels, slightly acidic, neutral and slightly alkaline. After rhizobox filling, the front plate was removed and tungsten shots (Rottweil ultimate 12/76, 3.5 mm, 90-95% W, 10-5% alloying elements, e.g. Ni, Fe) and tungsten powder (Inframat® Advanced Materials™, 2 µm) were placed onto the soil surface (Figure 71). A nylon membrane was fixed between the soil and the front plate and boxes were closed again. One rhizobox for each pH level was incubated without W input, used as control. Rhizoboxes were incubated for 3 weeks at room temperature and at 80% of the soils maximum water holding capacity (i.e. water content 36%, 34% and 32% respectively for acidic, neutral and alkaline soil).

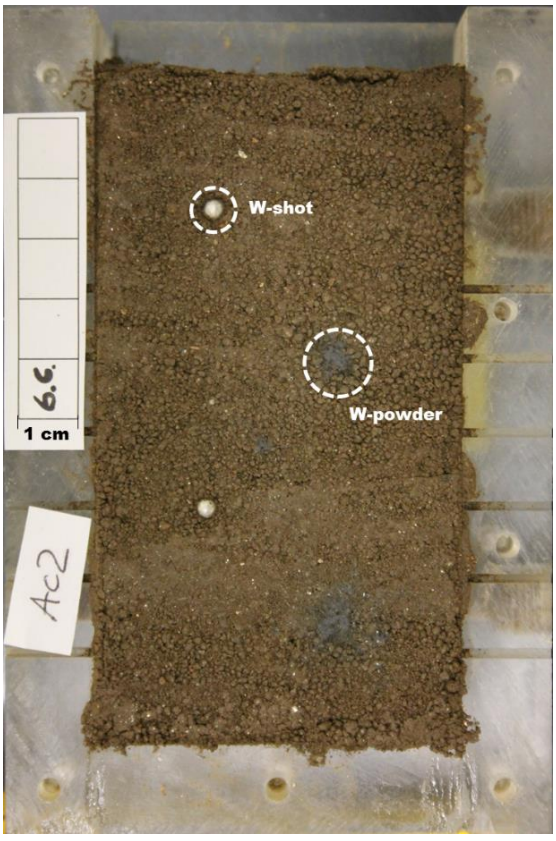

Figure 71: Picture of a rhizobox with W shots and W powder in acidic soil.

2.2.2. Optode preparation

Low-pH optode (LO) foils were prepared according to the recipe previously developed. The pH sensor cocktail was prepared with the sensitive dye DClFODA and the reference dye ziegelrot at 0.5% / 5% (w/w) of hydrogel dissolved in ethanol. After complete dissolution, the sensor cocktail was coated onto polyester foil with a 1 mil bar knife.
The detailed protocol is presented in appendix 4.

2.2.3. Optode calibration

Optode calibration was carried out in rhizobox filled with phosphate buffer. As the soil solution (obtained by centrifuge at 15300 g for 10 minutes) presented different levels of conductivity, ionic strength (IS) of buffer was adjusted with NaCl, to reach 5, 10 and 45 mM. Calibration was performed for each ionic strength level.
Homogeneity of one optode foil from this batch production was also evaluated in buffer solution. An ROI of 20 cm^2 was virtually cut into 1 cm^2 sub-areas. The ratio mean was calculated for each sub-area. The standard error between sub-area was of 0.0015. We considered optode foil production homogeneous. Consequently, calibrations were performed on one small piece of the optode foil used for the rhizobox application experiment.

2.2.4. Soil pH imaging

Prior to the experiment, pictures of tungsten shots and powder on soil surface were taken with the pH imaging set-up to evaluate light reflectance from the W shot. No signal was observed. However, to ensure a homogeneous background, the nylon membrane applied during the incubation was left in place for the measurement. Also, nylon membrane protected soil surface from disturbance when re-opening the rhizobox. After 3 weeks of incubation, rhizoboxes were opened and pieces of optode were taped onto the front plate (Figure 72).
Pictures were taken after one hour of contact between soil and optode. During this contact time, rhizoboxes were protected from light and placed upside down to ensure a good contact between soil and optode. Measurement were carried out in a black box and a black picture was taken without excitation light to record the camera sensor noise. The excitation light was provided with blue LEDs at 445nm covered with a 475 nm short-filter. Emission light were recorded by a DSLR camera combined with a 495 nm long-pass filter. After the measurements, front plates

with optodes were put in buffer solution overnight and measurements were carried out in phosphate buffer to check the integrity of the optode after W contact, especially for W powder. In solution, the optode signal should be homogeneous in both channels. After contact with some specific compounds, optodes might be stained as it was observed by Pradier [78]. Commercial pH planar optodes were used to image pH changes in the rhizosphere of *Eucalyptus grandis*. It appeared that after a short contact time, optodes were irreversibly stained probably due to root exudates.

Finally, at the end of the experiment, the soil under the optode was collected. Soil solution was extracted and pH was measured.

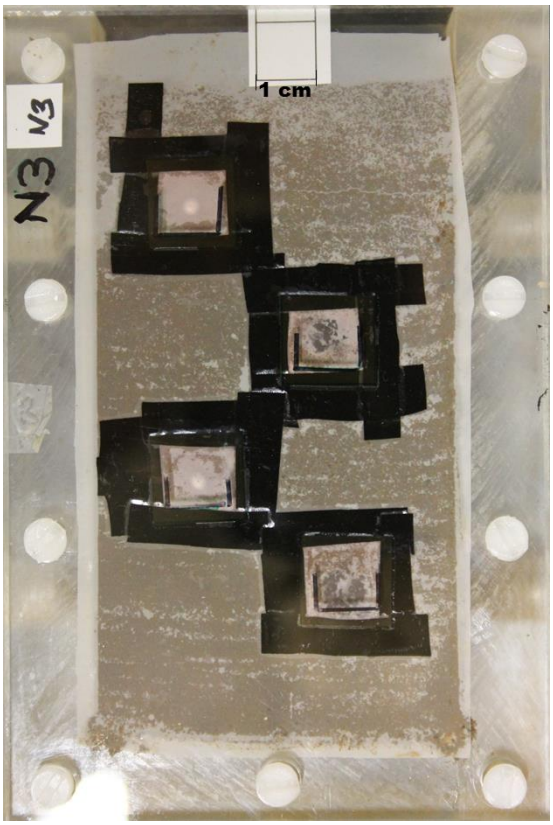

Figure 72: Picture of rhizobox with tungsten input, nylon membrane and Low pH optodes.

2.3. Results

2.3.1. Optode calibration

Optode calibration was carried out with an ionic strength close to IS of soil solutions. Since the IS differed for the different liming treatments, a separate calibration model was determined for

acidic, neutral and alkaline soil application. Calibration data analysis was achieved on 200 x 200 pixels' area equivalent to 2 cm^2. The spatial resolution was of 70 µm x 70 µm. Signal ratio was calculated using Red signal divided by Green signal (R/G). Calibration models were well described by a sigmoidal model (R^2>0.999) as displayed in Figure 73.

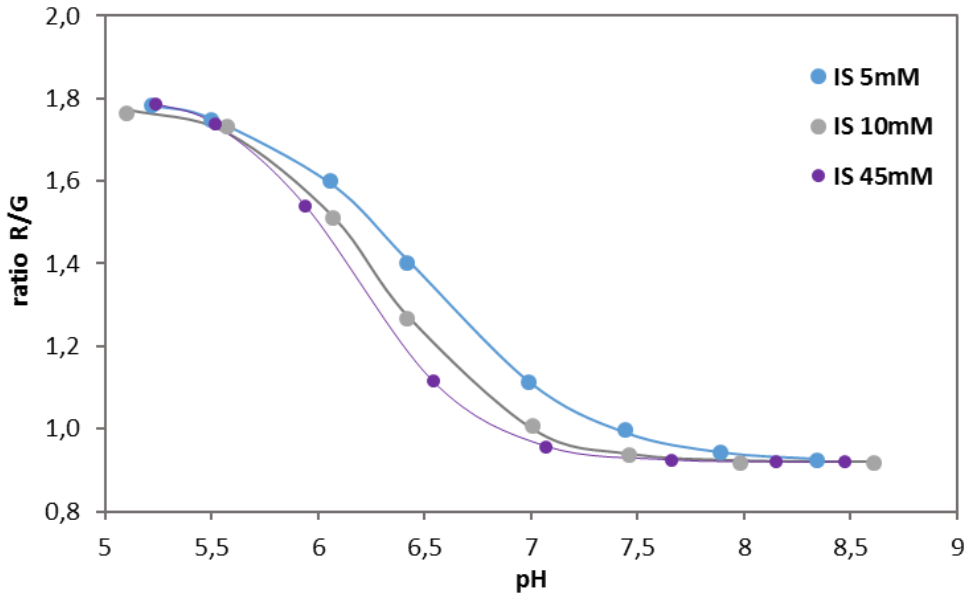

Figure 73: Calibration curve of LO optode at 5mM, 10mM and 45mM ionic strength. (Ratio is the mean of 14400 pixels' ratio values)

2.3.2. Soil pH imaging

After black correction of Green and Red images, the ratio Red/Green was calculated. A median filter (2 pixels' radius) was applied on the ratio image reducing the noise. Then the calibration model corresponding to each soil was applied to the ratio images using a macro command. Figure 74 displays pH maps of 120 x 120 pixels (equal to 70 mm^2) for each treatment. The spatial resolution was of 70 x 70 µm.

Firstly, strong pH differences were observed between soils as expected. Soil pH measured by optode was respectively 5.3 (±0.08, n=4), 6.4 (±0.14, n=2) and 6.8 (±0.03, n=2) for acidic, neutral and alkaline soil. This value was obtained by mean calculation of 120 x 120 pixels' area. Spatial variation was comprised between 0.1 pH unit (neutral and alkaline soil) and 0.4 pH unit for acidic soil. The spatial variation was higher for acidic soil as the pH value was at the limit of pH application range of LO optodes. Moreover, about 65% of pixels could not be transformed in pH value as the ratio value was outside the calibration range. It means that pH

mean value of acidic soil was probably below pH 5.2. The alkaline soil was more neutral than we expected and its value was in the calibration range of Low-pH optode. pH measurement of soil solution after experiment showed a shift compared to optode measurement: 4.9, 6.1 and 7.4 respectively for acidic, neutral and alkaline soil. It has to be considered that soil solutions were prepared few days after optode measurement.

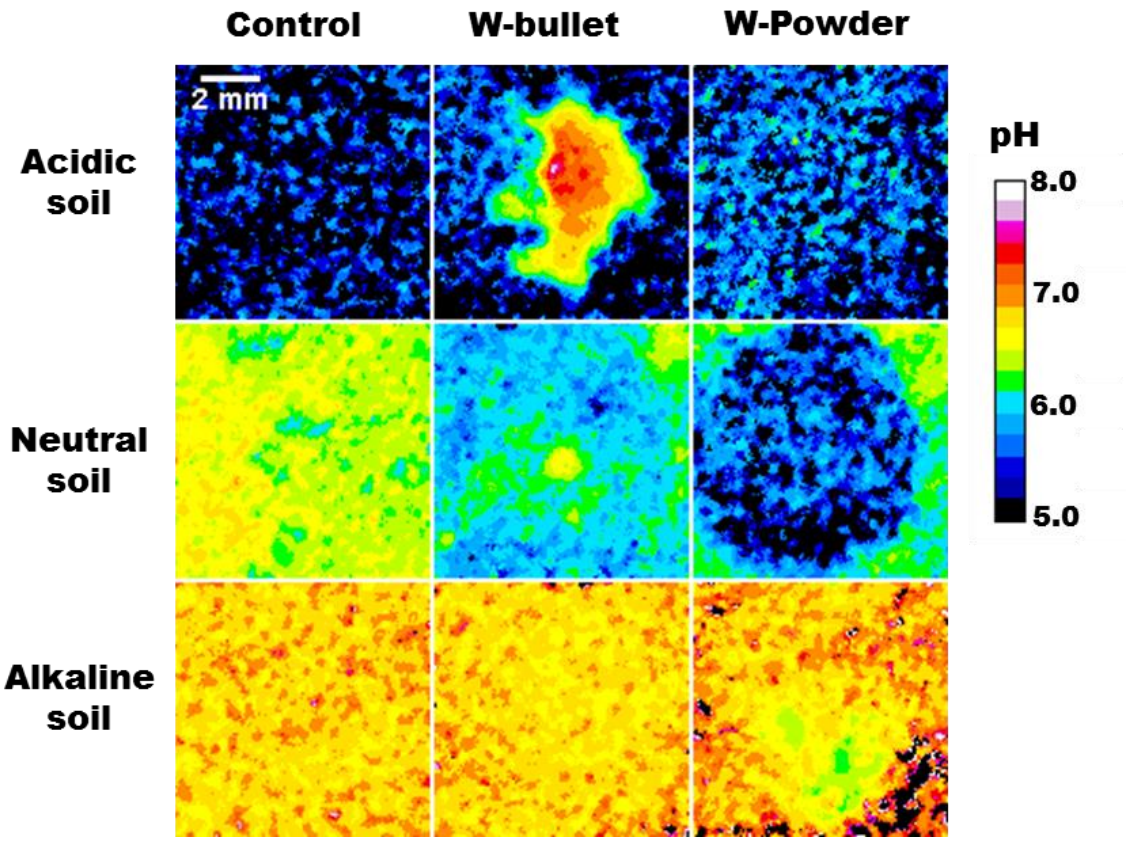

Figure 74: Typical pH map for soil control (Bulk), W-shot and W powder.

W-powder input resulted in a substantial acidification in neutral soil with a pH mean of 5.6 whereas the surrounding soil was at pH 6.1. Acidification was also observed in alkaline soil with surrounding soil at 6.9 and acidification spot close to pH 6.3. No acidification was observed for the acidic soil. Pictures of optodes in buffer after soil application showed some unexpected signal heterogeneities of the applied optodes. In homogeneous solution, signal received on the Green and Red channel should be homogeneous. As we can see in Figure 75, optode signal was not homogeneous in the buffer solution, especially for LO optodes placed on W powder in the acidic and neutral soil. Only green channel was impacted with dark spots on the picture corresponding to a decrease of pixel intensity. As the result, ratio picture presented

heterogeneities too. The green channel recorded fluorescence emitted by the pH-sensitive dye. One explanation might be an irreversible interaction between DClFODA and tungsten changing optical properties of the indicator dye. Consequently, the signal changes recorded in the W powder incubation experiment might not be due to pH changes only. It is not possible to remove such a fake signal and discriminate signal due to pH changes from signal due to W interactions with the sensor layer. Even though the pH decrease observed is in agreement with the literature [101], no reliable results about the effect of W powder on soil pH can be obtained if optode integrity is not maintained during the optode application time. This clearly demonstrates that theses planar optodes are not well adapted for such experimental conditions.

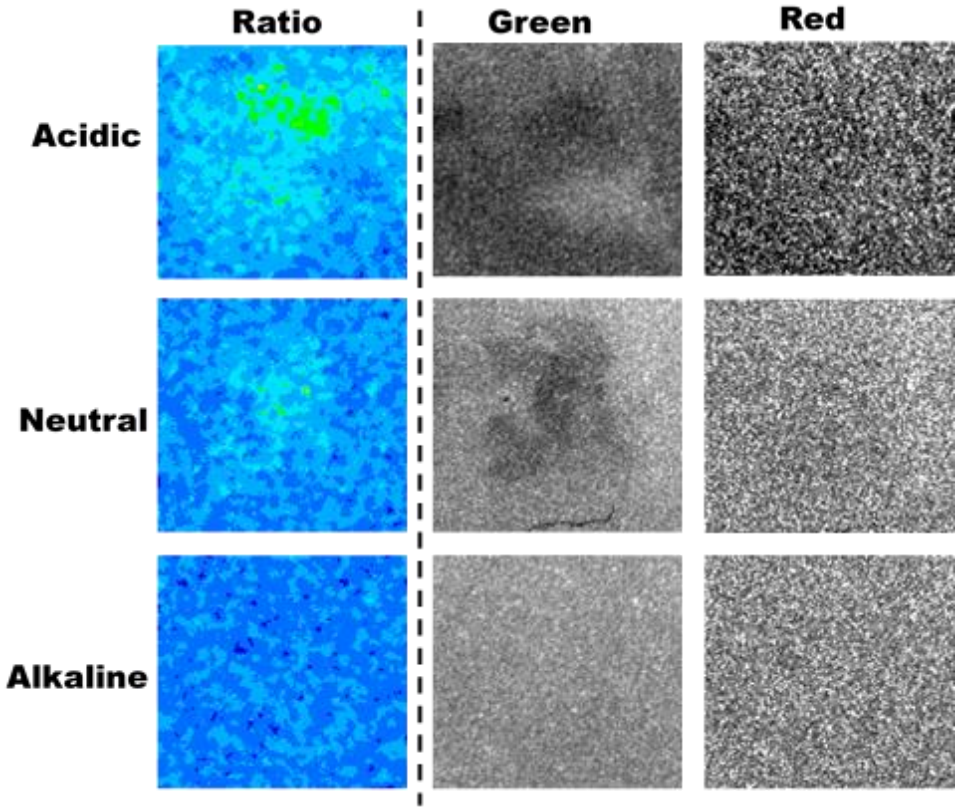

Figure 75: Ratio, Green and Red images (pixels values) of LO optodes in buffer solution used previously on W-powder.

The incubation of **W shots** in soils with increasing pH resulted in different pH patterns compared to W powder. In the acidic soil, alkalinisation was observed around W bullets. Also, in the neutral soil, alkalinisation was visible around W-bullet as well as a pH decrease in a larger area. Finally, in alkaline soil, a pH profile of horizontal transect showed a slight acidification in alkaline soil around W shot (Figure 76).

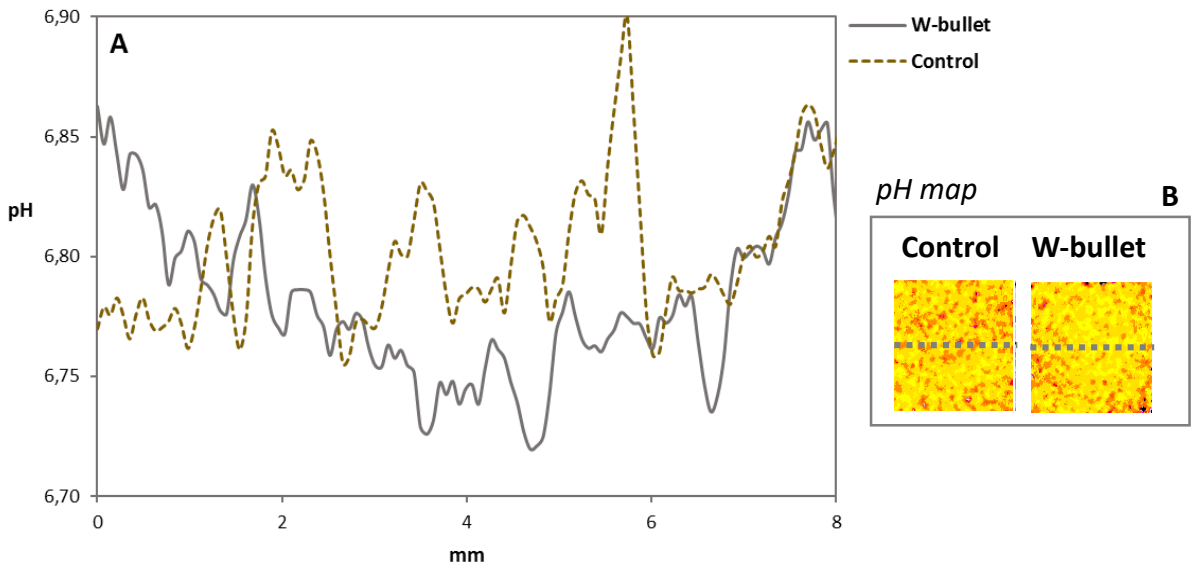

Figure 76: pH profile of horizontal transect of LO (A) and pH map (B)

In acidic conditions, an increase in pH could be explained by the sorption of tungstate to soil particles (S) and the concurrent release of hydroxyl ion [101].

$$S\text{-}OH + WO_4^{2-} \longrightarrow S\text{-}WO_4^{-} + OH^{-} \quad (12)$$

W shots contained 90-95% of W and 5-10% of alloying elements such as nickel (Ni), iron (Fe), cobalt (Co) and copper (Cu). These alloying elements can change W speciation during the oxidation process. The oxidation of alloys combined with the depletion of oxygen concentration leads also to an increase of pH as described below:

$$Ni \longrightarrow Ni^{2+} + 2e^{-} \quad (13)$$

$$O_2 + 2H_20 + 4e^{-} \longrightarrow 4OH^{-} \quad (14)$$

Moreover, in acidic conditions, tungstate polymerization is accompanied by the consumption of protons. All these processes could explain the pH increase observed around W-shot in acidic soil.

In alkaline condition, oxidation of W occurs with the formation of mobile WO_4^{2-} and release of protons [98]. This might explain the slight decrease of pH around W shot in alkaline soil.

$$W + 2H_2O \longrightarrow WO_2 + 4H^+ + 4e^- \quad (15)$$

$$WO_2 + H_2O \longrightarrow WO_3 + 2H^+ + 2e^- \quad (16)$$

$$WO_3 + H_2O \longrightarrow WO_4^{2-} + 2H^+ + 2e^- \quad (17)$$

Finally, in neutral soil, we could have a combination of W oxidation resulting in a pH decrease and oxidation of alloying elements close to the W shots leading to pH increase.

2.4. Conclusion

This rhizobox experiment demonstrated the applicability of LO in soil to image pH around W bullets. It was possible to observe spatial changes of pH with soil pH at sub-mm scale. This experiment was repeated afterwards by Christina Roschitz (PhD, BOKU university) with a longer incubation time for W shots and presented similar patterns. Optode technique could be useful for a better understanding of W speciation in soils and long-term pH monitoring could be also considered.

Regarding imaging pH in soil amended with W powder, the obtained signal was compromised by unwanted interactions of W powder with the components of the sensor layer. This fake signal was also observed with commercially available pH planar optodes (PreSens) with a much bigger impact (data not shown). These results demonstrate the need to check the integrity of the optode after use to avoid misinterpretation of signal ratio even after a short-term experiment.

General conclusion

The objectives of this work were (1) to develop protocols for the reliable construction of oxygen optodes as well as pH optodes for the neutral and alkaline pH range (2) to adapt optode construction and application for soil-root environments, (3) to deploy pH and oxygen optodes in two application projects. Optode signal detection was based on the ratiometric RGB approach. To achieve these objectives, initial prototypes were improved step by step, leading to finalized optode recipes and a significantly better knowledge of crucial aspects of optode design for soil application.

Oxygen optode development was successfully conducted resulting in a final recipe adapted for oxygen monitoring in the range of 0-100% of air saturation and a reliable construction process based on commercially available fluorophores. Further tests in flooded soil showed that optical insulation was not critical when O_2 optodes are applied in plant-soil experiments to reveal the O_2 dynamics in the rhizosphere of plants grown under paddy field conditions. Luminescence emitted by roots was found to be negligible compared to the optode signal. A white translucent nylon membrane as optical insulation placed between soil and optode reduced the background signal heterogeneity even further while keeping optode performance unchanged. Thus, structures behind optode were still visible allowing the observation of root growth during the experiment. The drawback using an external membrane is the reduction of spatial resolution due to smearing which is induced by the thickness of the membrane. Lifetime of O_2 optodes was also studied in flooded soil over a period of 4 weeks revealing signal drift over time. This experiment demonstrated the importance of checking the optode performance when conducting long-term experiments in such a complex system. Finally, O_2 optodes were applied to image spatio-temporal dynamics of oxygen in the rhizosphere of rice grown under paddy field conditions. Oxygen hotspots were clearly identified around roots and changes in oxygen concentrations along the roots were observed over a 24-hour monitoring period. Our results confirmed the suitability and the potential of this optode to visualize oxygen dynamics in plant-soil systems.

Despite intensive testing, there are still additional experiments that could further secure this optode setup or help to improve it. Firstly, the optical insulation study could be complemented by a quantification of signal changes depending on the type of background such as a comparison of optode signals in soil and in water at similar oxygen concentration levels. To do that, adapted

oxygen sensors such as microsensors or optode spots combined with optic fibers (PreSens GmbH) should be applied simultaneously to have an accurate control of oxygen concentration in soil without disturbing the system. Also, camera settings (aperture, exposure time, sensitivity) could further improve optode measurement through reduction of noise and brightness enhancement. These aspects were beyond the scope of this work.

Low-pH optode development also led to a reliable optode construction protocol, dedicated to a pH working range from 5.5 to 7.5, which is adapted for slightly acid to near-neutral soil environments. In contrast to oxygen optodes, the absence of optical insulation was critical as the luminescence emitted by roots was higher than the optode background signal. Only a non-transparent optical insulation could suppress this artefact. However, whenever it is important to see the structures behind the optode, we propose to apply the inverse ratio calculation to convert the signal to pH as this reduces the weight of the artefact signal as root luminescence is wavelength dependant. Like for O_2 optodes, the application of an external nylon membrane between optode and the soil/root surface was also found to improve the homogeneity of the background signal. This experiment further highlighted the need to critically assess the background luminescence prior to any optode-based measurement of pH. Moreover, the influence of soil water-content on optode measurements was studied showing that optodes can be applied on non-saturated soil but measurements should be only done after a sufficient contact time, as we found that the duration of contact required for achieving a stable optode signal increase with decreasing soil water content. No reliable optode signal was obtained at soil water content below 12% of the soil maximum water holding capacity due to the need of a sufficient amounts of water for the hydrogel matrix to swell as well as a limited quality of contact between optode and soil at low soil water content.

Finally, the application project in soil demonstrated the suitability of this optode to monitor pH changes around point contaminant sources, in this case a weathering tungsten ammunition shot at sub-millimetric scale. However, pH optodes applied on metallic tungsten powder incubated with soil showed altered signals after soil application due to irreversible changes to the optode matrix. Again these results demonstrated the importance to check optode integrity and performance after use.

This work could be completed with a useful lifetime study in soil, at different levels of water content. Also, the water content study carried out with a sandy soil could be extended by tests with a clayey soil as the physical properties may differ. As for oxygen optode, the effect of

different camera settings on pH measurements by optodes could also further be explored. Brightness could be thus enhanced since titanium oxide was found to be incompatible with pH probes.

Critical steps of the development of the **high pH optode** were achieved, however additional experiments to improve its performance and applicability to soil environments could not be carried out due to time constraints. The recipe proposed allows pH measurement in the range of pH from 6.2 to pH 9.5, which met the requirements for monitoring pH changes in the alkaline soil pH range. In addition, tests showed that the optical set-up dedicated to low-pH optode could also be used also for high-pH optodes. Simultaneous measurement of both pH optodes without changing the optical setup is therefore possible. This development work should be completed by a study of ionic strength effect and an improvement of brightness. Moreover, as this optode is transparent, the need of optical insulation should be explored.

In general, the optode tests that we have conducted might also be complemented by a study of photostability, probe leaching especially for pH optodes. In addition, storage conditions and pre-conditioning before use could also be assessed.

Next to optode construction, analytical performances of optodes designed should be tested to assess analytical limits, as well as accuracy and uncertainty. Also, spatial homogeneity of optode foil production and its impact on obtained results is not hardly ever documented. The use of accuracy profiles as analytical tools might be an innovative approach to validate sensor homogeneity and performance. An application of accuracy profile to images obtained by oxygen optodes in this work gave useful information about oxygen measurement uncertainty. Based on this approach, relative uncertainty ranged from 1% at 100% air saturation to 9% at 5% of air saturation. This type of data analysis could bring more detailed insights into the data extracted from optodes, for example to reliably discriminate significant pH or oxygen variation from that related to measurement uncertainty and to obtain a better knowledge of quantification limit.

In summary, this work highlighted the complexity of optode design particularly for soil application. Important insights about optode applications in soil were revealed, which have not been discussed so far in scientific literature. Also, the development of home-made optodes allows to individually adapt the system to one’s needs and account for constraints that are inherent to soil application. This is not possible with the commercial optode systems. Typically, pH optodes suitable for an alkaline pH range are not commercially available and these

commercial planar optodes are non-transparent. The flexibility and adaptability of self-constructed optodes is highly valuable for research teams that apply optodes in a wide range of environmental studies. Nevertheless, the understanding of methodological constraints and application specific limitations is crucial for accurate chemical imaging with planar optodes. This work significantly contributed to deepen our understanding on environmental optode applications, particularly in plant-soil systems.

Appendix

APPENDIX 1 / EGU 2017 – Abstract

Imaging pH and oxygen at the soil-root interface by planar optodes: a challenging technology to study dynamic rhizosphere processes.

Gabrielle Daudin[1,2,3], Eva Oburger[1,2], Hannes Schmidt[4], Sergey Borisov[7], Céline Pradier[5], Christophe Jourdan[5], Claire Marsden[6], Daniela Obermaier[8], Dagmar Woebken[4], Andreas Richter[1], Walter Wenzel[2], Philippe Hinsinger[3].

[1]*Division of Terrestrial Ecosystem Research, Department of Microbiology and Ecosystem Science, University of Vienna, Althanstrasse 14, A-1090 Vienna, Austria*

[2] *Rhizosphere Ecology and Biochemistry Group, Department of Forest Soil Sciences, Institute of Soil Research, University of Natural Resources and Life Sciences, Konrad Lorenz-Strasse 24, 3430 Tulln, Austria*

[3] *INRA, UMR Eco&Sols, Place Viala, 34060 Montpellier, France*

[4] *Division of Microbial Ecology, Department of Microbiology and Ecosystem Science, University of Vienna, Althanstrasse 14, A-1090 Vienna, Austria*

[5] *Cirad, UMR Eco&Sols, Place Viala, 34060 Montpellier, France*

[6] *SupAgro, UMR Eco&Sols, Place Viala, 34060 Montpellier, France*

[7] *Institute of Analytical Chemistry and Food Chemistry, Graz University of Technology, Stremayrgasse 9, A-8010 Graz, Austria*

[8] *PreSens Precision Sensing GmbH, Am Biopark 11, 93053, Regensburg, Germany*

Roots do not only take up water and nutrients from surrounding soil but they also release a wide range of exudates, such as low molecular weight organic compounds, CO_2 or protons. Root-soil interactions trigger heterogeneous rhizosphere processes based on differences in root activity along the root axis and with distance from the root surface. Elucidating their temporal and spatial dynamics is of crucial importance for a better understanding of these interrelated biogeochemical processes in the rhizosphere. Therefore, monitoring key parameters at a fine scale and in a non-invasive way at the root-soil interface is essential. Planar optodes are an emerging technology that allows in situ and non-destructive imaging of mainly pH, CO_2 and O_2. Originated in limnology, planar optodes have recently been applied to soil-root systems in laboratory conditions. This presentation will highlight advantages and challenges of using planar optodes to image pH and O_2 dynamics in the rhizosphere, focusing on two RGB (red-green-blue) approaches: a commercially available system (PreSens) and a custom-made one. Important insights into robustness, accuracy, potentials and limitations of the two systems applied to different laboratory/greenhouse-based experimental conditions (flooded and aerobic rhizobox systems, plant species) will be addressed. Furthermore, challenges of optode measurements in the field, including a first case study with *Eucalyptus grandis* in Brazil, will be discussed.

APPENDIX 2 / Titanium oxide supplementary test: comparison of different products

Context and objectives

Titanium oxide is added to the sensor layer of oxygen optodes. Titanium oxide particles act as light scattering center and enhance brightness of the optode. Different particles sizes are available which is a crucial point in terms of light scattering properties.

As the titanium oxide used for the optode development is not commercially available anymore, two others references were tested:

- nanopowder, 21 nm particle size, n° CAS 13463-67-7
- rutile, nanopowder < 100 nm particle size, n° CAS 1317-80-2

Table of titanium oxide references

Reference product	**Particle size**	**Comments**
UV-Titan P170 (Merck)	14 nm	Used for optode development work.
Sigma-Aldrich 718467	21 nm	To test
Sigma-Aldrich 637262	< 100 nm	To test

Materials and method

- *Optode preparation*

Oxygen optodes were prepared according to the recipe developed (appendix 3). PtOEP and Macrolex Yellow were mixed with TiO_2 particles and polystyrene and dissolved in chloroform. Sensor mix was then coated onto a polyester foil with a 1 mil bar knife. One optode was prepared with TiO_2 21 nm particle size (21), and second one with TiO_2 rutile <100 nm particle size (rut).

- *Optode calibration*

Optode was stuck on a front plate of a rhizobox filled with water and mixed with N_2 gas to adjust oxygen content. Images were taken with the optical set-up dedicated to oxygen optode measurement (DSLR camera combined with a 530 nm emission filter and excitation light with blue LED at 445 nm).

Results

Figure 77 presents the calibration curve of both optodes. Both optodes presented a typical Stern-Volmer shape, with a range of ratio value similar to the one of oxygen optodes prepared with TiO_2 used during the development work. However, optode 21 showed a very high standard deviation (from 14% at 0% of air saturation to 27% at 100% of air saturation) which was unusual compared to the developed optode (3% of standard deviation at 0% of oxygen).
Also, a look at individual green and red channel showed a strong difference of pixel intensity between the optodes 21 and rut one. Optode 21 emitted much less light than the rut one. The red channel presented a maximum pixel value at 35 for optode 21 and 298 for optode rut. This strong difference of pixel intensity indicates that the TiO_2 rutile did not enhance light and probably absorbs it. Thus, even if the calibration curve of both optodes presented a similar trend to the one developed in this study, pixel values on the green and red channels were very low for the optode 21. The titanium oxide 21 nm particle size is not adapted for optode application, as it does not scatter light. The optode with the titanium oxide rutile presented pixel intensity similar to the one prepared with TiO_2 P-170 used for the development work. It seems adapted to optode application.

This short experiment showed the necessity to test any new reference of titanium oxide before use for optode application.

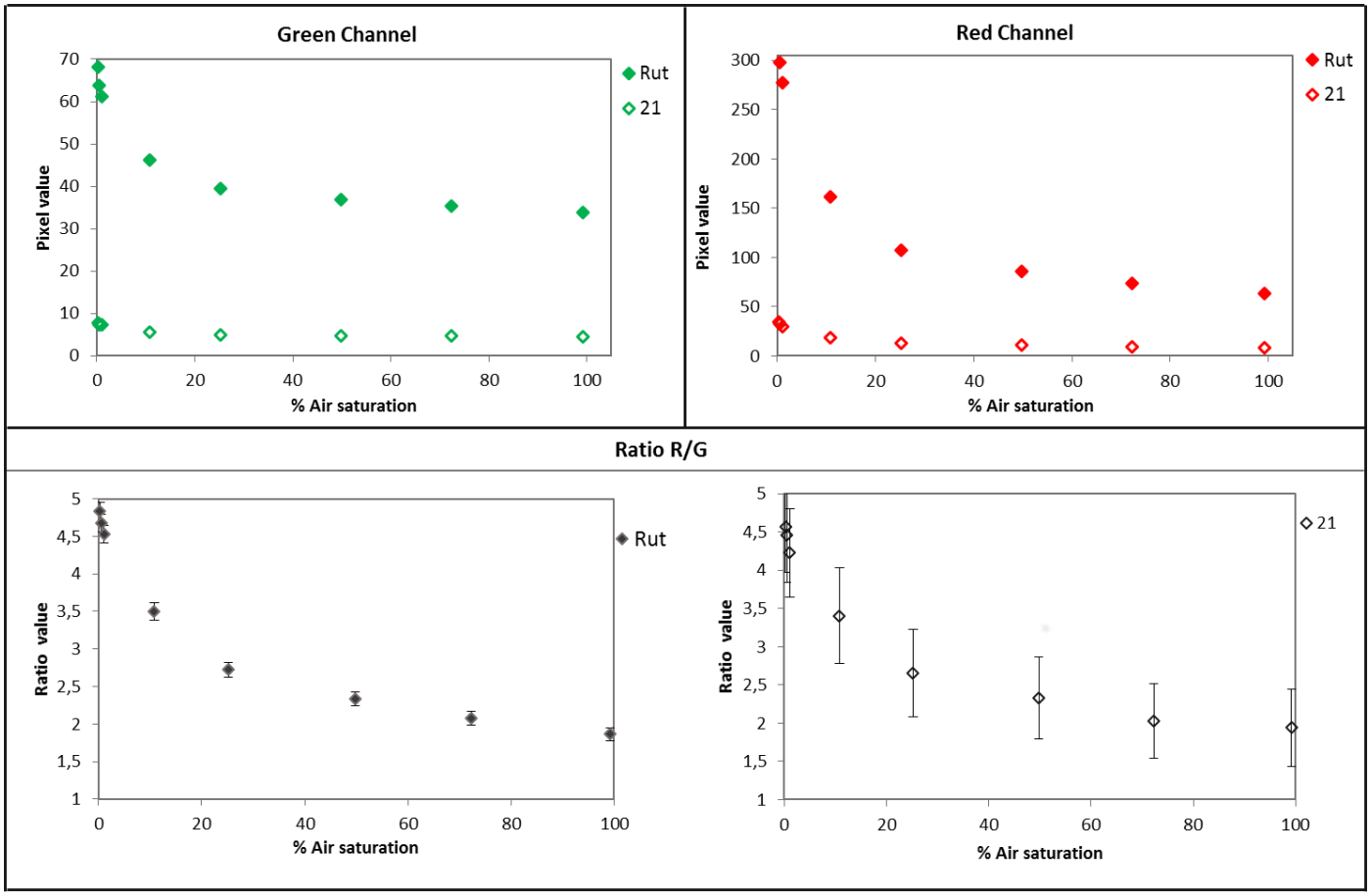

Figure 77: Calibration curve of oxygen optode made up with rutile <100 nm (rut) and 21 nm (21) titanium oxide. Up: Pixel values (mean) of green and red channels. Down: calibration curve expressed from ratio Red/Green.

APPENDIX 3 / Protocol: preparation of oxygen optode

Chemicals

PtOEP (platinum(II)-octaethylporphyrin)
Macrolex Yellow 10GN
Titanium oxide (P170, UV-Titan, Merck)
Polystyrene 260 000 g/mol
Chloroform
Ethanol (technical grade)
Acetone (technical grade)

Materials

Vial
Magnetic stirrer
Polyester foil Melinex 506, 125 µm
Bar knife, 1 mil
Glass plate

Sensor mix preparation

Table of amounts for about 4 optode foils:

Chemicals	**weight**
PtOEP	1.5 mg
Macrolex Yellow	1.5 mg
Titanium oxide	300 mg
Polystyrene	200 mg
Chloroform	3 g

In a small vial, weight first PtOEP and Macrolex Yellow. Add the bar magnet. Adjust the weight of titanium oxide, polystyrene and chloroform regarding on the weight of PtOEP and Macrolex. Close the vial and add parafilm to avoid evaporation of chloroform. Protect the vial from light exposure with aluminium foil.

Mix with magnetic stirrer for about 4 hours, until complete dissolution of all of components.

Coating of the sensor mix

The coating is prepared in a fumehood.

Clean carefully the bench in the fumehood to remove dust.

Put a glass plate on the bench. Clean it with ethanol then acetone.

Carefully clean a piece of polyester foil (half of A4 paper size) with ethanol then acetone. Avoid scratch on the foil.
Fix it on the glass plate, with tape or few drops of acetone between the foil and the glass plate.
Clean the 1 mil bar knife with ethanol then acetone.

Pipette sensor mix with a glass pipette, about ¾ of the glass pipette (≈ 1.5mL), and drop quickly on to the polyester foil. Then coat with the bar knife. (See the picture below).
Quickly, carefully clean the bar knife with chloroform. Then with ethanol.

Let the optode foil to dry, few minutes in the fumehood, then in a dark place.
Store it between pieces of paper, and protected from light.

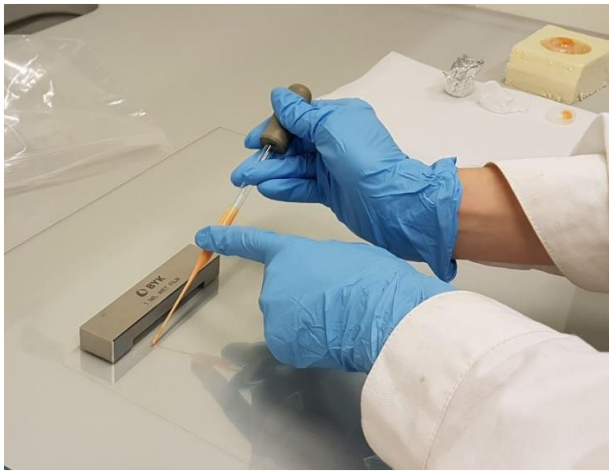

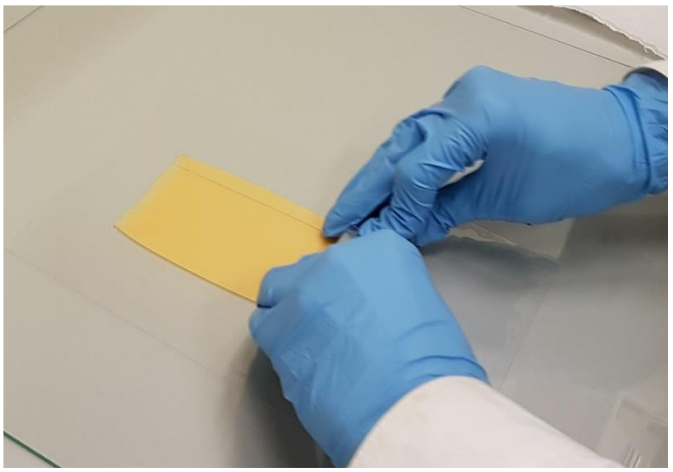

APPENDIX 4 / Protocol: preparation of Low pH optode (pH range: 5.5 – 7.5)

Chemicals

DClFODA (2',7'-dichloro-5(6)-N-octadecyl-carboxamidofluorescein)
Ziegelrot
Hydromed D4
Ethanol (analytical grade)
Ethanol (technical grade)
Acetone (technical grade)

Materials

1 Vial
Magnetic stirrer
Polyester foil Melinex 506, 125 µm
Bar knife, 1 mil
Glass plate

Sensor mix preparation

Table of amounts for about 7 optode foils:

Chemicals	**weight**
DClFODA	2.5 mg
Ziegelrot	25 mg
Hydromed D4	500 mg
Ethanol (analytical grade)	3 g
Water	0.33 g

In a small vial, weight first DClFODA and Ziegelrot. Add the bar magnet. Adjust the weight of hydromed, ethanol and water regarding on the weight of DClFODA. Close the vial and add parafilm to avoid evaporation of ethanol. Protect the vial from light exposure with aluminium foil.

Mix with magnetic stirrer for about 4 hours, until complete dissolution of all of components.

Coating of the sensor mix

The coating is prepared in a fumehood.

Clean carefully the bench in the fumehood to remove dust.

Put a glass plate on the bench. Clean it with ethanol then acetone.

Carefully clean a piece of polyester foil (half of A4 paper size) with ethanol then acetone. Avoid scratch on the foil.

Fix it on the glass plate, with tape or few drops of acetone between the foil and the glass plate.
Clean the 1 mil bar knife with ethanol then acetone.

Pipette sensor mix with a glass pipette, about ¾ of the glass pipette (≈ 1.5mL), and drop quickly on to the polyester foil. Then coat with the bar knife. (See the picture below).
Quickly, carefully clean the bar knife with ethanol. Then with ethanol.

Let the optode foil to dry, few minutes in the fumehood, then in a clean dark place.
Store it between pieces of paper, and protected from light.

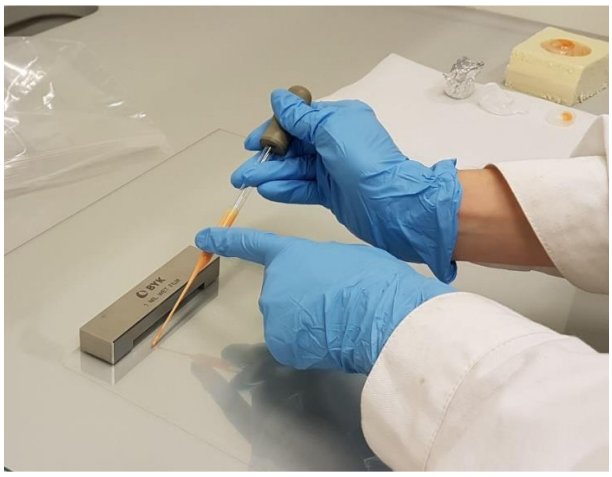

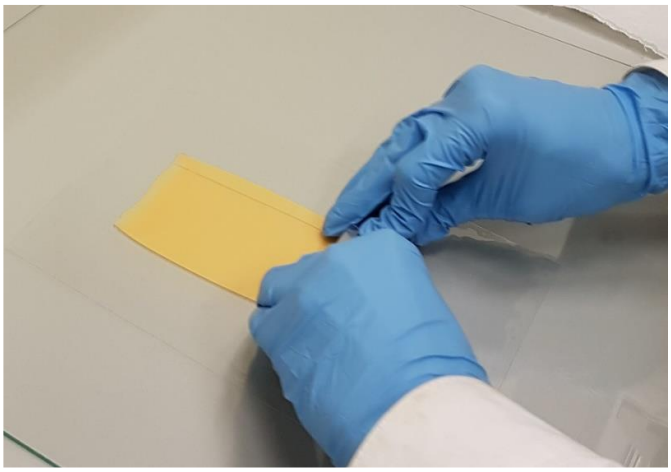

APPENDIX 5 / Protocol: preparation of High pH optode (pH range: 6.5 – 9.5)

Chemicals

d-HPTS (lipophilic derivative of 8-hydroxy-1,3,6 pyrenetrisulfonic)
Macrolex Yellow 10GN
Hydromed D4
Ethanol (analytical grade)
Ethanol (technical grade)
Acetone (technical grade)

Materials

1 Vial
Magnetic stirrer
Polyester foil Melinex 506, 125 µm
Bar knife, 1 mil
Glass plate

Sensor mix preparation

Table of amounts for about 5 optode foils:

Chemicals	**weight**
d-HPTS	3 mg
Macrolex Yellow	3 mg
Hydromed D4	200 mg
Ethanol 90% (Analytical grade)	1.8 g

In a small vial, weight first d-HPTS and Macrolex Yellow. Add the bar magnet. Adjust the weight of hydromed, ethanol regarding on the weight of d-HPTS. Close the vial and add parafilm to avoid evaporation of ethanol. Protect the vial from light exposure with aluminium foil.

Mix with magnetic stirrer (low speed) for about 4 hours, until complete dissolution of all of components.

Coating of the sensor mix

The coating is prepared in a fumehood.

Clean carefully the bench in the fumehood to remove dust.

Put a glass plate on the bench. Clean it with ethanol then acetone.

Carefully clean a piece of polyester foil (half of A4 paper size) with ethanol then acetone. Avoid scratch on the foil.
Fix it on the glass plate, with tape or few drops of acetone between the foil and the glass plate.
Clean the 1 mil bar knife with ethanol then acetone.

Pipette sensor mix with a glass pipette, about ¾ of the glass pipette (≈ 1.5mL), and drop quickly on to the polyester foil. Then coat with the bar knife. (See the picture below).
Quickly, carefully clean the bar knife with ethanol. Then with ethanol.

Let the optode foil to dry, few minutes in the fumehood, then in a clean dark place.
Store it between pieces of paper, and protected from light.

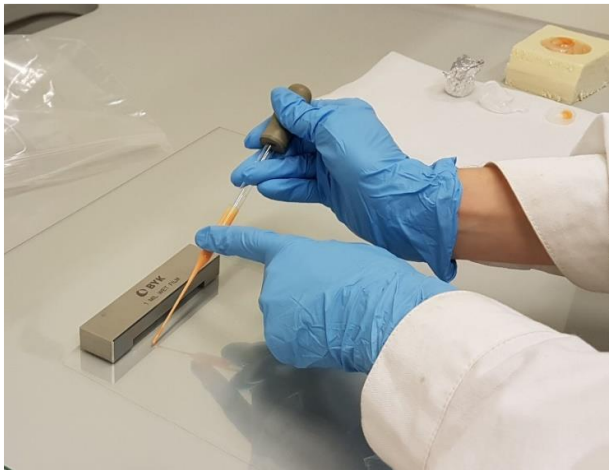

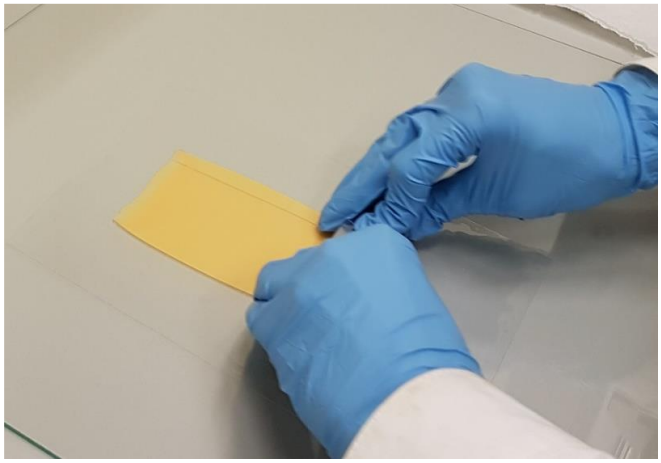

References

[1] KEESSTRA S. D. *et al.* The significance of soils and soil science towards realization of the United Nations Sustainable Development Goals. *SOIL,* 2016, 2, 111–128

[2] YOUNG I. M., CRAWFORD J. W. Interactions and Self-Organization in the Soil-Microbe Complex. *Science,* 2004, 304**,** 1634–1637.

[3] GLUD R.N. *et al.* Planar optrodes: a new tool for fine scale measurements of two-dimensional O2 distribution in benthic communities. *Marine Ecology Progress Series,* 1996, 140, 217–226

[4] BLOSSFELD S., GANSERT D. A novel non-invasive optical method for quantitative visualization of pH dynamics in the rhizosphere of plants. *Plant Cell and Environment,* 2007, 30**,** 176–186.

[5] HINSINGER P. *et al.* Rhizosphere: biophysics, biogeochemistry and ecological relevance. *Plant and Soil,* 2009, 321, 117–152.

[6] WENCEL D. *et al*. Optical Chemical pH Sensors. *Analytical Chemistry,* 2014, 86, 15–29.

[7] CAMMANN K. *et al.* The Cambridge definition of chemical sensors. in *Proceedings of the Cambridge workshop on chemical sensors and biosensors. Cambridge University Press, New York*. 1996.

[8] STICH M. I. J. *et al*. Multiple fluorescent chemical sensing and imaging. *Chemical Society Reviews,* 2010, 39, 3102–3114.

[9] LAKOWICZ, J. R. *Principles of Fluorescence Spectroscopy*. 3rd Edition. Springer US. 2006. 954 p.

[10] SCHÄFERLING M. The Art of Fluorescence Imaging with Chemical Sensors. *Angewandte Chemie International Edition,* 2012, 51, 3532–3554.

[11] ZHU Q. *et al*. Two-dimensional pH distributions and dynamics in bioturbated marine sediments. *Geochimica et Cosmochimica Acta, 2006,* 70, 4933–4949.

[12] LARSEN M. *et al.* A simple and inexpensive high resolution color ratiometric planar optode imaging approach: application to oxygen and pH sensing. *Limnology and Oceanography-Methods*, 2011, 9, 348–360.

[13] LIEBSCH G. *et al.* Fluorescent imaging of pH with optical sensors using time domain dual lifetime referencing. *Analytical Chemistry,* 2001, 73, 4354–4363.

[14] KREUZEDER A. *et al.* In situ observation of localized, sub-mm scale changes of phosphorus biogeochemistry in the rhizosphere. *Plant and Soil,* 2018, 424, 573–589.

[15] KOREN K. *et al*. In-vivo imaging of O2 dynamics on coral surfaces spray-painted with sensor nanoparticles. *Sensors and Actuators B: Chemical,* 2016, 237, 1095–1101.

[16] KOREN K. *et al.* Tuning the dynamic range and sensitivity of optical oxygen-sensors by employing differently substituted polystyrene-derivatives. *Sensors and Actuators B: Chemical,* 2013, 176, 344–350.

[17] OGURI K. *et al*. Platinum octaetylporphyrin based planar optodes combined with an UV-LED excitation light source: An ideal tool for high-resolution O2 imaging in O2 depleted environments. *Marine Chemistry,* 2006, 100**,** 95–107.

[18] ZHU Q. *et al*. High-performance planar pH fluorosensor for two-dimensional pH measurements in marine sediment and water. *Environmental Science & Technology,* 2005, 39, 8906–8911.

[19] HAKONEN A., HULTH S. A high-performance fluorosensor for pH measurements between 6 and 9. *Talanta,* 2010, 80, 1964–1969.

[20] HAKONEN A., HULTH S. A high-precision ratiometric fluorosensor for pH: Implementing time-dependent non-linear calibration protocols for drift compensation. *Analytica Chimica Acta,* 2008, 606, 63–71

[21] SCHRÖDER C. R. *et al.* pH Fluorosensors for use in marine systems. *Analyst,* 2005, 130, 907–916.

[22] KÖNIG B. *et al*. Fabrication and test of sol–gel based planar oxygen optodes for use in aquatic sediments. *Marine Chemistry,* 2005, 97, 262–276.

[23] WANG X., WOLFBEIS O. S. Optical methods for sensing and imaging oxygen: materials, spectroscopies and applications. *Chemical Society Reviews,* 2014, 43**,** 3666–3761.

[24] MOßHAMMER M. *et al.* Design and Application of an Optical Sensor for Simultaneous Imaging of pH and Dissolved O2 with Low Cross-Talk. *ACS Sensors,* 2016, 1, 681–687.

[25] KERMIS H. R. *et al.* Dual Excitation Ratiometric Fluorescent pH Sensor for Noninvasive Bioprocess Monitoring: Development and Application. *Biotechnology Progress,* 2002, 18, 1047–1053.

[26] JIANG Z. *et al*. Design and Fabrication of a Ratiometric Planar Optode for Simultaneous Imaging of pH and Oxygen. *Sensors,* 2017, 17, 1316.

[27] MEIER R. J *et al*. Referenced luminescent sensing and imaging with digital color cameras: A comparative study. *Sensors and. Actuators B: Chemical,* 2013, 177, 500–506.

[28] HAKONEN A. *et al*. Digital colour tone for fluorescence sensing: a direct comparison of intensity, ratiometric and hue based quantification. *Analyst,* 2014, 139**,** 3524–3527.

[29] HAKONEN A. *et al.* Analytical performance during ratiometric long-term imaging of pH in bioturbated sediments. *Talanta,* 2010, 81, 1393–1401.

[30] JOVANOVIC Z. *et al.* Rhizosphere O2 dynamics in young Zostera marina and Ruppia maritima. *Marine Ecology Progress Series,* 2015, 518**,** 95–105.

[31] BLOSSFELD S. *et al.* The dynamics of oxygen concentration, pH value, and organic acids in the rhizosphere of Juncus spp. *Soil Biology & Biochemistry,* 2011, 43, 1186–1197.

[32] BLOSSFELD S. *et al*. Quantitative imaging of rhizosphere pH and CO2 dynamics with planar optodes. *Annals of Botany,* 2013, 112**,** 267–276.

[33] LARSEN M. *et al*. O2 dynamics in the rhizosphere of young rice plants (Oryza sativa L.) as studied by planar optodes. *Plant and Soil,* 2015, 390, 279–292.

[34] ZHU K. *et al*. Spatial Oxygen Distribution and Nitrous Oxide Emissions from Soil after Manure Application: A Novel Approach Using Planar Optodes. *Journal of Environmental Quality,* 2014, 43, 1809–1812.

[35] SCHREML S. *et al.* 2D luminescence imaging of pH in vivo. *Proceedings of the National Academy of Sciences,* 2011, 108, 2432–2437.

[36] ZHU Q., ALLER, R. C. A rapid response, planar fluorosensor for measuring two-dimensional pCO2 distributions and dynamics in marine sediments. *Limnology and Oceanography: Methods,* 2010, 8, 326–336.

[37] PEDERSEN L. *et al*. A nitrate sensitive planar optode; performance and interferences. *Talanta,* 2015, 144, 933–937.

[38] STROMBERG, N. Determination of ammonium turnover and flow patterns close to roots using Imaging optodes. *Environmental Science & Technology,* 2008, 42, 1630–1637.

[39] WAICH K. *et al*. Fluorescence sensors for trace monitoring of dissolved ammonia. *Talanta,* 2008, **77,** 66–72.

[40] ZHU Q., ALLER R. C. Planar fluorescence sensors for two-dimensional measurements of H2S distributions and dynamics in sedimentary deposits. *Marine Chemistry,* 2013, 157**,** 49–58.

[41] KRAUSE C. *et al*. pH-Insensitive Ion Selective Optode: A Coextraction-Based Sensor for Potassium Ions. *Analytical Chemistry,* 1999, 71, 1544–1548.

[42] BORISOV S. *et al*. A novel planar optical sensor for simultaneous monitoring of oxygen, carbon dioxide, pH and temperature. *Analytical and Bioanalytical Chemistry,* 2011, 400, 2463–2474.

[43] CAO Z. *et al*. A fluorosensor for two-dimensional measurements of extracellular enzyme activity in marine sediments. *Marine Chemistry,* 2011, 123, 23–31.

[44] SCHROEDER C. R. *et al*. Time-resolved pH/pO_2 mapping with luminescent hybrid sensors. *Analytical Chemistry,* 2007, 79, 60–70.

[45] KAUTSKY H. Quenching of luminescence by oxygen. *Transactions of the Faraday Society,* 1939, 35, 216–219.

[46] KLIMANT I. *et al.* Fiber-optic oxygen microsensors, a new tool in aquatic biology. *Limnology and Oceanography,* 1995, 40, 1159–1165.

[47] BORISOV S. M., KLIMANT, I. Ultrabright Oxygen Optodes Based on Cyclometalated Iridium(III) Coumarin Complexes. *Analytical Chemistry*, 2007, 79**,** 7501–7509.

[48] BALEIZAO C. *et al*. Dual fluorescence sensor for trace oxygen and temperature with unmatched range and sensitivity. *Analytical Chemistry*, 2008, 80**,** 6449–6457.

[49] HOLST G., GRUNWALD B. Luminescence lifetime imaging with transparent oxygen optodes. *Sensors and Actuators B: Chemical*, 2001, 74, 78–90.

[50] FREDERIKSEN, M. S., GLUD, R. N. Oxygen dynamics in the rhizosphere of Zostera marina: A two-dimensional planar optode study. *Limnology and Oceanography,* 2006, 51, 1072–1083.

[51] PRECHT E. *et al*. Oxygen dynamics in permeable sediments with wave-driven pore water exchange. *Limnology and Oceanography, 2004,* **49,** 693–705.

[52] VALEUR, B. *Invitation à la fluorescence moléculaire*. De Boeck, 2004. 202 p.

[53] HULTH S. *et al*. A pH Plate Fluorosensor (Optode) for Early Diagenetic Studies of Marine Sediments. *Limnology and Oceanography*, 2002, 47, 212–220.

[54] BORISOV S. M. *et al*. Fluorescent poly(styrene-block-vinylpyrrolidone) nanobeads for optical sensing of pH. *Sensors and Actuators B: Chemical*, 2009, 139, 52–58.

[55] WEIDGANS B. M. *et al*. Fluorescent pH sensors with negligible sensitivity to ionic strength. *The Analyst*, 2004, 129, 645.

[56] STAHL H. *et al.* Time-resolved pH imaging in marine sediments with a luminescent planar optode. *Limnology and Oceanography-Methods*, 2006, 4, 336–345.

[57] RUDOLPH N. *et al*. Spatio-temporal mapping of local soil pH changes induced by roots of lupin and soft-rush. *Plant and Soil*, 2013, 369, 669-680.

[58] SCHREML. S. *et al.* A sprayable luminescent pH sensor and its use for wound imaging in vivo. *Experimental Dermatology*, 2012; 21, 951–953.

[59] PreSens. pH Sensor Foils SF-LV1R - https://www.presens.de/products/detail/ph-sensor-foils-sf-lv1r.html. (Accessed: 23rd April 2018)

[60] HAN C. *et al.* High-resolution Imaging of pH in Alkaline Sediments and Water Based on a New Rapid Response Fluorescent Planar Optode. *Scientific Reports,*2016, 6, 26417.

[61] KUZYAKOV Y., BLAGODATSKAYA E. Microbial hotspots and hot moments in soil: Concept & review. *Soil Biology and Biochemistry*, 2015, 83, 184–199.

[62] HINSINGER P. *et al.* Rhizosphere geometry and heterogeneity arising from root-mediated physical and chemical processes. *New Phytologist*, 2005, 168, 293–303.

[63] HINSINGER P. *et al.* Origins of root-mediated pH changes in the rhizosphere and their responses to environmental constraints: A review. *Plant and Soil, 2003*, 248, 43–59.

[64] COLMER, T. D. Long-distance transport of gases in plants: a perspective on internal aeration and radial oxygen loss from roots. *Plant Cell and Environment*, 2003, 26, 17–36.

[65] YORK L. The holistic rhizosphere: integrating zones, processes, and semantics in the soil influenced by roots. *Journal of Experimental Botany,* 2016, 67, 3629–3643.

[66] PEDERSEN L. L *et al*. Measuring biogeochemical heterogeneity at the micro scale in soils and sediments. *Soil Biology and Biochemistry*, 2015, 90, 122–138.

[67] HÄUSSLING M. *et al*. An Improved Method for Non-destructive Measurements of the pH at the Root-Soil Interface (Rhizosphere). *Journal of Plant Physiology,* 1985, 117, 371–375.

[68] JAILLARD B. *et al.* pH mapping in transparent gel using color indicator videodensitometry. *Plant and Soil,* 1996, 183, 85–95.

[69] ZHANG H., DAVISON W. Performance Characteristics of Diffusion Gradients in Thin Films for the in Situ Measurement of Trace Metals in Aqueous Solution. *Analytical Chemistry,* 1995, 67, 3391–3400.

[70] HOEFER C. *et al.* Localized Metal Solubilization in the Rhizosphere of Salix smithiana upon Sulfur Application. *Environmental Science & Technology,* 2015, 49, 4522–4529.

[71] SPOHN M. *et al*. Soil zymography – A novel in situ method for mapping distribution of enzyme activity in soil. *Soil Biology and Biochemistry,* 2013, 58, 275–280.

[72] RUDOLPH-MOHR N. *et al*. Mapping water, oxygen, and pH dynamics in the rhizosphere of young maize roots. *Journal of Plant Nutrition and Soil Science,* 2017, 180, 336–346.

[73] RUDOLPH N. *et al.* Dynamic oxygen mapping in the root zone by fluorescence dye imaging combined with neutron radiography. *Journal of Soils and Sediments,* 2012, 12, 63–74.

[74] RUDOLPH-MOHR N. *et al*. A multi-imaging approach to study the root-soil interface. *Annals of Botany, 2014,* 114, 1779–1787.

[75] ALONY A., LINKER R. Development of a laser-induced fluorescence imaging system for root activity and rhizosphere visualisation. *Biosystems Engineering*, 2013, 114, 466–473.

[76] SANTNER J. *et al.* Two decades of chemical imaging of solutes in sediments and soils – a review. *Analytica Chimica Acta,* 2015, 878, 9–42.

[77] ZHU K. *et al*. Heterogeneity of O_2 dynamics in soil amended with animal manure and implications for greenhouse gas emissions. *Soil Biology and Biochemistry,* 2015, 84, 96–106.

[78] PRADIER, C. *Rôles fonctionnels des racines fines profondes en plantation d'eucalyptus au Brésil sur sols pauvres en nutriments et en situation hydrique limitante. Réponse à une situation hydrique limitante*. Thèse de Doctorat : Montpellier SupAgro, 2016.

[79] HOEFER C. *et al*. Integrating chemical imaging of cationic trace metal solutes and pH into a single hydrogel layer. *Analytica Chimica Acta*, 2017, 950, 88–97.

[80] MAYR T. *et al.* Light Harvesting as a Simple and Versatile Way to Enhance Brightness of Luminescent Sensors. *Analytical Chemistry,* 2009, **81,** 6541–6545.

[81] ALVA A. K. *et al.* Relationship between ionic strength and electrical conductivity for soil solutions. *Soil Science, 1991,* 152, 239.

[82] PAPKOVSKY D. B. *et al.* Phosphorescent polymer films for optical oxygen sensors. *Biosensors and Bioelectronics,* 1992, 7, 199–206.

[83] QUARANTA, M. *et al*. Indicators for optical oxygen sensors. *Bioanalytical Reviews,* 2012, 4, 115–157.

[84] LIM C.-J., PARK, J.-W. Luminescent oxygen-sensing films with improved sensitivity based on light scattering by TiO2 particles. *Sensors and Actuators B: Chemical,* 2017, 253, 934–941.

[85] ZHOU Z. *et al*. Enhanced Photoluminescence of Oxygen Sensing Films through Doping with High Dielectric Constant Particles. *Advanced Functional Materials,* 2007, 17, 3530–3537.

[86] MOHR G. J. *et al*. Application of a novel lipophilized fluorescent dye in an optical nitrate sensor. *Journal of Fluorescence,* 1995, 5, 135–138.

[87] WILLIAMS P. N. *et al.* Localized Flux Maxima of Arsenic, Lead, and Iron around Root Apices in Flooded Lowland Rice. *Environmental Science & Technology,* 2014, 48, 8498–8506.

[88] SCHREIBER C. M. *et al.* Monitoring rhizospheric pH, oxygen, and organic acid dynamics in two short-time flooded plant species. *Journal of Plant Nutrition and Soil Science,* 2012, 175, 761–768.

[89] RUDOLPH-MOHR N. *et al.* Non-invasive imaging techniques to study O_2 micro-patterns around pesticide treated lupine roots. *Geoderma,* 2015, 239, 257–264.

[90] CHRISTEL W. *et al.* Spatiotemporal dynamics of phosphorus release, oxygen consumption and greenhouse gas emissions after localised soil amendment with organic fertilisers. *Science of The Total Environment,* 2016, 554–555, 119–129.

[91] WANG Z. *et al*. Accuracy of Visible and Ultra-Violet Light for Estimating Live Root Proportions with Minirhizotrons. *Ecology, 1995,* **76,** 2330–2334.

[92] RUBOL S. *et al*. 2D visualization captures the local heterogeneity of oxidative metabolism across soils from diverse land-use. *Science of The Total Environment,* 2016, 572, 713–723.

[93] ROGER P. A. et al. Microbiological management of wetland rice fields. In meeting soil microbial ecology. Dekker, new york, 1993. pp 417–455.

[94] ARMSTRONG W. *et al*. Root adaptation to soil waterlogging. *Aquatic Botany,* 1991, 39, 57–73.

[95] GREEN M. S., ETHERINGTON J. R. Oxidation of Ferrous Iron by Rice (Oryza sativa L.) Roots: A Mechanism for Waterlogging Tolerance? *Journal of Experimental Botany,* 1977, 28, 678–690.

[96] DIXON R., KAHN D. Genetic regulation of biological nitrogen fixation. *Nature Reviews Microbiology,* 2004, 2, 621–631.

[97] FEINBERG M. Validation of analytical methods based on accuracy profiles. *Journal of. Chromatography A,* 2007, 1158, 174–183.

[98] KOUTSOSPYROS A. *et al*. A review of tungsten: From environmental obscurity to scrutiny. *Journal of Hazardous Materials,* 2006, 136, 1–19.

[99] STRIGUL N. *et al.* Influence of speciation on tungsten toxicity. *Desalination,* 2009, 248, 869–879.

[100] STRIGUL N. *et al.* Effects of tungsten on environmental systems. *Chemosphere,* 2005, 61, 248–258.

[101] DERMATAS D. *et al.* Solubility, Sorption, and Soil Respiration Effects of Tungsten and Tungsten Alloys. *Environmental Forensics, 2004,* **5,** 5–13.

***In situ* measurements of pH and O_2 by planar optodes: improvements and adaptations for soil and rhizosphere applications.**

Résumé

Le sol est un milieu très hétérogène, lieu d'interactions biogéochimiques complexes à fine échelle affectant le fonctionnement des écosystèmes à plus large échelle. La connaissance de leurs dynamiques spatio-temporelles reste limitée car difficile d'accès. Les optodes planaires sont une technologie émergente permettant le suivi des dynamiques du pH et de l'oxygène de manière non-invasive et à l'échelle infra-millimétrique. Son principe est basé sur l'interaction réversible entre une sonde fluorescente et l'analyte, combiné à un système de détection optique. L'objectif de ce travail a été de développer et d'adapter une optode oxygène et deux optodes pH (gamme de pH entre 5.5-7.5 et 6.5-9.5) pour le suivi de processus biogéochimiques dans le sol et la rhizosphère. L'effet des conditions expérimentales sur la mesure a été particulièrement étudiée, telles que l'hétérogénéité structurale, l'humidité du sol, la durée de l'expérimentation. Les résultats ont montré la nécessité de vérifier l'impact de l'hétérogénéité du système lors de l'utilisation d'optodes transparentes. La mesure peut aussi être affectée par les processus biogéochimiques du sol renforçant la nécessité de vérifier l'intégrité de l'optode après application. Ces optodes ont été appliquées à deux études de cas : le suivi (1) de la dynamique d'oxygène dans la rhizosphère du riz immergée et (2) des gradients de pH autour d'apport de tungstène dans des sols non saturés en eau.

Mots-clés : optode planaire, sonde pH, sonde oxygène, fluorescence, sol, rhizosphère, imagerie

Abstract

Soil is a highly heterogeneous system in which complex biogeochemical interactions occur at fine scale affecting ecosystem functioning at larger scale. Knowledge of spatio-temporal dynamics of soils processes is still scarce as access and continuous monitoring is challenging. Planar optodes are an emerging technology allowing the imaging of pH and oxygen dynamics in a non-invasive way and at sub-mm scale. It is based on the reversible interaction between protons or oxygen with a sensitive fluorescent probe and combined with a dedicated imaging set-up. The objective of this work was to develop and adapt oxygen and pH optodes (pH range of 5.5–7.5 and 6.5-9.5) for monitoring soil chemical processes as well as soil-root interactions. In addition, we focused on determining the effect of soil experimental conditions on optode measurements, including background heterogeneity, soil water content and experiment duration. Results revealed the need to test and overcome effects of background heterogeneity when working with transparent optodes, Moreover, depending on experimental condition, optode signals were occasionally found to be affected by biogeochemical processes, highlighting the necessity to assess optode performance after its application to soil. Improved optodes were applied in two case studies: the imaging of (1) oxygen dynamics in the rhizosphere of flooded rice and of (2) pH changes around metallic tungsten sources in non-water saturated soil.

Keywords: planar optode, pH sensor, oxygen sensor, fluorescence, soil, rhizosphere, chemical imaging